TECHNICAL UNIVERSITY OF VIENNA
DIPLOMA THESIS

INSTITUTE OF CHEMICAL TECHNOLOGIES AND ANALYTICS

Characterisation of Passive Check Valves in Microsystems

Submitted in satisfaction of the requirements for the degree of Diploma- engineer /eng./
of the Technical University of Vienna
in cooperation with the Fraunhofer EMFT

Barbara Leikam
Mentor at the Fraunhofer EMFT: Lorenz Grünerbel
Mentor at the TU Vienna: Univ. Prof. Dipl.- Ing. Dr. Peter Ertl

July 19, 2021

Statutory Declaration

I declare that I have authored this thesis independently, which I have not used other than the declared sources/resources. I have explicitly marked all material quoted either literally or by content from the used sources.

Munich, 19.07.2021

Signature

Acknowledgements

I would like to thank very much my supervisor, Lorenz Grünerbel, in Microdosing Systems at Fraunhofer EMFT for making this opportunity possible for me and providing his valuable guidance and support throughout my thesis.

A special thanks goes to the Technical University of Vienna, particularly Professor Ertl, for supervising and correcting my thesis. Also a huge thank you goes to Silvia Schobesberger, who has always been a reliable source of support for all my questions throughout my work.

I want to thank all the nice and helpful colleagues from the department of Microdosing at the Fraunhofer EMFT. A friendly and welcoming atmosphere was always improving working conditions and allowing for questions if necessary.

Finally, and most importantly, I am very grateful to my parents for providing me with huge support and love throughout my years of study. My heartfelt and greatest thanks are due to them for this.

Contents

Abstract

A trend towards miniaturisation can be observed in many industries. Among other things, the quest for more performance and the reduction of mass and energy consumption have favoured this trend in recent years. This is also the case in medical and laboratory technology. For some applications, micropumps offer opportunities for integration into microdosing systems and thus contribute to the miniaturisation of devices. Possible areas of application for the piezoelectric steel diaphragm micropump manufactured at Fraunhofer EMFT include negative pressure therapy for wounds, the dosage of medicines and hydraulic prostheses. Precise dosing is essential here, which is why the behaviour of all the components of the micropump must be studied in detail and the interrelationships understood. One of these complex components is the microvalve. The behaviour of passive valves is strongly dependent on the fluidic properties of the medium used. The literature research has shown that there are deficits in the investigation of microvalves with liquid as the medium. One reason for this is that the valves are not visible during normal operation of the micropump, as the actuator diaphragm is located above the valves. Therefore, no experimental measurements are known describing the behaviour of the valves under the influence of liquids. However, measurements are necessary to validate the derived valve models. For this purpose, a new measurement method is being developed to investigate the quasi-static and dynamic behaviour of valves under the influence of air and water and to characterise the valve behaviour. This opens up new possibilities for more detailed observation and derives optimisation options.

Kurzfassung

In vielen Branchen ist ein Trend zur Miniaturisierung zu beobachten. Unter anderem haben das Streben nach mehr Leistung und die Reduzierung von Masse und Energieverbrauch diesen Trend in den letzten Jahren begünstigt. Auch in der Medizin- und Labortechnik ist dies der Fall. Für einige Anwendungen bieten Mikropumpen Möglichkeiten zur Integration in Mikrodosiersystemen und tragen in diesem Sinne zur Miniaturisierung von Geräten bei. Potentielle Einsatzgebiete für die, an der Fraunhofer EMFT hergestellten, piezoelektrische Edelstahlmikropumpe sind unter anderem die Unterdrucktherapie von Wunden, die Dosierung von Medikamenten und hydraulische Prothesen. Hierbei kommt es auf eine exakte Dosierung an, weshalb das Verhalten aller Komponenten der Mikropumpe genau untersucht und die Zusammenhänge verstanden werden müssen. Eines der komplexen Bauteile stellt das Mikroventil dar. Das Verhalten der passiven Ventile ist stark von den strömungstechnischen Eigenschaften des verwendeten Mediums abhängig. Eine Literaturrecherche hat ergeben, dass Defizite bei der experimentellen Charakterisierung von Ventilen, unter Einfluss von Flüssigkeiten, vorhanden sind. Ein Grund hierfür ist, dass die Ventile unter normalem Betrieb der Mikropumpe nicht sichtbar sind, da sich die Antriebsmembran oberhalb der Ventile befindet. Daher sind keine experimentellen Messungen bekannt, die das Verhalten der Ventile unter dem Einfluss von Flüssigkeiten beschreiben. Messungen sind jedoch notwendig, um die abgeleiteten Modelle für Mikroventile zu validieren. Zu diesem Zweck wird eine neue Messmethode entwickelt, um das quasistatische und dynamische Verhalten von Ventilen unter dem Einfluss von Luft und Wasser zu untersuchen und das Ventilverhalten zu charakterisieren. Dies eröffnet neue Möglichkeiten zur genaueren Betrachtung und leitet Optimierungsmöglichkeiten ab.

1   Introduction

In recent years, research on microelectromechanical systems (MEMS) has gained fundamentally new achievements for many industrial applications and offers completely new technologies with entirely new innovations. As with all microsystem technologies, micropumps are miniaturised devices and have numerous advantages, such as high quantities by low production costs, a small physic size and weight, portability, low power consumption, and the possibility for integration with other microfluidic devices.
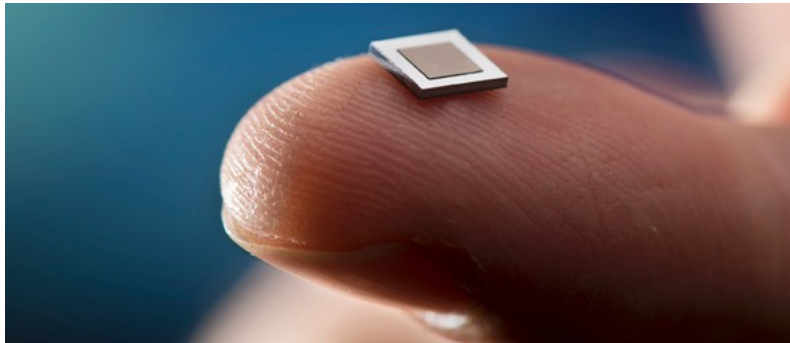
Figure 1:   The smallest micropump in the world Si-micropump, 3.5mm x 3.5mm @Fraunhofer EMFT [1]

Micropumps have functional dimensions in the micrometre range and are transporting tiny volumes of liquids or gases. Whenever microfluidics plays a role within devices, small volumes have to be manipulated and controlled. Hence, the micropump is fundamental for active micro-dosing systems, and it can be mentioned as the "beating heart of microfluidic" [2]. Over the past few decades, research and development have been contributed to the rapid development of a wide range of MEMS with different functions.

Especially in the field of medicine, miniaturisation has advanced and reshaped the industry. Since the first MEMS for insulin delivery systems was introduced by Jan Smiths in 1980, [3],micropumps have been developed for various medical applications but are still rarely found on the medical market [4]. However, every application requires different performance parameters and needs, therefore a unique micropump solution with clear specifications [5]. The trend of miniaturising medical devices, in particular, was supported by different factors. Small medical devices minimize patients trauma and reduce the length of hospital stays and thereby lower the costs. Also, an ageing population, a push for more personalized treatment and increasing availability of healthcare leads to more wearable devices. In addition, many medical applications can theoretically be realized much more effectively due to reducing the size or even enabling new treatments in the first place. Micropumps offer possible solutions

for some of these requests. For future prognoses, micropumps will play an ever-greater role in medical treatments. According to MarkedResearchFuture, the annual growth rate of the global micropump sector will rise from 2018 till 2027 up to 19.4%, and the forested key payers are the sectors biotechnology and pharmaceutical companies, hospitals, and diagnostic centres, and research institutes [6].

To guarantee an accurate and precise fluid dosing system for medical applications, understanding the micropump's relevant components and how it can be controlled is indispensable. To meet the requirements of a complex microfluidic system, microvalves are important components for optimisation and are the focus of this thesis.

1.1 Motivation and objectives

A variety of micropumps are fabricated using microfabrication techniques and have a wide range of possible industrial applications. The piezoelectrically driven microdiaphragm pumps made of stainless steel and developed by the Fraunhofer EMFT also offer various potential application areas. These pumps can be used in the field of laboratory or medical technology, where extremely small quantities of gases and liquids are metered. With these pumps, the focus is on miniaturisation to achieve the required pumping performance reliably but still cost-effectively. These pumps could establish themselves on the market in the future, especially in the medical sector. The micropumps may, among other things, be used for treatments like wound therapy, medical implants like drug delivery systems or artificial sphincter implants, pump infusions, and autonomous cell culture devices.

Considering the fact that the European population is the most aged in the world and chronic diseases, for example, diabetes mellitus, are more likely within increasing age. Also the number of drug dosing systems will rise. While 2019 in Europe, 30 of 100 persons aged 65 (or over), it is projected that the number of older persons is reaching 49 in 2050 [7, 8]. Furthermore, from 2017 to 2019, an increase of 25 % was objected of diabetes patients in Germany [9].

Also, the possible treatment of chronic wounds by micropumps is an important point. In Germany, about 2.7 million people are suffering from chronic wounds with different disease entities [10]. Recent studies have shown a promising and effective treatment called Negative Pressure Wound Therapy (NPWT). Compared to the conventional chronic wound treatment in Subcutaneous Abdominal Wound Healing Impairment(SAWHI), significantly more

wounds were closed within 42 days treated with NPWT [10].

In addition, portable devices are a great opportunity to improve these people's lives by the possibility to use medical devices independently. The portable devices are taking part in being an important requirement between hospital and in-home treatment. Coupled with increasing medical costs and the push for shorter hospital stays has supported the need for wearable medical devices. The population nowadays wants to be flexible. Where patients once had to contact a doctor's office or other clinical settings for healthcare, they now can use devices without leaving their homes. As a result of these dynamic changes in the medical healthcare sector, a new focus has been driven towards smaller, lighter, and more portable medical equipment. Also, the need to automate home-use devices is necessary due to inaccurate dosage that could cause long-term patient consequences.

To enable a flexible and portable treatment, pump miniaturisation is one focus at Fraunhofer EMFT [11]. In microfluidic systems, small parameter deviations can lead to large system changes and could pose a risk to the user or patient and can change the operating point. Therefore, a thorough understanding of all aspects of the micropump is mandatory for patient safety. The passive diaphragm microvalves are a sensitive component of the micro diaphragm pump. Precise and controllable dosing is necessary, particularly in the case of medical devices. The optimisation of micropumps for certain applications requires an exact understanding of the individual components. The high fluid resistance of the valves is, for example, a limiting factor for the flow rate. In addition, unavoidable small backflows through the closed valve counteract reduce the pumping capacity.

Most of the dosage systems in medical applications are dealing with fluids that are applied to the patient. However, nowadays, only a few examples of micropumps are used in industry, and the technology is not commonly used due to immense micro-system challenges [12]. More research needs to be done to understand better the complex fluid behaviour in microvalves and thus of the whole micropump system.

In particular, the behaviour of the valves of the piezoelectric pump under the influence of water is poorly researched compared to air. Since the valves of a micropump are usually located within a closed pump system, it is challenging to visually analyse their performance under operating conditions. When using air as a medium, it is relatively easy to observe the valve displacement through an optical measuring device. The escaping air at the valve does not affect the sensitive measurement sensors. With water measurements, the situation is quite different, and it is impossible to measure under free conditions without damaging

the measuring equipment.

As a result, little information is available on the behaviour of passive microvalves with water as a medium. However, this information is important for further optimisation of the valves and thus also of the entire pump. Therefore, the aim of this diploma's thesis is to determine the behaviour of the passive microvalves experimentally and to characterise the valves on the basis of their different behaviour in the medium air and water.

1.2   Outline of the thesis

In this paragraph, the structure of this paper work is schematically Figure 2 drawn and should give a visual overview of the practice regarding this diploma thesis.

After the introduction (1), the theoretical background chapter (2) describes the basic knowledge of all necessary microfluidic components. Explanations of the general fundamentals of micropumps and microvalves are given in this chapter. Also, the considered ortho-planar valve within relevant variables mechanical parameters are introduced, and the methods for valve characterisation in fluidic microsystems are reviewed. After establishing the basics and state-of-the-art methods for fluidic valve characterisation, the third chapter (3) presents the implementation of the valve characterisation for medium air and water. Therefore, analytical and experimental fluidic analyses of the valve behaviour are described separately. The fourth chapter (4) represents and discusses the results of the experimental methods. Finally, in the fifth chapter (5), a conclusion is drawn out, and an outlook on future developments is given.

1. Introduction

2. Characteristics of microvales
    +
    Methodes for valve characterization
    in differentmediums

3. Implementation of valve characterization for mediumair and water

    Analytical analyse   +   Experimental analyse

4. Experimental results for medium air and water
    +
    Discussion

5. Conclusion
    +
    Outlook
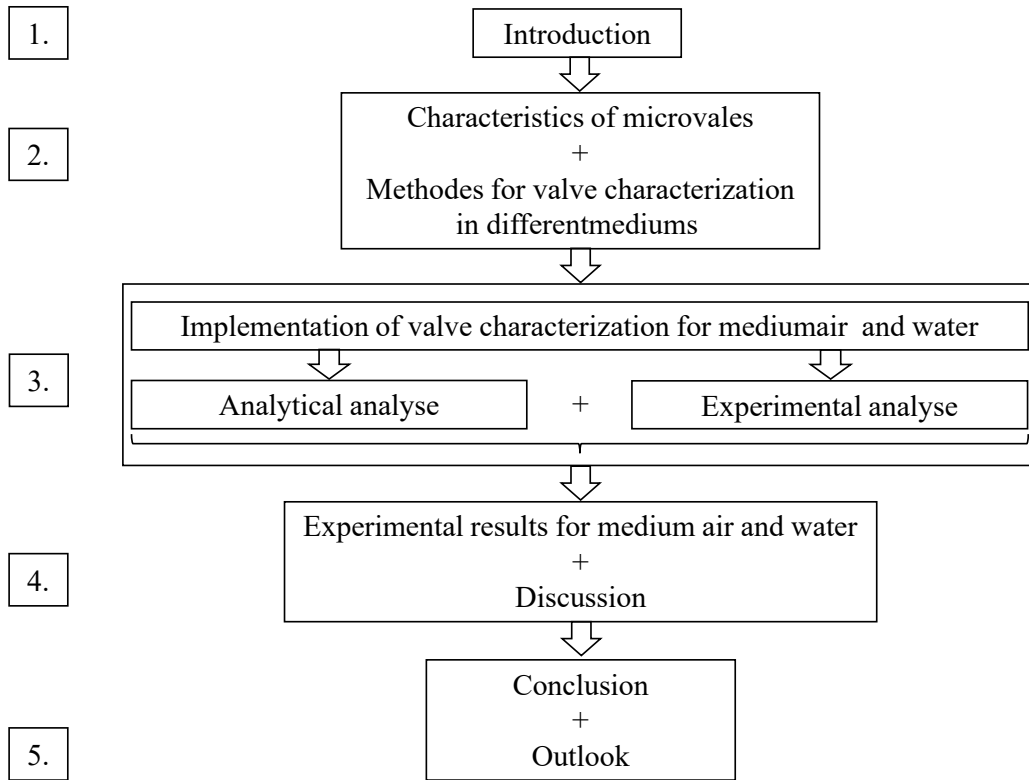
Figure 2: Structure of the diploma thesis

2   Theoretical background

The second chapter gives a short overview of micropumps and obtains deeper insight into microvalves focusing on the ortho-planar diaphragm microvalves, that is characterised in this diploma thesis. The chapter ends with the current state of the art of the methods for valve characterisation within different mediums.

2.1   Micropumps

A micropump is a pump of reduced size and is a device that can control and deliver the working fluid (gas or liquid) in small volumes on a nano/microliter order, from a reservoir to a target. The optimal micropump should provide adequate flow control, high back pressure, a wide range of flow rates within lower power consumption. The individual, variable design of micropumps allows effectiveness and suitability for a diversity of applications [13].

2.1.1   Classification

Over the last years, micropumps have been classified in many ways. However, based on the actuation principle (Figure 3), micropumps are often classified broadly into two types [14]:

1. **Non-mechanical pumps** or dynamic pumps use characteristic fluid properties such as polarizability or electrical conductivity to generate flow.

2. **Mechanical pumps** or displacement pumps are systems where mechanical energy is transferred to the fluid in the form of one or more moving elements.

The non-mechanical micropumps directly interact within the working fluid through electrical-, chemical-, or magnetic means. Hence, no moving parts are needed and simple microstructures are possible. A few examples of non-mechanical micropumps are electrohydrodynamic-, magnetohydrodynamic-, electroosmotic-, electrochemical- and acoustic streaming pumps [13].

In comparison, the mechanical (displacement type) micropumps require a physical actuator to drive pulsating fluid flow due to periodic moving mechanical parts like an oscillating diaphragm or a rotor that applies pressure. Furthermore, displacement pumps can be

categorized into the reciprocating type, which means either an oscillating diaphragm or a reciprocating piston. In addition, the rotary type comprising gears or vanes also falls into this category. The rotary pump principle, in which the fluid demand is created, e.g. by rotating blade movements, has a negative effect due to unfavourable friction effects in the microscopic range. In conclusion they are therefore only rarely used. As shown in Figure 3,
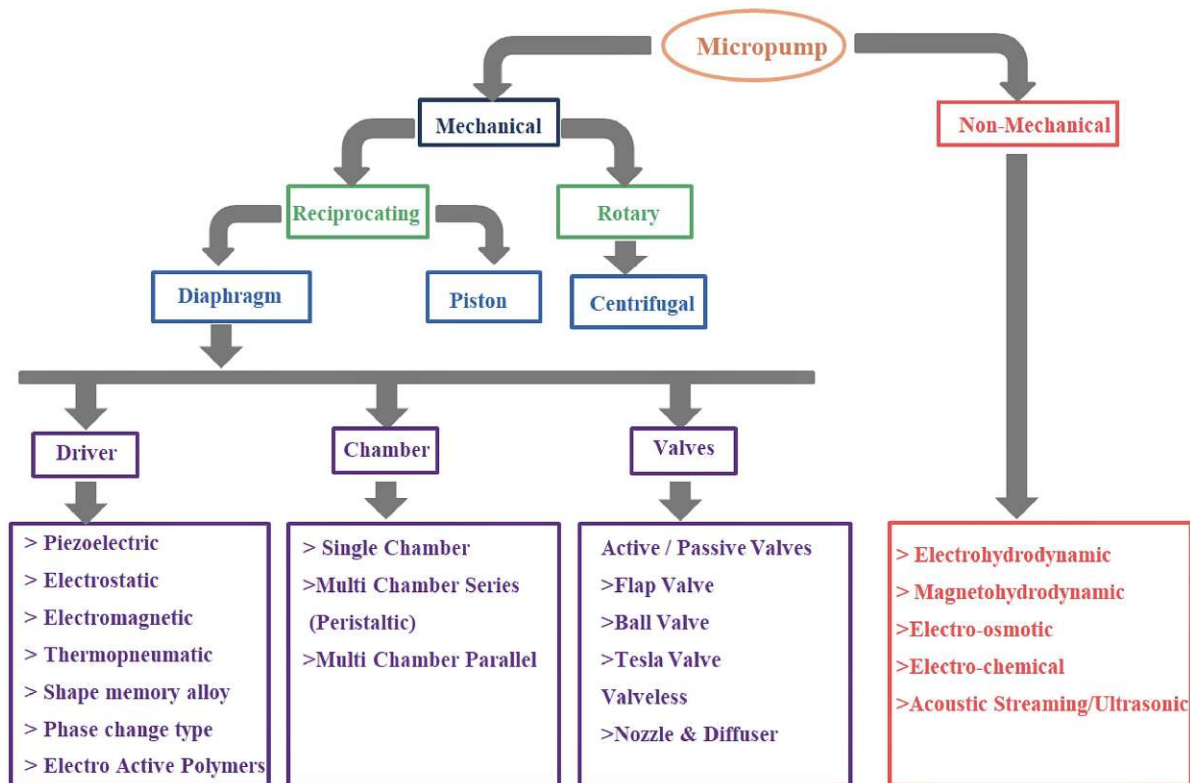
Figure 3: Classification of micropumps [13, S. 36]

the outcome parameters of a mechanical micropump depends strongly on the variation of the driven actuator principle, the number of chambers and the used valves. A few examples of mechanical pumps are piezoelectrically -, electrostatic -, electromagnetic -, thermopneumatic, electrostatically actuated micropumps [13]. Also, the type of chamber with single-, multi-series- and the multi parallel chambers is a crucial factor in order of the valve function [15]. The goal hereby is always to maximize the flow rate by supplying more energy. Apart from the driving principle and the chamber, the last component to complete a working mechanical micropump is the valves mainly classified into active- and passive valves.

Fraunhofer EMFT is researching micropumps elsewhere in the area of medical technologies for many years and has formed a product portfolio of silicon, stainless steel, and titanium

diaphragm micropumps. In the following Table 1, all technical parameters of the Fraunhofer EMFT piezoelectrical diaphragm pumps are listed.

Table 1: Overview of technical micropump parameters of the product portfolio at Fraunhofer EMFT [16]

Micropump types	Unit	µP015v1	µP024Av2	µP026v1	µP303	µP304
Material		silicon	silicon	silicon	steel	steel
Weight pump chip	g	0.07	0.06	0.03	13	5
Size pump chip	mm^3	7x7x0.8	7x7x0.7	7x7x0.6	OD=30,t=2	OD=20,t=2
Operation voltage +	V	285	150	60	300	240
Operation voltage -	V	-70	-60	-20	-80	-60
Stroke volume	nl	80	140	50	20000	6000
Back pressure air	kPa	90	60	30	20	25
Suction pressure air	kPa	-50	-50	-20	-20	-20
Blocking pressure water	kPa	550	140	80	31	75
Max. pump rate air	µl/min	500	1000	300	200000	50000
Max. pump rate water	µl/min	150	300	60	80000	16000

This paperwork focuses on the mechanical piezoelectrical driven stainless steel diaphragm micropump, type µP304) (see Table 1), developed by Fraunhofer EMFT. The mechanical micropump provides relatively high flow rates compared to smaller pumps like the silicon one.

2.1.2 Piezoelectrical displacement micropump

The stainless steel diaphragm micropumps (µP304), by Fraunhofer EMFT, can generate a high flow rate on the scale of microfluidics. The generated flow rates are up to 50 ml/min in air and up to 16 ml/min in water (Figure 4). Metal pumps are more suitable for larger dosage volumes, for example, infusion systems, tumour- or wound therapy or active implants [11, 17]. Furthermore, Lab-on-Chip-Systems, cell culturing, and tissue engineering could be promising approaches [18].

Figure 4: Types of stainless steel micropumps (µP303 and µP304) [17]

The main elements of the micropump are the diaphragm with the piezoelectric actuator (1), two valve foils (2, 3) for inlet and outlet, and the pump body (4). The different layers are welded together as depicted in Figure 5.
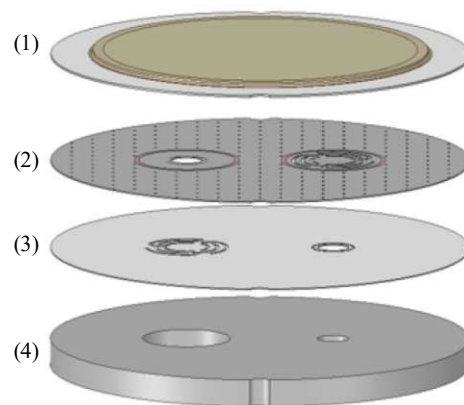
Figure 5: Components of the stainless steel piezoelectrical diaphragm micropump of Fraunhofer EMFT: (1) piezoelectrical actuator, (2, 3) valve foils, (4) pump body

The base body, the pump chamber diaphragm and the two valve foils are connected by laser beam welding. The piezoelectric bending transducer is applied to the diaphragm by adhesive bonding and pre-stressed during the adhesive curing phase. A convex pre-curvature of the pump chamber is created. The thickness of the adhesive layer is approximately a few micrometres. The flexible membrane is positioned above the main pump valve foil, centred between the inlet and outlet valves. The space between the bottom side of the membrane and the top side of the valve chips forms a pump chamber [5].

Working principle

The most common form of mechanical micropumps is displacement pumps [19]. In general, the diaphragm displacement pump design consists of three components (see Figure 6(a)):

1. **Pump chamber** which is filled with the applicable fluid during pumping action.

2. **Actuator** for actuating the pumping action.

3. **Flow rectification components** like either passive or active valves or simply two nozzles for controlling the in- and outlet flow in one direction.

The actuator converts electrical signals into an up-and downward movement of the diaphragm. This periodic volume change of the pump chamber causes alternating negative and positive pressures. The fluid is sucked in through the inlet valve by the negative pressure in the chamber (see Figure 6(b)) and forced through the outlet valve by the subsequent overpressure (see Figure 6(c)) [5, 13]. Another important parameter considering the flow rectification component is the cracking pressure which is the minimum differential upstream pressure between inlet and outlet at which the valve will operate.
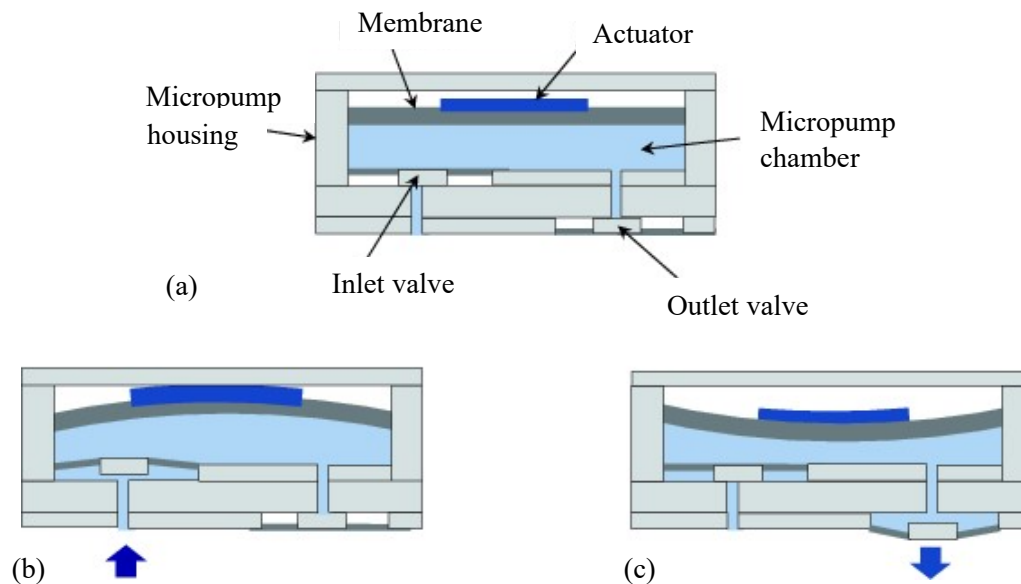
Figure 6: Principle of membrane actuation for micropumps (a) Membrane in the initial flat configuration, (b) membrane bowing upwards during the suction stroke, (c) membrane bowing downwards during the discharge stroke [14, S. 1079]

Piezoelectrical actuation An actuator is a device that converts a specific form of energy into another one, mainly into some kind of motion. The provided external driving force is then used for driving the fluid inter alia in microfluidic systems.

In a piezoelectrically driven actuator, the basinal principle converts electrical energy into mechanical energy using the inverse piezoelectric effect. The piezoeffect describes the phenomenon that pressure shifts electrical charges in various crystals such as quartz and tourmaline. Furthermore, electric fields have the ability to deform piezoelectric materials. This effect is called the "inverse piezoelectric effect". Especially polycrystalline ferroelectric ceramics such as barium titanate (BaTiO) and lead zirconate titanate (PZT) show higher deflections and induce larger electric voltages, respectively [20].

MEMS with piezoelectric actuator principle has been designed for various applications and are often found in the literature [15, 21–25]. In the course of this diploma thesis, a diaphragm micropump with the actuation principle explained above is also used. This pump is made out of stainless steel and, due to its material properties, can be used, among other applications, for high precision drug injection and active hydraulic implants are in the high flow range [20]. Stiffer materials like stainless steel, copper, silicon, etc., offer higher force and faster response and enable high flow generation [18].

Apart from the actuator principle, the two valves are susceptible components to meet the requirements of the micropumps. Moreover, the focus of this diploma thesis is on microvalves, and consequently, this topic will be discussed in more detailed as follows.

2.2 Microvalves

Microvalves form the foundation of various microfluidic systems. The component enables fluid manipulation by selectively allowing or hindering fluid flow. Microvalves control routing, timing and regulates the flow between two fluidic ports and are mandatory components of the micropump [26]. Due to a variety of different valves, the first step is the classification of microvalves.

2.2.1 Classification

Many different valve types have been developed over the last few years, and a possible collection is shown Figure 7. A commonly used classification scheme for microvalves is the

separation into active- and passive microvalves. While active valves are actively controlled and regulated by utilizing an additional external energy source, passive valves are influenced exclusively by the system's intrinsic elements.

In general, active valves can be separated into mechanical, non-mechanical systems, while passive microvalves are separated into mechanical valves (check valves) and non-mechanical (valveless) valves. Non-mechanical microvalves take advantage of fluid properties to regulate fluid flow without moving parts. In comparison, mechanical microvalves are characterised by their movable parts, which regulate the flow by changing position. By the aim of external systems like pneumatic means or built-in modular, external active microvalves can be actuated. Active microvalves can be subdivided according to the present switching behaviour into normally open (NO), normally closed (NC). NO valves are in an open position when inactive, while NC valves are in a closed position. When energy is supplied, NO valves are closed, and NC valves are opened. Hence, depending on the valve type, fluid flow or interruption is established. Both NO and NC valves require constant energy to achieve the change of the initial position.

Non-mechanical microvalves take advantage of fluid properties to regulate fluid flow. Moreover, passive non-mechanical microvalves, also known as the "valveless" type, enable flow by the interaction of geometry and fluidic. The passive flow is realized in a diffuser, abrupt, liquid triggered, burst and hydrophobic valves.

Analogue to the micropumps, active mechanical microvalves can be directly triggered by magnetic-, electric-, piezoelectric-,thermal-, bistable- or other actuation methods. For bistable valves, only energy pulses for the transition between the states to switch is necessary.

Passive mechanical valves are mostly incorporated in reciprocal displacement micropumps. They can be briefly be categorized into flaps, membranes, balls or mobile structures, which are all suitable as the moving parts of the micropump. The valves just open because of forwarding pressure, and a diode like characteristic can be observed. Because no direct energy is required for the one-way valve behaviour, no further energy source than the actuation energy of the actuator is necessary and makes the passive mechanical valve very suitable for small-sized and low weight consuming micropumps. These properties make the passive mechanical microvalves very suitable for reciprocal displacement pumps.

The Fraunhofer EMFT uses a passive ortho-planar check valve design (see Figure 8) in the combination of the piezoelectrical diaphragm micropump out of stainless steel. The combination of check valves and piezoelectric micropumps can achieve high output flow and

Categories			
Active	Mechanical	Magnetic	External magnetic fields
			Integrated magnetic inductors
		Electric	Electrostatic
			Electrokinetic
		Piezoelectric	
		Thermal	Bimetallic
			Thermopneumatic
			Shape memory alloy
		Bistable	
	Non-mechanical	Electrochemical	
		Phase change	Hydrogel
			Sol–gel
			Paraffin
		Rheological	Electro-rheological
			Ferrofluids
	External	Modular	Built-in
			Rotary
		Pneumatic	Membrane
			In-line
Passive	Mechanical	Check valve	Flap
			Membrane
			Ball
			In-line mobile structure
	Non-mechanical		Diffuser
		Capillary	Abrupt
			Liquid triggered
			Burst
			Hydrophobic valve

Figure 7: valve characterisation [26, S. 15]

high back pressure [27]. Since the valve disc moves parallel to its surface, the behaviour of the valve displacement is straightforward. When pushing on the central disc in a perpendicular direction to the plate, the valve arms or beams bend and apply a spring force to the central disc [28].

Figure 8: ortho-planar spring valve
by Fraunhofer EMFT

Two identical foil structures are superimposed to form the two valves (intake and exhaust valve), with the upper foil rotated 180 relatives to the lower foil. The micro structuring of the two valve foils can be seen in Figure 8, where the left structure functions as a valve cover and the right structure as a valve seat. When the valve foils are placed, the two complementary structures, valve cover and valve hole are superimposed and aligned with corresponding blocking direction at the inlets and outlets.

Some parameters are relevant for the typical spring valve behaviour.

2.2.2   Passive diaphragm check valves

Passive membrane or diaphragm check valves can be generally categorized into bridges, holes, or bumps membranes [26]. Bridge type valves [26], also known as wheel check valves, [29] consist of a fixed ring, valve arms (beams), and valve plate. Springs were a platform movably coupled to a base. Being movable linearly with respect to the base along at least a portion of an axial direction perpendicular to both a base surface and a platform surface are called ortho-planar springs [28, 30]. The ortho-planar valves have a compact flat design requiring little space and are also easy to fabricate. Ortho-planar mechanisms means the mechanisms with links, that can be simultaneously located in a plane with motion out of that plane [31] .The advantage of the ortho-planar design is the stable parallel out-of-plane deflection and has shown good sealing characteristics [30]. The passive membrane (diaphragm) bridge type check valve (see Figure 9) is often used to achieve large movable distances [24, 27, 32–38]. The check valves are a susceptible component, so that leakage of the valves reduces back

pressure and the pumping rate of the micropump [20, 26, 39].

(a) (b) (c)

valve arm   fixed ring   valve plate
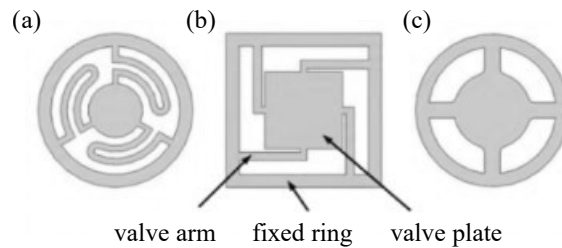
Figure 9: (a) crank arm wheeled check valves (b) parallel straight arm wheeled check valve (c) intersecting straight arm wheeled check valve [40, S. 5]

Another classification criteria are the valve arm geometry and can be separated into crank arm and straight arms. The straight arm wheel valves are further divided into intersecting and parallel types (see Figure 9).

In general, the working principles of check valves are similar to the diodes in the electrical circuit. They provide only a small fluidic resistance in the forward flow direction, and in the opposite direction, it does not allow fluid to pass through [29, 41]. However, low forward flow resistance, large operational reverse pressure and negligible leakage are critical common performances of most of these micro check valves. Also, the frequency response of the microvalves plays a significant role where a high-frequency response is expected [33]. Most ortho-planar diaphragm check valves are made out of stainless steel, beryllium bronze, silicon, and PET [40]. Wheeled check valves are usually moulded by laser cutting and nickel electroforming process [29].

Assumptions on ortho-planar microvalves

To be able to interpret the valve behaviour further, spring models based on the geometry and assumptions regarding the ortho-planar valves are outlined. In the case of a very simplified model of the valve, it can be assumed that the valve cover deflection only runs parallel to the plane and that the central disk is non-formable. The curved beams can be simplified as straight segments within a simple straight beam attached at one end and guided at the other. In addition, it is presumed

Figure 10: Simplified Straight bar model [42]

that all the force is applied at one point, the central disc, and is evenly distributed over each valve arm. The so-called straight bar model is illustrated in Figure 10 [42]. Inspired by the

described so-called straight bar model, a few various constants for the valve design and the valve behaviour are defined as follows [42, 43]:

l = Beam length

j = Number of arms

h = Beam height

b = Beam width

F = Vertical force on one arm

E = Young's modulus

I = Moment of inertia

Following expressions considering the deflection (z) and the stiffness (k_s):

$$F = \frac{F_{total}}{j} \quad \text{and} \quad I = \frac{bh^3}{12} \tag{1}$$

with

$$k_s = \frac{12EI}{l^3} \tag{2}$$

The total spring stiffness is expressed as:

$$k_{total} = j \cdot k_s \tag{3}$$

In summary, a smaller number of arms means a lower spring constant. Still, also rotation around the suspension axis is more likely, and unexpected displacement of the central disc could appear. For example, a valve design with one or two folded beams could have spring constants 20 times lower than that of the four beams.

In more complex analytical models, the valve arms are no longer represented as rigid beams, instead the curves of the valve arms and their torsion are integrated into the calculations. Therefore the ortho-planar valve is divided into a different sections within their beam arms. Such a procedure for the model formation of ortho-planar valves is presented in some papers and can be looked up under the references below [30, 42, 44]. Due to the complexity of the valve shape, FEM simulations are often used to determine the spring stiffness [21].

In general, the spring stiffness plays a major role in the fluid flow into the micropump

chamber. It is necessary to find the spring stiffness to determine the deflection of the valve and net flow into the pump chamber. Furthermore, general practical limitations in the use of this type of valve should be mentioned.

1. **Low stiffness:** within low stiffness, the spider spring gives a large opening area.

2. **Low fluid resistance:** the injection substance has to pass through the spring cuttings

3. **Spring symmetry:** the central disc of the spring should stay parallel to the fixed outer disc.

However, not only the geometry of the valve influences the behaviour of the valves, but also the welding radius around it.

Welding radius of the metal foils
The goal of laser welding of the metal foils is always to closely connect between elements. With regard to the valves, the two valve foils should be attached to each other. Through an optical measuring method (profilometer), a 3D image of the valves can be created, and an optical inspection is possible. The foils' distortion can be detected in the form of an initial valve gap are visualised in Figure 11. In the optimum case, no valve gap appears. It can be
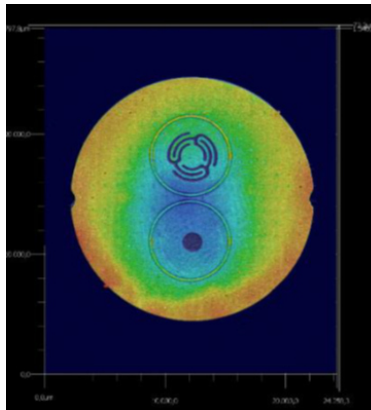
Figure 11: Optical measurement of the film distortion on the complete pump

assumed that the valves with a narrower weld radius have a much stronger pre-load, and an increase of the gaps appears in comparison to valves within a larger welding radius.

Further explanations for the initial gap are necessary and discussed below.

Initial gap

 In addition, unavoidable small backflows through the closed valve counteract the desired result of fluid delivery and thus reduce the pumping performance. For a more detailed understanding of the behaviour of the ortho-planar spider spring valve, the following paragraph describes the operation using sketches showing the valve in cross-section (see Figure 12).

The valve cover always overlaps the valve seat to such an extent that it is located centrally above a fine recessed channel of the valve seat. The valve cover is connected to the outer platform by the valve arms (= spring elements), and the opening mechanism can be seen in Figure 12(a). The gap height between the valve cover and the valve seat is usually zero and limits or prevents the flow at low pressures.

By exerting pressure on the valve plate through the fluidic volume flow, the valve is opened if a higher pressure appears than spring force due to the stiffness of the valve beams. The central disc moves upwards, and the fluid flows due to the valve clefs. Due to the installation or manufacturing processes of the very thin diaphragm microvalves, it is possible to create an undesirable initial gap due to tensions on the spring beams, which curve as a result upwards. In this case, the gap between the valve seat and the valve cover is not zero at low pressures. This allows the flow to move against the desired flow direction and is further referred to as the initial gap (see Figure 12(b)). Also, high-pressure leakage is possible. This phenomenon occurs at high pressures and without any gap between the valve seat and cover and can happen due to plastic deformation (see Figure 12(c)). Due to the manufacturing process, the existing pre-bending of the valve arms means that the cover is already slightly raised in the initial position. To close this initial gap, the spring stiffness
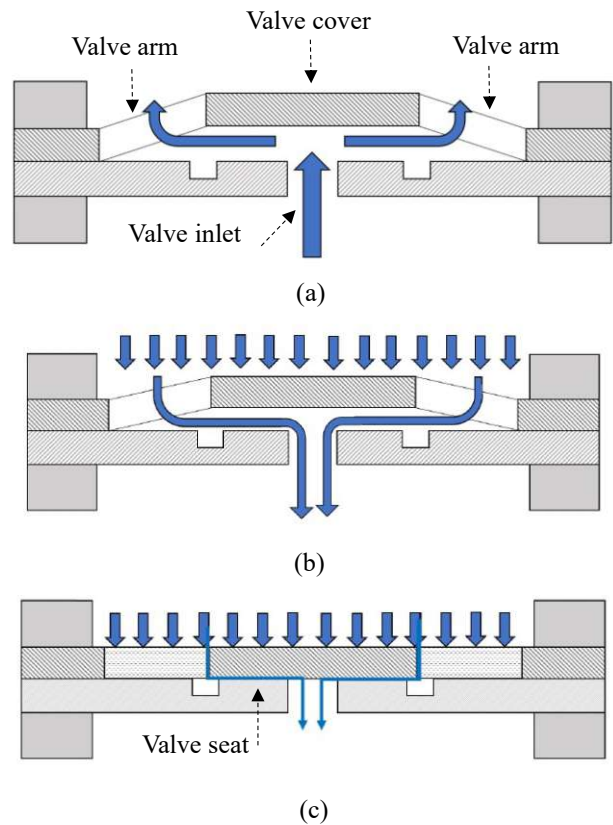
Figure 12: (a) Flow of the fluid by lifting the valve cover (b) Initial gap leakage rate due to existing gap between valve cover and valve seat at low pressures (c) High pressure leakage rate in closed condition at high pressures [45, S. 20–21]

must be overcome in the negative z-direction. After all mechanical design considerations about ortho-planar diaphragm check valves are given, methods for validation and characterisation of the microvalves in fluidic systems are discussed in the following section.

2.3 Methods for valve characterisation with different media

The high fluidic resistance of the valves is a limiting factor for the flow rate. In addition, unavoidable small jerk flows through the closed valve work against the desired result of fluid delivery and thus reduce the pumping performance. High flow optimisation of the valve characteristics is therefore essential. For this purpose, it is necessary to precisely understand the effects of individual valve parameters, for example, on the flow and leakage rate.

Different techniques have been used for analysing and optimizing valve parameters in the literature, but most of the experiments focus on air. Especially for medical applications, it is obligatory to analyse the fluid behaviour with liquids because many medical applications deal with liquids such as drugs.

Literature review: All reviewed methods of characterisation of passive check microvalves and their optimisation principles can be categorized first in the medium used for the experimental characterisation of valve performance. In this context, air [27, 33, 34, 38], nitrogen gas, DI-water [32, 33, 35, 46, 47] and methanol [32, 48] can be found in the literature. Methanol is used to minimize the bubble generation and maximize the measurements' accuracy with fluids.

After separating the specific medium, valve characterisation has been simulated by analytical simulations [34, 35, 38, 49–51] or experimentally tested by flow measurements [34, 38, 46, 48, 49]. Interesting parameters are the flow rate, reserve fluid flow (leakage), and the deflection of the valves. Often the actuator was also considered when testing the performance of the valve, which makes sense in the content of the working principle but extends influences while measuring. This work focuses on the experimental methods to analyse flow characteristics in passive microvalves.

For getting an overview of all performed methods for valve characterisation within different mediums, the specific parameters are listed Table 3.

Table 3: Experimental methods for check valve characterisation,

Ref.	Parameter	Experiment explanation	Medium
[38]	Flow rate	The flow rate was measured by soap-film flow-meter and the output pressure through a U-type pressure gauge. Different check valves were tested on the actuators, and the performance of the proposed piezoelectric pump was done. The fluid behaviour was calculated based on Poiseuille's law.	Air
[36]	Flow rate	The test characterisation was performed by a specifically designed valve holder while different pressures were applied. The measured flow rate is proportional to the pressure differences applied, and also durability tests have been made.	DI- water
[33]	Frequency	A polytec doppler vibrometer was used to measure frequency response, and a laser beam was focusing on the top of the valve flap. A plumbed zirconate titanate (PZT) ceramic plate was employed to excite the valve into vibration mounted on a large stainless-steel base block with the microvalve on top, and increasing frequencies were applied (up to 100kHz). The first modal frequency of the valve obviously occurs at 17.7 kHz.	Air
[33]	Deflection	The valve deflection was measured indirectly (not with fluid) through a dc motor, and a linear PZT actuator was combined. A force transducer is attached to the PZT actuator. The force sensor tip was attached to the flap membrane through the valve orifice, and displacement and force are gained through the data acquisition board.	Air
[33]	Flow rate	For flow measurements, the microvalve was mounted in a package with inlet and outlet ports, and a maximum water flow rate of 35.6 ml/ min was measured at a pressure difference of 65.5 kPa.	DI- water

Ref.	Parameter	Experiment explanation	Medium
[34]	Flow rate	First, an ANSYS simulation is made with a relatively low youth modulus. Here, the valve disc moves parallel to its surface, and the behaviour of the valve displacement behaviour is straightforward, and a linear model with a constant stiffness is assumed. For characterisation, a large water reservoir with variable surface heights was used to justify the pressure across the microvalve. The water reservoir was at the same height for each measurement to generate constant inlet pressure and was measured with a pressure sensor. By determining the velocity of DI-water or air in the outlet tube, the flow rated was given.	DI-water Air
[34]	Backflow	Backward pressure was applied to measure the leakage out of the reverse flow.	DI-water/ Air
[35]	Flow rate	The pressure droplet with DI across the valve was measured in a capillary with known diameter and gave information about the flow rate. Again, a large reservoir of water with different heights emulates the inlet pressure during the measurements.	DI-water
[32]	Backflow	For forward and reserve fluid flow characteristics, a burred is used as a liquid supply reservoir. The pressure transducer, which produces a DC output proportional to the pressure at the reservoir base, is used to determine the height of liquid in the column.	Methanol/ DI-water

Ref.	Parameter	Experiment explanation	Medium
[32]	Deflection	For deflection measurements, the nitrogen gas flows through the microvalve controlled using a mass flow controller and pressure transducer. The pressure transducer is used for logging the corresponding pressure at the valve inlet. The valve plate deflection changes were measured at the centre of the valve using a 4 mg stylus. (Surface metrology is the measurement of small-scale features on surfaces). The calculated deflection should be proportional to the pressure to the power of $1/3$, and the initial deflection of the valves argues the differences through the measurements. The gas flow characteristics differ from the fluid characteristics because gas behaves as compressible, whereas liquids are incompressible.	Nitrogen gas
[46]	Flow rate	For characterisation, an experimental setup, as usual, an air compressor, pressure-controlled liquid reservoir, a fixture holding for the microfluidic structure and a waste reservoir with electronic balance was used. The balance measured the outflow of the DI water under certain pressure applied, and the DI water mass changes for one minute were calculated.	DI-water
[27]	Deflection	For displacement measurements, a Kean LK2000 laser micrometre was used. It is considered that the total opening displacement of the valve is separated into the opening displacement of the check valve caused by inertial force(X_i), and (X_p) is the opening displacement of the check valve caused by pressure difference. The study on the check valve opening, which is driven by the inertial force provided by the vibration of the piezoelectric vibrator and a special setup	Air

Ref.	Parameter	Experiment explanation	Medium
[27]	Flow rate	Electronic soap film flowmeter (GL-103B electronic soap film flow meter) used to measure the output flow of piezoelectric micropump under the conditions of no-load and output flow can be directly digital read. The output pressure of the piezoelectric micropump can be measured using a U-type pressure gauge. The pressure force was eliminated using a special measurement setup with two laser micrometres, a data acquisition system, a driving power supply, a check valve, a piezoelectric vibrator, and a fixed bracket.	Air
[52]	Displacement	A PI P-603.3S2 piezoelectric actuator is controlled in feedback with an integrated strain gauge displacement sensor. The force applied to the microvalve is measured with a Futek LSM250 load cell at 10.00V supply voltage and is transferred to the valve plate through a stiff glass needle	Air
[52]	Flow rate	For fluidic measurements, a Bronkhorst P-602CV pressure controller is used to control a dry nitrogen gas flow through the valve, which is subsequently measured using a Bronkhorst F-111B gas mass flow meter	Air
[53]	Displacement	A PI P-603.3S2 piezoelectric actuator is controlled in feedback with an integrated strain gauge displacement sensor. The force applied to the microvalve is measured with a Futek LSM250 load cell at 10.00V supply voltage and is transferred to the valve plate through a stiff glass needle	Air
[52]	Flow rate	For fluidic measurements, a Bronkhorst P-602CV pressure controller is used to control a dry nitrogen gas flow through the valve, which is subsequently measured using a Bronkhorst F-111B gas mass flow meter	Air

Conclusion: The reviewed papers show a lack of measurements with liquid as medium and deflection of microvalves. A bridge check valve allows a one-way flow of air and liquid between two points in the microfluidic process. In particular, changes in deflection are challenging to measure with different, forward fluid pressures.The gas flow characteristics differ from the fluid characteristics and will be explained in more detail in chapter three. No measurement has been found containing the valve deflection with liquids.

For actuators, the deflection is always measured by optical measurements: MTI- 2100 fiber-optic measurement [24], laser vibrometer (Polytec) [48], force microscope (AFM) [54] and Laser Displacement Sensor [47]. This is easily possible due to a closed system and measuring on top of the micropump. For measuring the valve deflection in the centre of the microvalve by an optical measurement, a closed system is an obstacle.

In addition, for the characterisation of check valves, special clamping fixtures for the valve foils are used in the literature [27, 45, 46, 51, 55]. These fixings introduce the risk of plastic deformation to the valves, and the results may be biased. In this context, a characterisation system must be found that avoids external forces on the valve.

For a more detailed understanding of the valve behaviour, a new measurement setup needs to be developed. The next step is to establish a measurement system for valve deflection, which can be found in chapter three.

3   Characterisation of valves with medium gas and liquid

Chapter three is presenting the characterisation methods with gas (air) and liquid (DI-water). Therefore, the fluid system and the valve deflection within the differences between air and liquid as a medium are explained analytically. The analytical part includes an explanation of the analogy between electronic and flow properties. Moreover, the characteristics of the used media are explained, and an insight into the system's characteristics of the following measurements is given. After these considerations are done, the experimental implementation follows. All necessary considerations to fulfill the task of an experimental characterisation for a passive check valve are explained within the experimental part. This section includes the sample preparation, a simplified network model of the check valves, the calibration of the measurement setup and the material, and methods of the measurement setups.

3.1   Analytical system description

In this section, the passive check vales are first examined from the analytical side. This acquired knowledge is intended to assist in analysing and interpreting the measurements carried out afterwards.

3.1.1   The analogy between electronics and fluidic

To characterise the passive check valves, it is first important to understand their functional principle. For this purpose, the analogy between electronics and flow properties is used. Thus, the electronic properties of components can be converted into microfluidics characteristics. The basic analogizes listed Table 4 below. In the characteristic line of a diode (check valve), the microfluidic variables are shown in parentheses [56].

<div align="center">

Table 4: Basic electrical-microfluidic analogy [56]

Electrical varibale	microfluidic variable
Voltage (v)	Pressure (p)
Current (i)	Flow rate (q)
Charge (q)	Volume (V)
Energy = v·q	Energy= p·V
Power = v ·i	Power= p ·Q

</div>

The electronics are derived from a wide range of components with specific transmission

characteristics. The fundamental principle of an electronic diode consists of allowing electric current to flow in one direction but not in the opposite. As already mentioned (see section 2.2.2), the microfluidic device which is most comparable to a check valve is an electronic diode. In the ideal case, this device also permits the fluid flow only in a single direction. The characteristic curves of the electronic and microfluidic diode and of a check valve are the same. In the following Figure 13, this characteristic curve is represented under (a) and (b) is demonstrating the OFF and ON regions of a diode with regard to the behaviour of a valve.
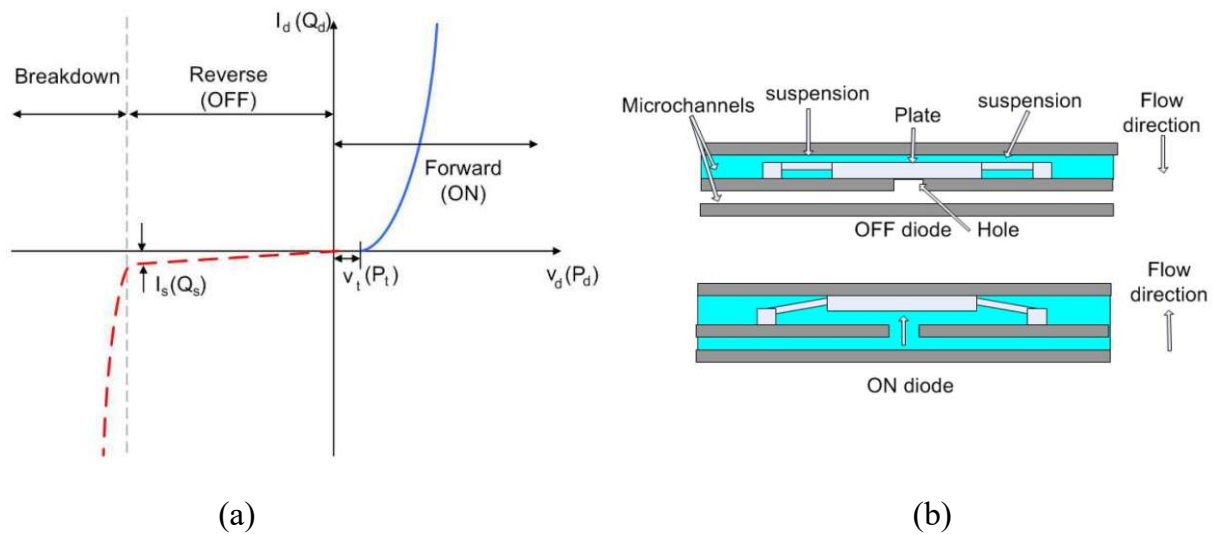
Figure 13: Behaviour of check valves and diodes [57, S. 11]: (a) Plot of a microfluidic and electronic diode (b) Working principle of a check valve

The most important equations relating to Figure 13 (a) are mentioned first, and the microfluidic variables are shown in parentheses [56, 57].

- $i_d(q_d)$ diode current (positive in forward direction)
- $v_d(P_d)$ voltage across the diode (measured from anode to cathode)
- $v_t(P_t)$ forward threshold voltage
- $i_s(q_s)$ reverse bias saturation current (or scale current)

At a certain pressure (P_t), the check valve begins to allow the flow of fluids (q_d). This pressure corresponds to the forward threshold voltage (v_t) in an electronic diode. Above that pressure, an ON state is reached, and the microfluidic diode allows the fluid to flow (forward range). Below this pressure, the diode is in the off-state, and the flow is considered

blocked. Hence, this effect is known as the reverse region. At high reverse voltage, the plate of the check valve breaks due to high backward pressure. This is the equivalent of the avalanche effect of an electronic diode due to a high reverse voltage (breakthrough region). In the so-called breakdown region, the diode begins to conduct in the reverse direction. Moreover, the leakage rate (q_s) of a diode is the equivalent of the reverse leakage (i_s) rate and is the flux between the plate and the hole due to the backward pressure [57, 58].

The exp-function of the diode characteristic makes dealing with the characteristic equation complicated. Therefore, for the practical handling of diodes, an approximation for the forward region is often used.

Electronic components are often operated at a fixed operating point (AP). The circuitry limits the current and voltage of the diode to an environment around the characteristic point $(v_d(P_d); i_d(q_d))$. If the voltage and current spacing around the operating point are sufficiently small, the nonlinear characteristic can be replaced for the calculation by its tangent at the operating point [59].
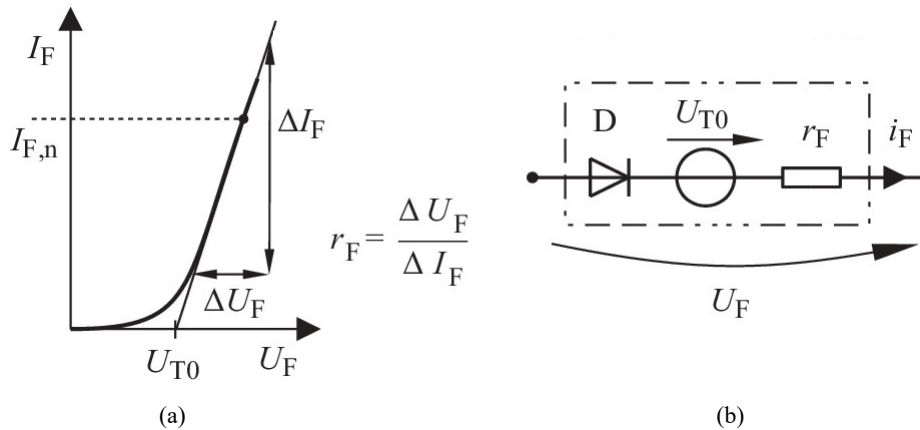
Figure 14: Modelling of a diode: (a) characteristic curve of a diode (ideal valve) in the flow direction with a tangent at the nominal point (b) diode substitute model [59, S. 21]

In the literature, $I_d(q_d)$ and $v_d(p_d)$ are often found as i_f and, v_f indicating the forward range of the diode [59]. As the forward current increases, the plot shows that the value of r_F approaches a constant level, the ohmic path resistance RS. This kink-curve contains only two parameters:

- the differential resistance r_F (slope resistance) and
- the threshold voltage U_{T0} or as mentioned before v_t.

The forward pressure v_t is the threshold at which the check valve opens, and the fluid begins to flow and can be estimated experimentally. The differential resistance (r_f) can be calculated based on experiments.

Compact models as an electric analogy can be used to investigate the interrelationships of individual components in fluidic systems. In the case of micropumps, this has been done in several cases [53, 56, 57, 60, 61]. Marus Herz designed an electrical network model for a silicon micropump with passive check valves (flap-type) [53].
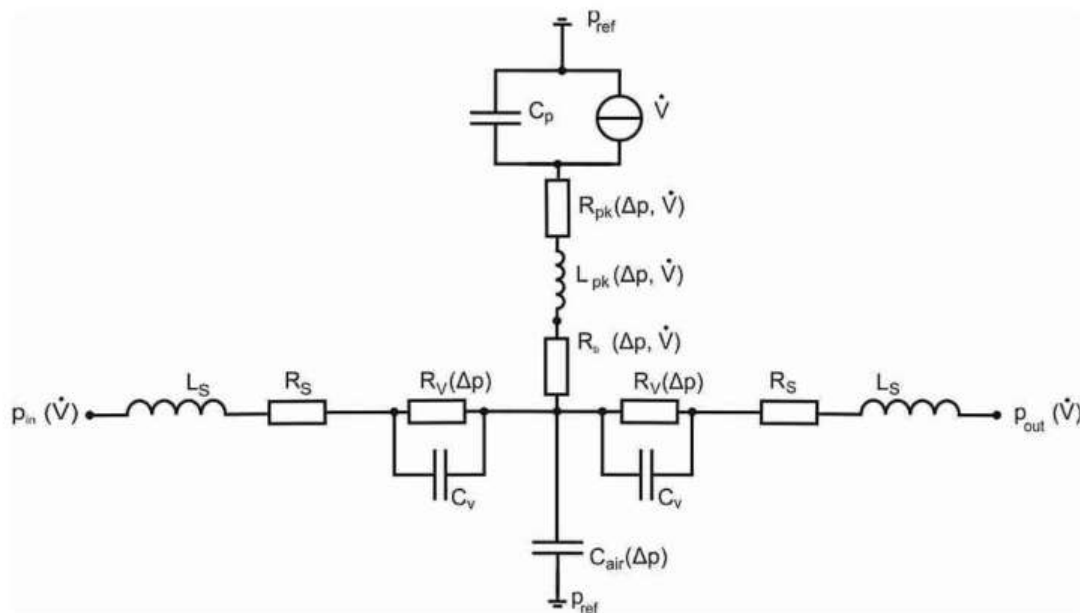
Figure 15: Electrical network model of a micropump [53, S. 82]

In general, coils are used to represent fluidic inductance and resistors are used to represent fluidic resistance. P_{in} applied pressure on the inlet valve, P_{out} is the pressure applied on the outlet valve, The circuit above and below the horizontal series circuit between P_{in} and P_{out}, the pump camper and actuator principle are described.

In fluidic systems, all components have a strong interaction between the surrounding fluid and the moving structure. The design and integration of these moving components into a network is one of the most difficult tasks in pump systems [61]. As mentioned earlier, a valve can be considered as an element with two different linear mechanical impedances in the forward and reverse directions. A basic principle for realizing the two passive check valves is a series connection of two valve resistances that describe the pressure required to open the valve [61]. In the water analogy, capacitors represent movable membranes to describe a damping behaviour through a change in volume (charging and discharging process of the

capacitor) [62].

In the model above (see Figure 15), the capacitor describes the volume displacement through the valve at different valve deflections. The connection between opening resistance R_v and the volume changes depending on the valve deflection x is expressed by a parallel connection of capacitor (C_v) and resistor (R_v). Formulas used in the literature for calculation of the resistance R_v and the capacitor C_v can be found under Appendix A.
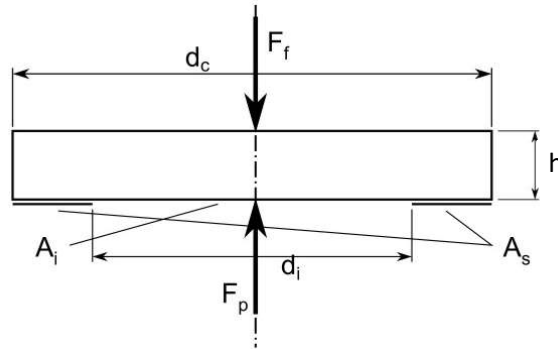
Figure 16: Forces on the central disc [63]

When calculating the capacitor as well as the resistance, the deflection of the valve at applied pressure plays a decisive role. This opening behaviour will be investigated experimentally later on. According to Hook's law, the pressure-dependent deflection of the check valve z can be simplified as follows [21, 63]:

$$z = \frac{(A_i) \cdot (\triangle p)}{k_{total}} \tag{4}$$

where A_i is the surface of the inlet, dp the pressure difference and k_{total} the valve stiffness depending on the sum of valve beams.

Since experimental measurements of the valve behaviour under the influence of water and air will be investigated in the further course, a description of the two media is necessary.

3.1.2 Characteristics of gas and liquid

Fluids are the collective term for liquids and gases. Substances can occur in three states of aggregation, the solid, liquid and gaseous state. The binding forces of the molecules determine the different states of aggregation. While the molecules and atoms of solid substances are firmly bonded in a lattice structure, the particles of liquids can be easily shifted and ex-

changed. In gases, the molecules move freely in the available space. Using the temperature-pressure diagram (see Figure 17), it can be determined into which phases a substance can be divided and the state of aggregation it is, depending on the pressure and temperature [64].
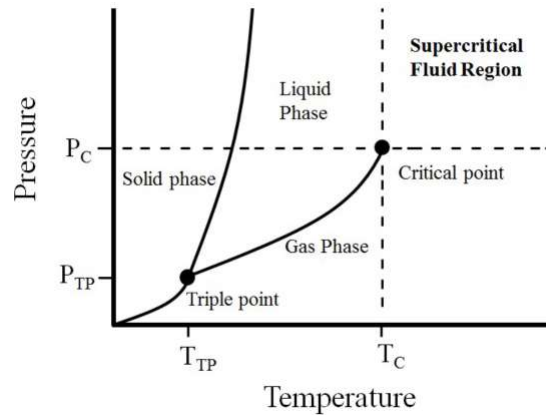
Figure 17: Change of state of matter in the p-T diagram [65, S. 5]

The following properties characterise a fluid [64]:

- It is a continuum.
- At rest, it can only absorb and transmit compressive forces at the surface.

The fluid at rest does not absorb tensile forces nor tangential forces. If the mechanical properties of fluids are also considered (Equation 5), a more detailed consideration of density (ρ) is useful, where the mass (m) is divided by the volume (V). At higher flow velocities or larger Mach numbers (Ma), the compressibility of the gas must be considered.

$$\rho = \frac{m}{V} \tag{5}$$

The density is a function of the pressure and the temperature p=f(p,T) [66, 67].

Incompressible fluids
If the fluid density does not change during a flow process, the fluid is called incompressible (p = constant). Fluids are incompressible at rest near the atmospheric state. The density change Ap/p of gases is still small and negligible even if the gas moves at low velocity with Mach numbers of Ma < 0.25. In this case, the density depends strongly on pressure and temperature, and the following equation is used for ideal gasses [64]:

$$\rho = \frac{p}{R \cdot T} \tag{6}$$

R is the ideal gas constant, p is the pressure in the closed system and T is the temperature in the system. The density is a function of the pressure and the temperature p=f(p,T).

For applied fluid mechanics in the ambient range of the atmospheric state, ideal fluids with constant density can be assumed ($\rho=$ constant), and density changes at low flow velocity (Ma < 0.25) in gases can be neglected and seen as incompressible ($\rho=$ constant) [64].

Compressibility of fluid

The change in density $d\rho$ of liquids at variable to pressure (isotherm) can be determined with the help of the compressibility coefficient (β_T) [64, 67]:

$$\beta_T = \frac{1}{E} \tag{7}$$

where E is Young's modulus. Compressibility describes the change in density or volume due to a change in pressure changes. For liquid flow, it resembles Hook's law:

$$\triangle p = -E \cdot \frac{\triangle V}{V_0} \tag{8}$$

V_0 is the volume at the beginning, and $\triangle V$ changes into volume, considering gas flow. The Boyle-Mariotte Law describes the circumstance that by reducing the volume, the pressure increases for constant temperature [67].

$$\triangle p = -p_0 \cdot \frac{\triangle V}{V_0} \tag{9}$$

There are many analogies between liquids and gases (because of the free displaceability of the particles). The main difference is the compressibility of the two media. However, flowing gases behave practically incompressible at $v \ll v_{soundvelocity}$ (Ma<0.25), i.e. there is no build-up of pressure waves [64].

Dynamic viscosity

The dynamic viscosity (η) connects the shear stress (τ) with the gradient perpendicular to the direction of movement dc/dn (=shear of the fluid) [64, 67]:

$$\tau = \eta \cdot \frac{\triangle v}{\triangle n} \tag{10}$$

The rate of change of shape of the fluid $\triangle c/\triangle n$ represents the displacement of the fluid layers relative to each other as the molecules move. It is the velocity gradient normal to the skin flow direction.

In simplified terms, all gases and fluids can be described as Newton's fluids and do not have tangential stress in their resting state. They are called Newtonian. They have a constant dynamic viscosity η, and the tangential stress is linear to the strain rate $\triangle c/\triangle n$.

The viscosities of water and air depend strongly on temperature but only slightly on pressure.

- Liquids: Viscosities become smaller with increasing temperature.
- Gases: Viscosities increase with increasing temperature.

In summary, all relevant parameters for the media air and water can now be collected in the Table 5.

Table 5: Relevant parameters considering medium water and air [64, 67]

	Parameter	Unit	Water	Air
Density p= 101.33 kPa at 20°C	ρ	[kg/m^3]	998.3	1.204
Young's modulus (isotherm)	E	[N/m^2]	$2 \cdot 10^9$	$1\text{-}1.4 \cdot 10^5$
Dynamic viscosity p= 101.33 kPa at 20°C	η	[Pa s]	$10.02 \cdot 10^{-4}$	$18.93 \cdot 10^{-4}$

Now all the essential properties of liquids and gases have been dealt with, the analytical difference between dynamic and static systems will now be discussed. Static and dynamic system behaviour will also be determined experimentally in the further course.

3.1.3 System characteristics

In this thesis, two kinds of systems are considered for valve characterisation: quasi-static measurements and dynamic measurements. Both will be explained as followed.

Quasi-stationary systems

If a physical process is carried out so that it can be considered exclusively as a sequence of equilibrium states, this process is called quasi-static or quasi-stationary. Therefore, the time scale on which a quasi-static process occurs must be much slower than when equilibrium is established (the relaxation time).Therefore, in terms of fluid mechanics, the same averaged flow state is present at any point in time as in steady-state flows.

A static system is characterised by the fact that each output value $y(t)$ always depends exclusively on the input value $x(t)$ present at the same time t.
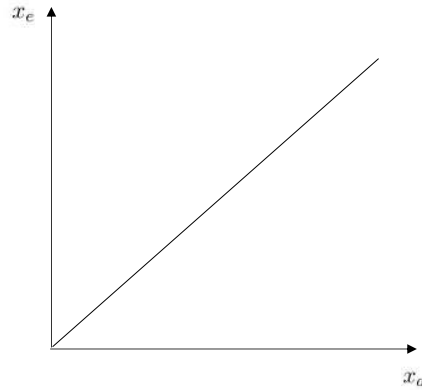
Figure 18: Example for static system behaviour

The behaviour of a static system (see Equation 11) can be described as follows, where x_e is the input signal, and x_a is the output signal:

$$x_e = f(x_a) \tag{11}$$

The function of an output variable from the input variable is referred to as a static characteristic curve.

Dynamic system

The relationship between the output and input signal is considered as a function of time (t). The dynamic transmission behaviour of a system describes the dependence of the output signal $x_a(t)$ on the input signal $x_e(t)$ when the system is at rest at time $t = t_0$. As shown in Figure 19 the reaction of the output variable $x_a(t)$ to a test signal $x_e(t)$ is recorded. It is shown how the output variable $x_a(t)$ of the system behaves if the input variable $x_e(t)$is increased abruptly at the time $t = t_0$ [68].The static behaviour between input signal x_e and output signal is described in Equation 12 as follows:

$$x_e(t) = f(x_a(t)) \tag{12}$$

The system performs oscillations and settles (due to damping) to a constant value, the steady-state.
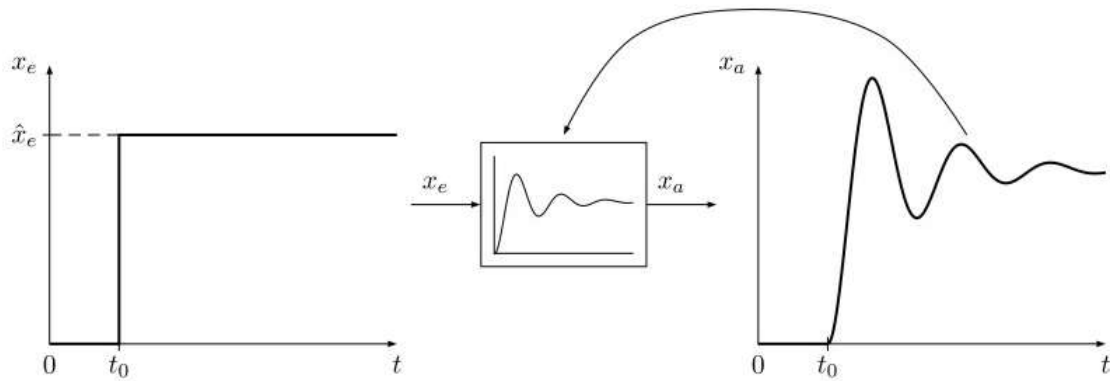
Figure 19: Example of the behaviour of a dynamic system in the event of an abrupt change in the input variable (qualitative progression) [68, S. 22]

The input/output behaviour of linear dynamic systems can always be described by a general linear differential equation (Equation 13) of n-th order with constant (time-invariant) coefficients:

$$a_n x_a^{(n)} + a_{n-1} x_a^{n-1} + ... + a_2 \ddot{x}_a + a_1 \dot{x}_a + a_0 x_a(t) = b_0 x_e(t) + b_1 \dot{x}_e + ... + b_q x_e^{(q)} \qquad (13)$$

Here, n corresponds to the highest derivative of the output variable $xa(t)$, ai and b_i are constant coefficients.

At the end of this paragraph, all important properties of the valve behaviour, the difference between the media, and the possible system behaviour of measurements are now determined analytically. These descriptions enable an experimental procedure to determine the valve characteristics.

3.2   Experimental characterisation

Now that the analytical prerequisites for the characterisation of passive check valves are formed, the next paragraph deals with the used experimental measurements to determine the valve behaviour in air and water. First of all, the principles of the measurement of the used sensors and systems are described. Subsequently, the variations of used valves and their preparation for the newly developed measurement method is presented. In the following, the calibration of this measurement setup for the valve deflection with water and air is validated due to calculation and measurements. At the end of this paragraph, all

materials and methods for all measurements for characterisation of the passive check valves are demonstrated.

3.2.1 Principles of the main measurement equipment

The laboratory provided by Fraunhofer EMFT was used for the experimental characterisation of ortho-planar valves. The measuring devices will be presented in the following. The measurements took place under cleanroom conditions.

Profilometer
Optical measuring methods as non-contact and non-destructive analysis and testing methods open up interesting possibilities. They can be used on reflect materials and are also suitable for sensitive surfaces. A profilometer is a measuring device for two- or three-dimensional measurement of microscopic topographies of the upper axis. The profilometer used for the test setup for measuring the valve deflection is a chromatic white light sensor from FRT GmbH (FRT Micro-Prof Optical Profilometer, FRT CWL-X (S/N2100/0253-08)). Monochromatic light is monochromatic visible light, in the general sense electromagnetic radiation of a precisely defined frequency or vacuum wavelength.
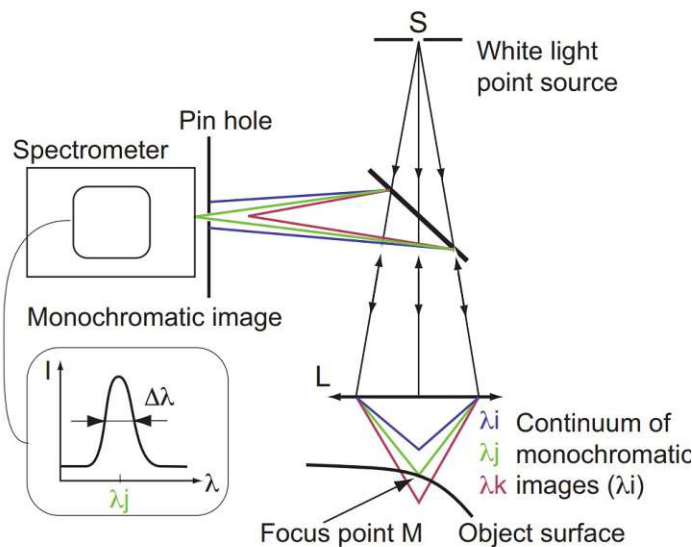
Figure 20: Micro-topographical principle [69, S. 4]

A chromatic lens (L) generates the white light source (S) image as a continuum of monochromatic images. As can be seen in Figure 20 the different wavelengths have different focal

points, depending on the specimen's height, a certain wavelength always achieves perfect focus. However, this is only true in a narrow height range as long as one wavelength of the light cone focuses (M). The backscattered light arrives at a pinhole P which filters out all wavelengths except a single wavelength (λj) and the sensor determines the structures on the sample at a working distance of 4 mm. The sensor in the measuring head measures the intensities of the reflected wavelengths, whereby the wavelength reaches the intensity maximum in focus. The maximum height measurement range depends on the measuring head. A 3 mm head was used for further measurements. Moreover, special software uses wavelength to determine the height of the sample at the focal point. By scanning and focusing many points on the sample, a three-dimensional topographic image can be created [69, 70].

Mass flow meter

The mass flow meter used is a product (mini CORI-FLOW) of Bronkhorst Deutschland Nord GmbH based on the "Coriolis effect". The flow meter consists of a loop-shaped tube, which is continuously vibrated by an exciter. Two pickup sensors at the rear and front end of the loop register the temporal and spatial change of the tube vibration. As long as there
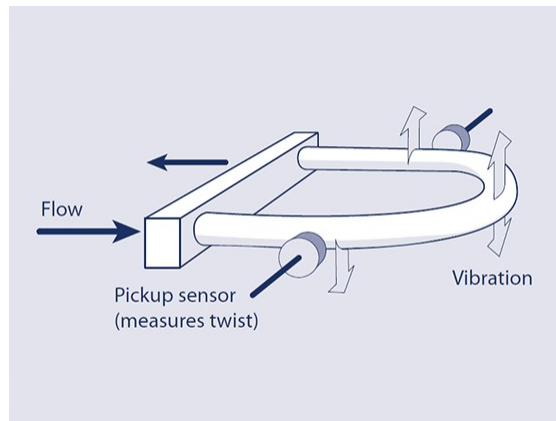
Figure 21: Flow measurement principle [71]

is no flow, the tube oscillates up and down uniformly at both ends. However, as soon as a medium flows through, the inertia of the liquid or gas causes a phase shift in the rocking motion, so that the sensors register different deflections of the tube. Here, the amplitude increases proportionally to the flow rate or flow velocity. The oscillation frequency of the tube, which is also detected by the sensors, is proportional to the density of the medium so that the volume flow can be determined from both measured values, and any air pockets can be detected [72].

Tube system

Tubing systems can significantly influence the dynamic or static valve deflection due to their viscous friction, mass inertia or even the elasticity of soft tubing. Steady-state flows can be estimated using Reynolds's number on the flow profile. Reynolds numbers below 1800-2300 are referred to as a laminar flow profile, above which the flow profile becomes increasingly turbulent. In contrast, the dynamic Reynolds number is used to determine the flow profile for unsteady flow processes within the excitation frequency and the flow velocity.

While the compressibility of water itself, at high pressures, causes a negligible volume change, the use of soft tubes can significantly affect the system's behaviour. In soft tubes, pressure expansion leads to uniform elongation and thus change in radius, which is not the case in rigid tubes.

Since the tube length is linearly incorporated into the flow resistance, the pressure drop due to viscous friction is almost negligible for short tube sections of a few centimetres. With a low Young's modulus such as PDMS, soft tubes can exhibit a corner frequency of up to 46Hz even at short tube lengths of 1.0 cm. In contrast, stiff tubes, e.g. PE with Young's modulus of 140 MPa, have a corner frequency that is 14 times higher even at a tube length of 25 cm. Thus, by choosing a stiff tube, the capacitance of the tube line becomes negligible [53].In the measurement setups used, care was taken to use rigid tubes with the shortest possible lengths to exclude any measurement inaccuracy due to the tube system.

Gas and liquid supply

In addition to the tube system, a large reservoir is used to compensate for variations in the supply.

Due to the measurements, it is necessary to take care of the water level in the reservoir. According to the hydrostatic law, under assuming of incompressibility of fluids, $\rho = \{const\}$, following equation can be given.

$$p(h) = \rho \cdot g \cdot h + p(0) \tag{14}$$

The height of the liquid column (h), the density of the liquid (ρ), The constant acceleration due to gravity (g) and the pressure on the top of the liquid column (p) are necessary for further calculations. In the case of Figure 22 the following conditions are given.

$$p_1 = p_2 \ \text{ and } \ p_3 = p_a \qquad\qquad \triangle p = \rho \cdot g \cdot \triangle h \tag{15}$$
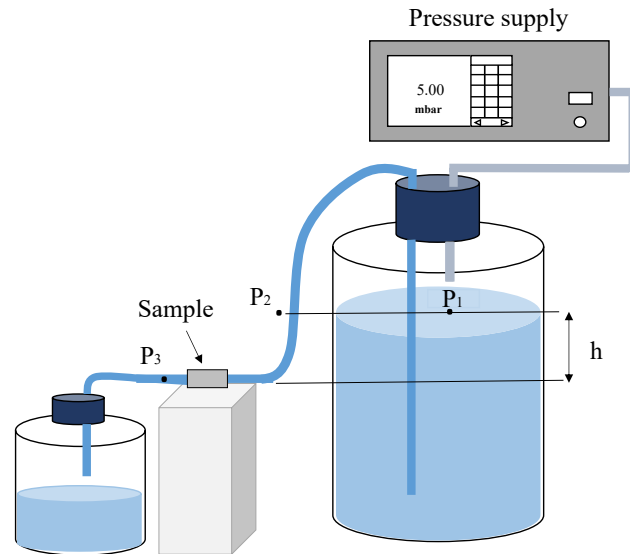
Figure 22: Principle of hydrostatic pressure within the tube and reservoir system

In case of a lower water level in the reservoir than the table height of the to be measured samples, a under pressure appears, and the hydrostatic pressure in the reservoir is smaller than the atmospheric pressure p_a at the end of the sample p_3. This implement falsifies the measurement result. The water level should be within all measurements at the same height and minimal higher than the sample level.

After all relevant measuring principles are explained, it will now be specified what the differences are between the valves used.

3.2.2   Valve samples

For valve characterisation, the top layer of the microvalve, the piezoelectric actuator, is removed, and only the two valve foils (1, 2) and the pump body (3) are used for further considerations (see Figure 23). A direct view of the valves should be made possible to describe their behaviour more precisely. Different types of ortho-planar valves were used to characterise the valves under the influence of different media.

Ortho-planar valve types
Three different valve series (V1.D1, V2.D1, V1.D2) were used to investigate the behaviour of the ortho-planar valves with air and water. These series differ essentially in two parameters: the geometric design and the welding radius of the valves. Both parameters are described
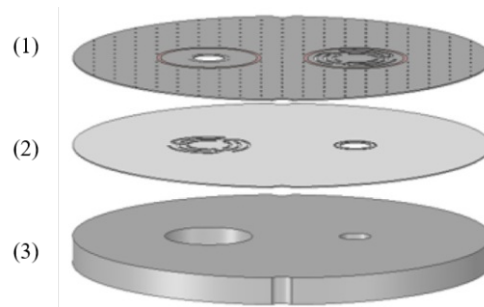
Figure 23: Components of valve samples (1, 2) valve foils, (3) pump body

in more detail under section 2.2.2. The valve design V1.D1 is referred to as "normal valves" in this work. This valve type is the usual design for the current stainless steel piezoelectric diaphragm micropumps by Fraunhofer EMFT. The structure of the used ortho-planar valve (V1.D1) is shown in the figure below (see Figure 24).
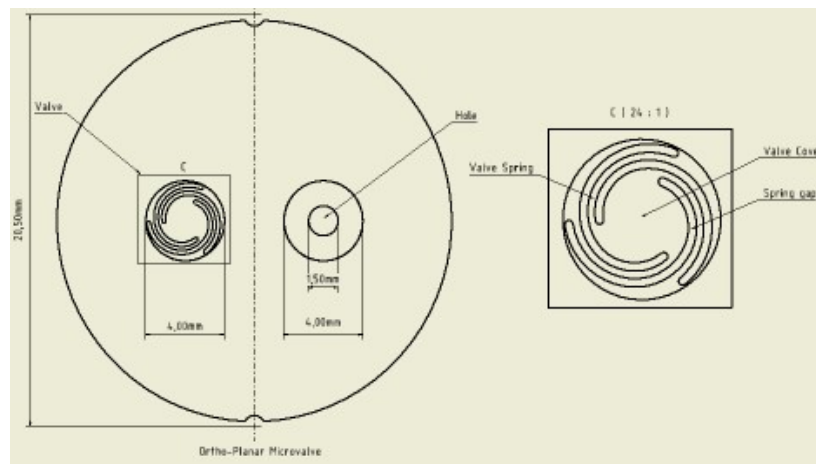
Figure 24: Ortho-planar valve (V1.D1)

Furthermore, V1.D2 will be mentioned as "valves with small welding radius" and V2.D1 as "valves with different geometry". The geometry of the valves is similar to the valve design of V2.D1, and the main difference is the only difference is the width (b) of the beams. At V2.D1, a stiffer spring stiffness (k_s) is expected due to widening the beam arms. In the case of the valves with a small welding radius, the same valve structure like V1.D1 is used, but the radius of the welding is smaller (D2). Due to the smaller welding radius, a pre-load on the valve is expected and thus a different behaviour to the valves, with a larger welding radius.

All specific valve parameters are given under Table 6.

Table 6: Valve parameters of valve type V1.D1,V2.D1 and V1.D2

	Parameter	Values	Unit
Young's modulus	E	$1.95 \ 10^{11}$	N/m^2
Beam height	h	$5.00 \ 10^{-5}$	m
Welding radidus (D1)	D1	$6.50 \ 10^{-3}$	m
Welding radidus (D2)	D2	$4.70 \ 10^{-3}$	m
Beam length	l	$3.00 \ 10^{-3}$	m
Beam width (V1)	b	$1.94 \ 10^{-4}$	m
Beam width (V2)	b	$2.00 \ 10^{-4}$	m
Diameter of the valve cover	d_s	$2.84 \ 10^{-3}$	m
Diameter of the valve inlet	d_i	$1.50 \ 10^{-3}$	m

Furthermore, the different valves are illustrated again under Table 7. A profilometer (described under section 3.2.1) was used to record the valves.

Table 7: Variation of valve parameters

Welding radius / Valve Design	D1: Ø 6.5 mm	D2: Ø 4.7 mm
V1: Cyclon Soft		
V2: Cyclon Stiff		
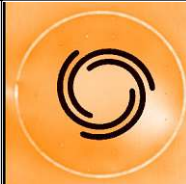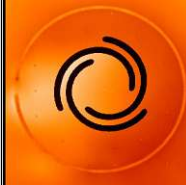
In general, it is suspected that a small welding radius increases the initial valve gap (see section 2.2.2) due to heat tension—the difference and also the beam width influences the flow behaviour. The relationship between the special design parameters within the valve behaviour is shown below (Figure 25).

Valves with thicker valve arms have a higher k_s and are stiffer. This will have an impact on the valve behaviour.

The different valve designs are chosen to investigate further a variety of design parameters in water and air. Working with medium water requires special preparation of the samples and filling the pumps with water. Significant matters are explained thereafter.
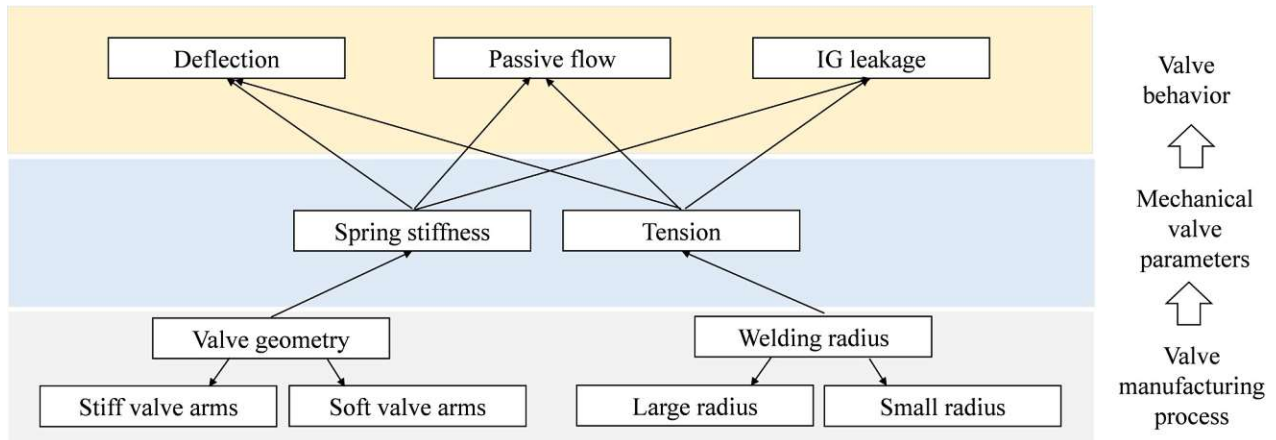
Figure 25: Variation of valve parameters

Preparation

Within the experimental part of the valve characterisation, preparation of the valve samples is necessary for optical measurements with medium water. As seen in the literature review in section 2.3, no methods for measuring valve deflection within water were found. The main concern is to build a closed system with the transparent surface for optical observation of valve behaviour. Furthermore, this covered system with a fixed volume,not as in the case of moving actuator diaphragms, can be used for other measurement methods with air and water as media.
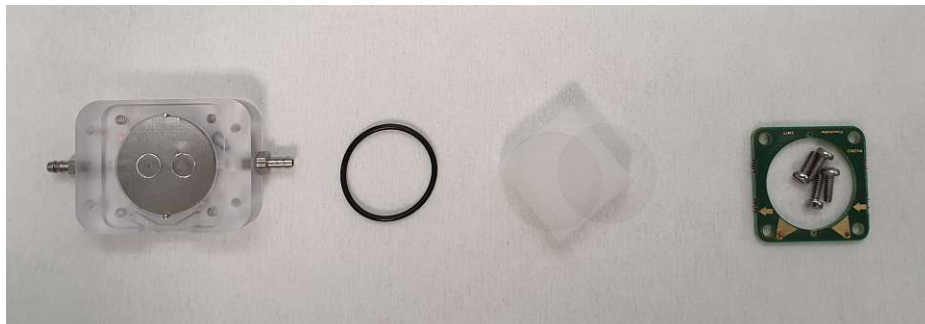
Figure 26: Prepreparation of the samples beginning from the left: micropump without actuator, Sealing ring, glass lip, screw fastening

The solution is therefore shown in Figure 26. First, a sealing ring FPM75 ($\varnothing$ 17 mm $\cdot$ 1 mm) is placed centrally on the top of the first valve foil, then the glass cover ($\varnothing$ 22 mm, No. 2) is placed and fixed by the screw fastening. For water measurements, the samples are filled with water close to the sensible optical sensor. The optical sensor for the measurements in the following context is a susceptible component in connection with water. Hence the

filling process must be separated from the measurement process. It is important to note that handling these sensitive valve samples is only possible in clean rooms. Particles have a huge impact on the behaviour of the valve and can block check valves and irreversibly damage the micropump.

Filling processes

The sample is connected to a tube system and a water reservoir via the inlet valve. Different pressure levels are applied by a pressure supply connected to the water reservoir. The working routine showed an optimal filling process without bubbles with pressure levels of 150 mbar to 50 mbar and again 150 mbar. While the fluid is pumped into the volume between the glass slide and the valve foil, gently tapping on the table is recommended to limit the inlet bubbles to a larger one, which then disappears by the pressure difference. The goal is always to ensure a filled chamber without phase differences in water and air.

After filling the chamber, three media are in the light path between sensor and valve sample: air, glass and water. Working with different media, comprised the fact of interfaces. A light source emits light beams divergently in all spatial directions, inhomogeneous media propagate rectilinearly. The speed of the light beam depends on the density of the medium in which it propagates.

Understanding the propagation within the different media is obligatory for further optical measurements to determine the valve deflection. In order to be able to guarantee the accuracy of the measurement results, the next step describes the measurement setup for the valve deflection, including the prepared valve samples with a glass pane.

3.2.3   Calibration of the measurement setup for valve deflection

The optical measurement setup for measuring the deflection of the valve cover contains the following relevant components for calculations and is shown as a schematic sketch (see Figure 27).

The prepared valve is placed in distance y_1 under the profilometer (1) and the monochromatic light beam (2). The valve is covered with the glass cover ($\varnothing$ 22 mm, No. 2) (3) and is placed on the seal ring FPM75 ($\varnothing$ 17 mm $\cdot$ 1 mm). The space between valve foils (5) and the glass plate is filled with DI-water (4). The pressure supply is entering through the inlet valve (7). Due to the pressure change, the valve deflection is then measured by the optical sensor above. More details about the optical measurement with the profilometer will be given
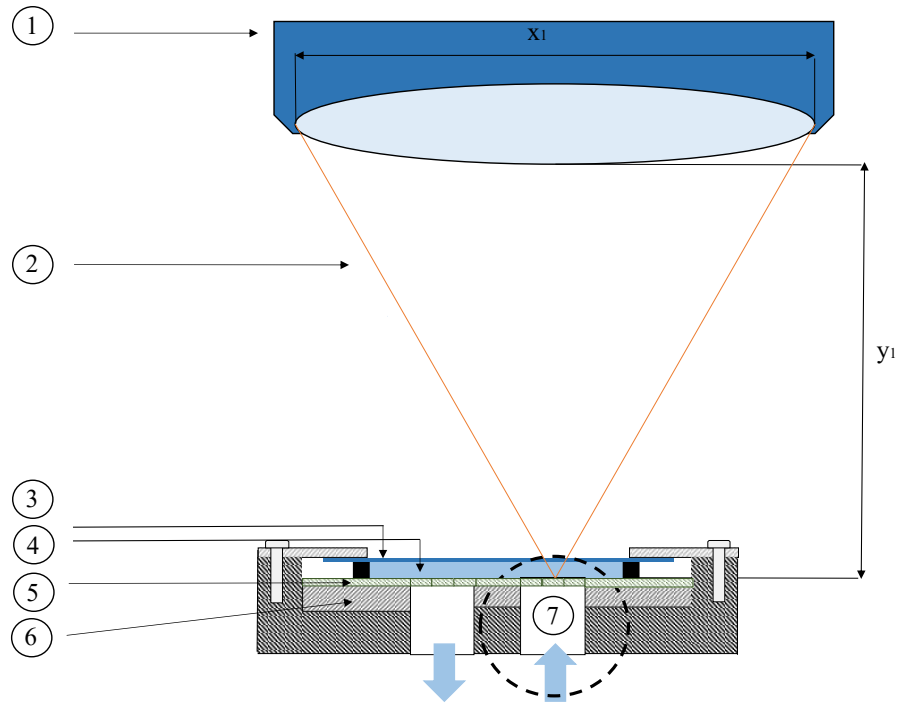
Figure 27: Measurement setup for calibration of the measurement method for the valve deflection

under the sections 3.2.5 and 3.2.1. The following paragraph is only intended to determine the behaviour of the optical measuring system for air and water.

The inlet valve (7) is the concerned valve to be measured, and a detailed few is given in Figure 28. Working with different mediums contain face shifts and interface sections. Till now, only measurements with medium air are done, and the impact of glass (3) and the deionized water (4) should be taken into considerations.

Calculations

Light rays change their direction and speed at the interfaces of media of different densities. The change in direction is also referred to as light refraction. The refractive index (n) is the ratio of the speed of light in the medium (c_M) to the vacuum speed (c_0) of light [73].

$$n = \frac{c_0}{c_M} \tag{16}$$

Parallel to the phase velocity, the wavelength in media also becomes smaller, while the light frequency remains constant.

Snell's law of refraction states that a light beam changes its direction when it passes into a

medium with a different density (phase velocity).The law only states how direction the light beam is deflected, but not how much is transmitted or reflected at the transition between the two media.In the case of total reflection, the real law of refraction is invalid.

The angles of incidence and refraction of the light are always given for the perpendicular to the boundary of the medium.

1. From the optically thin to the optically dense medium: refraction to the lot.

2. From optically dense to the optically thin medium: refraction from the lot.

Refraction to the perpendicular occurs when light passes from an optically thinner to an optically denser medium $(c_1) > (c_2)$ and the angle of incidence is always larger than the angle of reflection. In the case of transitions from an optically denser to an optically thinner medium, refraction from the perpendicular occurs $(c_1) < (c_2)$. The angle of incidence is then smaller than the angle of reflection [73].

In the setup (see Figure 27 (a)), first, the angle of incident (α) without any glass slide is calculated in medium air. The parameters for the further calculations are shown in Table 8.

Table 8: Calculation parameter for calibration of the valve deflection measurement setup (see Figure 27)

	Parameter	Values	Unit
Length lens	x_1	30.00	mm
Distance lens/sample (without glass)	y_1	29.50	mm
Distance glass/sample (seal ring)	y_2	1.00	mm
Thickness glass slide	y_3	0.20	mm
Refractive index air	n_a	1.0003	
Refractive index cover glass	n_g	1.5200	
Refractive index water	n_w	1.3330	

In the following Figure 28, the valve sample in combination with the glass plate and the light beam of the sensor head (profilometer) is shown enlarged.
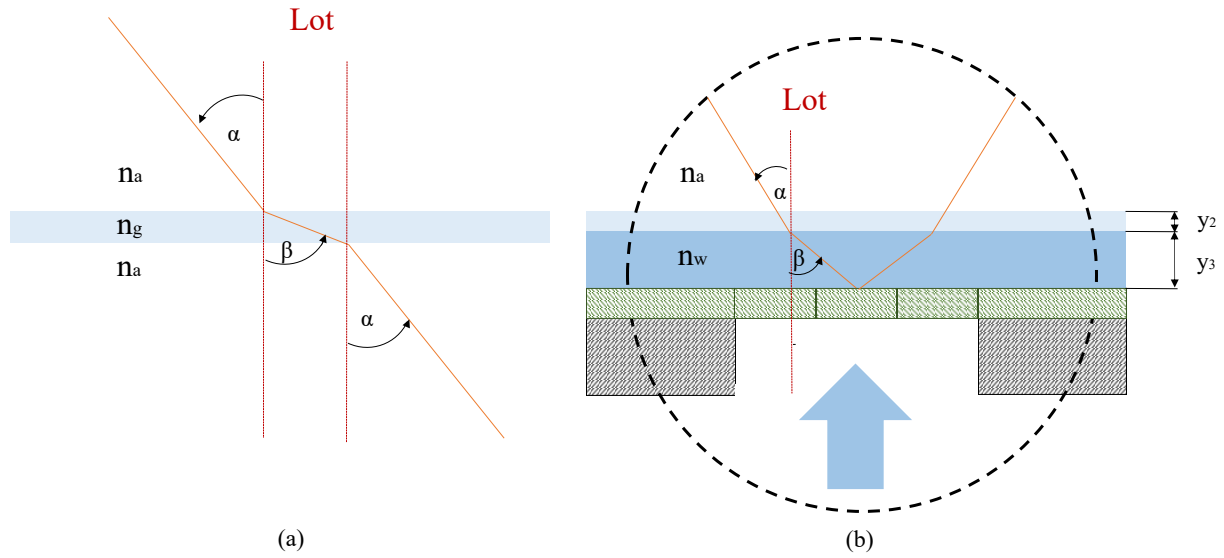
Figure 28: Measurement setup for calibration

The angle of incident is calculated with the angle function sinus.

$$\alpha = arcsin\Big(\frac{0.5 \cdot x_1}{y_1}\Big) \quad = 30.56° \tag{17}$$

Next, the phase shift between air and the glass slide is taken into considerations without medium water (see Figure 28 (a)). The light beam of the FRT travels through medium air (n_a) with a certain velocity and the incident angle (α) and hits the glass surface (n_g).

At interfaces of media with different densities, light rays change their direction and speed. After entering the medium air again, the conditions of the previous case are given, and α is the same angle as before. Within the refraction law states, the refraction angle is calculated as follows.

$$\beta = arcsin\Big(\frac{n_a}{n_g} \cdot sin(\alpha)\Big) \quad = 19.55° \tag{18}$$

Two flat, parallel surfaces at a distance of (d_p) form a plate offset. With this information Equation 17, the parallel offset (v) can be calculated with the equation below [73].

$$v = d_p\Big(\frac{\sin(\alpha - \beta)}{\cos(\beta)}\Big) \quad = 0.04mm \tag{19}$$

Since the parallel offset is vanishingly small in relation to the light beam, it is neglected in

the remainder of this section. For further calculations, it is accepted that no phase shift exists between the medium air and the 0.2 mm thin glass slide (see Figure 27).

In connection with water as a medium (see Figure 28 (b)), the result for β is:

$$\beta = arcsin\left(\frac{n_a}{n_w} \cdot sin\alpha\right) \quad = 24.72° \tag{20}$$

The relation between incident angle and reflective angle is then used to compare the measurement setup with medium air and water.

$$Factor_{water} = \frac{\alpha}{\beta} \quad = \frac{30.56°}{24.73°} \quad = 1.24 \tag{21}$$

In the following step, the $Factor_{water}$ is validated due to measurement validation of the calculated relationships and is used for comparison of air and water measurements.

Validation of refractory index

For calibrating or the measurement setup, foils with different thicknesses (see Table 9) were glued to the sample surface with double-sided tape (see Figure 32).
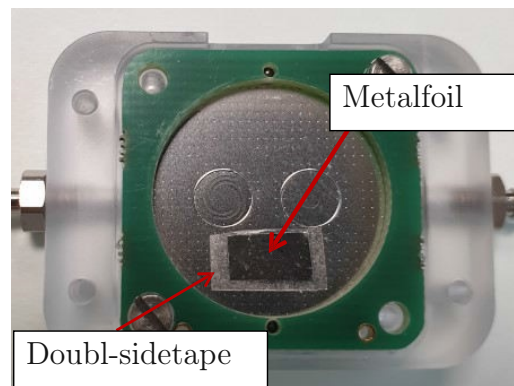
Figure 29: Valve sample with double-sidetape and metal foil

Various perennial trials have shown,that the best solution is to glue the complete metal foil with overhanging pieces of the glue strip. Better adhesion ensure stable results .

The thickness of those foils was measured by a 3D scan, using the profilometer (see section 3.2.1) for three different cases: (1) samples without glass slide (medium: air), (2) samples with glass slide (medium: air), (3) samples with glass slide (medium: DI-water).

Because the double-sided tape is transparent, the optical sensor (profilometer) cannot measure the correct height of the tape (18 μm). For correct results, first, the gluing part was

Table 9: Foil thickness

Metal foil thickness [µm]
10
30
50
100

measured without metal foils, and the height of the glue (h_g) was determined with 52 µm, which means an error offset of 34 µm. This error was considered in further measurements.

(a)

(b)

(c)
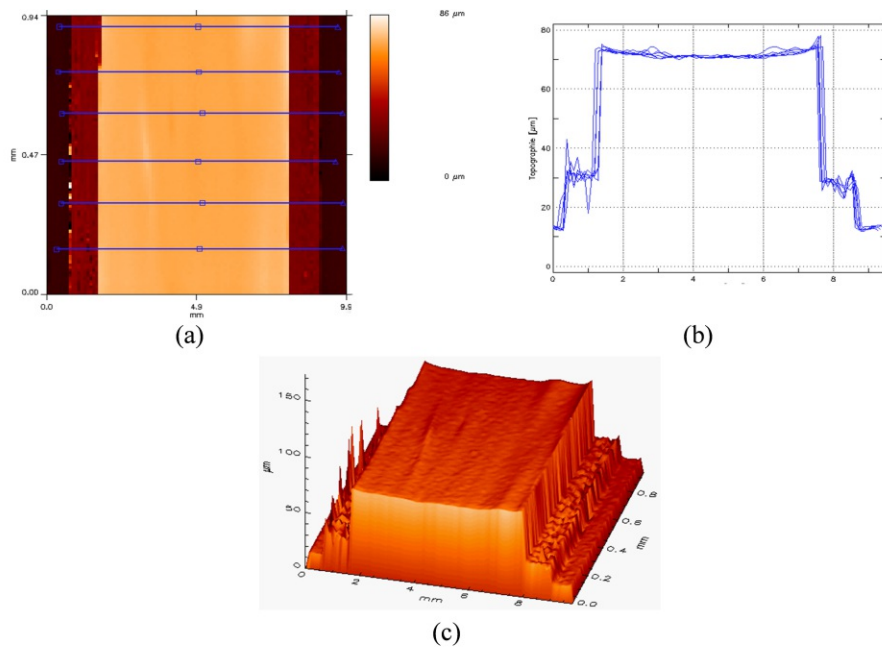
Figure 30: (a) 3D scan separated in 6 profiles (b) 2D image of a profile (c) 3D model of a 30 µm foil

For each 3D scan (Figure 32 (a)), the scans were split into six 2D profiles (see Figure 32 (b)) ,and the median was calculated to ensure accuracy. To facilitate comparison, the steps between the profile were always at the same height and uniformly distributed over the whole metal foil. Subsequently, the difference between the median of both glue sides and the median of the metal foil plate was calculated. In consequence, the offset of 34 µm was taken into considerations. For visualisation, three marked lines can be found in Figure 31. Each of them indicates a specific height for measuring the height
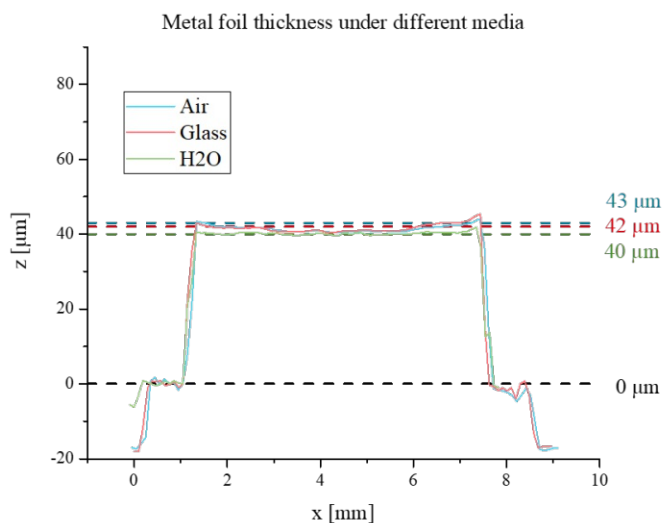
Figure 31: Different measured height for metal foil measurement under air (blue), sample with glass slide (red) and sample with glass slide and filled with water (green) conditions

of the metal foils within just air in between the profilometer and the sample, the sample with glass slide and at last the sample with glass cover and filled with water. The results differ from each other and can be found in Table 10.

Table 10: Results for metal foil thickness in air, with glass slide, with glass slide and water and the calculated factors

Foil thickness [µm]	Air [µm]	Glass [µm]	Water [µm]	$Factor_{water}$
10	9	8	6	1.33
30	29	29	23	1.26
50	45	45	38	1.18
100	101	102	85	1.20
Total factor				1.24

This table shows that the values between air and glass slide differ marginal. Caused through the fact of the resolution of the profilometer, just two significant digits are allowed. Someone also proofed this with previous Equation 19 and was so far expected. The calculated $Factor_{water}$, has also been confirmed with the experimental setup (see Equation 21).
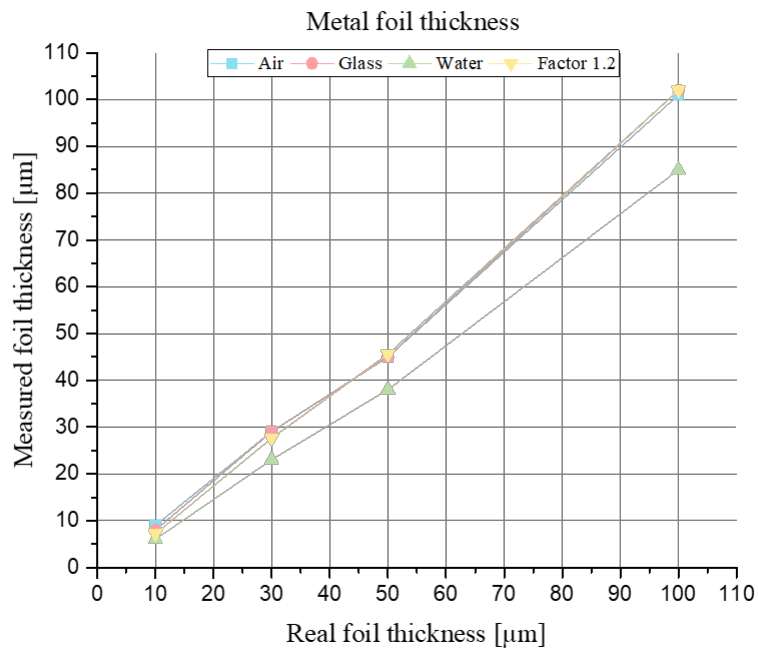
Figure 32: Results of the calibration with metal foils with the measurement conditions under air, glass, water and the water values multiplied with the Factor 1.2

In the Figure 31, the values of the water measurement were multiplied with the calculated Factor of 1.2. The straight line with air is congruent with the line that the water measurements, multiplied by the factor 1.2, have resulted in. In the future, water measurements in this setup made with the profilometer can be converted with the factor 1.2. Thus, a straight comparison of the measurements made under different circumstances (air and water) are possible.

After successfully calibrating the system, the specific network model for the valve samples with a glass plate is now described. This is essential to be able to draw the correct conclusions for the subsequent measurements.

3.2.4   Simplified network model for system behaviour

In cases of passive valves in the combination of piezoelectrical actuation principle [53, 56, 57, 60, 61], the valve deflection is caused due to the actuator movement above the microvalves by changing pressure. In this case, the actuator is replaced by a glass pane and the deflection

of the microvalves is only driven through pressure gradients between the inlet and the outlet valve. The following electrical network model is based on the considerations of Markus Herz [53]. In this system, the tube connections on the inlet and outlet valves are neglected, as their influence on the valve behaviour is marginal.
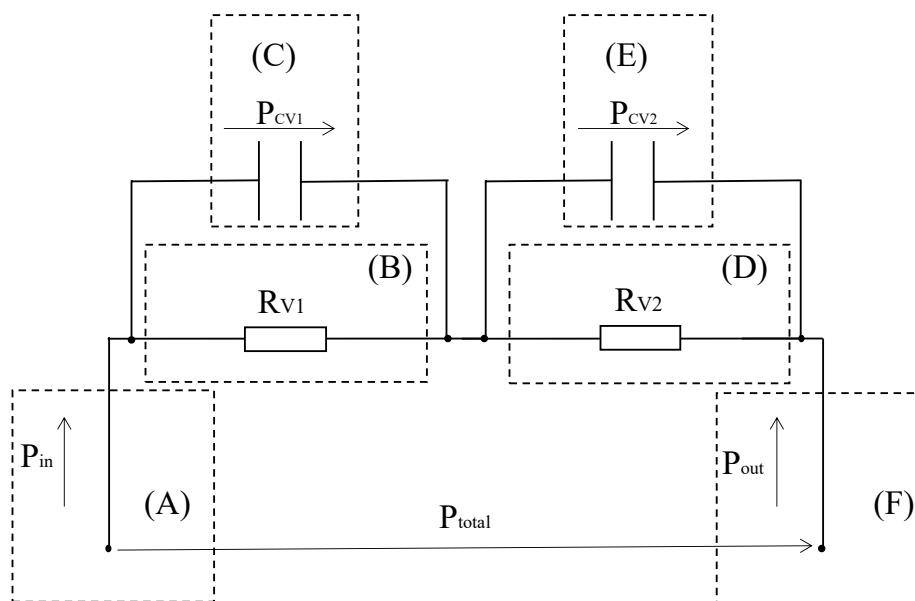
Figure 33: General analogous network modelling of the prepared valve samples: Pressure of the reservoir (A), the inlet valve resistance (B), the fluidic capacity dependent on the inlet valve displacement (C), the outlet valve resistance (D), the fluidic capacity dependent on the inlet valve displacement (E) and the back pressure (atmospheric pressure) (F)

In the circuit diagram shown above (Figure 33), the values of the resistors R_V and the capacitors C_V each depend on the pressure applied.

The variable pressure supply P_{in} (A) enters the inlet valve (B) and (C). Valve responding is represented by a parallel circuit of a resistor and a capacitor. The differential resistance R_{V1} describes the valve behaviour about the state at which the valve opens. After the valve has opened, it displaces the overlying volume ,and a capacitor C_{V2} is used to model this change of state. After the fluid passed the inlet valve at a certain pressure, it passes on to the outlet valve (C) after the fluid has crossed the inlet valve. The outlet check valve, opens with a differential resistance of R_{V2} and displaces volume according to C_{V2}. At last ,the back pressure is shown with P_{out} ,which is atmospheric pressure. The two diodes, inlet and outlet valve, should act equally and are seen as similar for further considerations. P_{out} is considered to be constant as long as the measurements are at the same place. P_{total} describes

the absolute pressure drop from P_{in} to P_{out}.

Static measurements

Considering quasi-static measurements the P_{in} (in Figure 33) is similar to a DC voltage source where the inlet pressure is seen as constant. A capacitor would work as isolator at a certain pressure by the power supply of a direct voltage source. Since the valve has a certain opening behaviour at constant pressure ,which is not time-dependent, no capacitor is required for the static case and is neglected. At the end ,a serial system out of pressure input (A), the resistor of the inlet valve (B), differential resistor of the outlet valve (D), and the output pressure (F) are designed.

If several voltage sources (= pressure sources) and resistors are connected in series, they form a series circuit. Because the components with their interconnected inputs and outputs form a line without branches, the same flow through them all. With serially connected components, the voltages in the series circuit are added together. This results in a total voltage that is the sum of all the individual voltages. In a series, currents is constant.

This fulfils Kirchhoff's mesh rule, which states that the sum of all voltages in a closed mesh is equal to zero:

$$P_{in} - P_{out} + i_{R_{V1}} \cdot R_{V1} + i_{R_{V2}} \cdot R_{V2} - U_{totla} = 0 \tag{22}$$

with

$$R_V = R_{V1} = i_{R_{V2}}$$

$$P_{out} = constant$$

The equation can then be simplified to:

$$P_{in} + 2 \cdot (i_V \cdot R_V) - P_{out} = P_{totla} \tag{23}$$

With the equation above, the overall system is considered, which includes both valves. however, for further valve characterisation, it is not the overall system that is decisive in this case but considering a single valve. Since the output voltage has a constant value, the two valves are considered identical by design, and therefore only the pressure difference is a variable. Consequently, the pressure difference must be halved in retrospect for the consideration of

one valve.

$$\frac{1}{2} \cdot P_{in} + i_V \cdot R_V - P_{out} = P_{totla} \tag{24}$$

This is taken into account for all subsequent measurements.

Dynamic measurements

In the dynamic case, the P_{in} (in Figure 33) is similar to a AC voltage source where the inlet pressure is changing over time. By power supply of an accelerating voltage source, a pressure depending capacitor is used to describe the valve's opening behaviour due to the displaced volume and is time-dependent. In the end ,a serial system out of pressure input (A), a parallel circuit containing the differential resistor (B) and the capacitor (C) of the inlet valve, a parallel circuit containing the differential resistor(D) and the capacitor (E) of the outlet valve, and the output pressure (F) is designed. Both valves are also to be considered identical in behaviour, and the input voltage is also halved afterwards to describe a valve (see Equation 24).

In the following section, all measurement setups for valve characterisation in air and water are described.

3.2.5   Quasi-static valve deflection measurements

For measuring the valve deflection, different experiments were done with normal valve geometries (V1.D1), normal valves with different smaller welding radius (V2.D1) and valves with different geometry (V1.D2). The three valve types are described further under Table 7. The setup used for deflection measurements is sketched below. The use of glass covers instead of the actuator diaphragm enables optical detection of the valve. Due to light refraction, the setup must be calibrated ,and distortion is considered during analysis (see section 3.2.3).

To measure the deflection of the passive check valve, the prepared microvalve is placed centrally on the electrically horizontal adjustable table of the profilometer (FRT Micro-Prof Optical Profilometer, FRT CWL-X (S/N2100/0253-08)). The valve cover deflects accordingly by the applied pressure due to a pressure generator (Mensor PC4000 Industrial Pressure Controller). With the water pressure or air pressure applied, the behaviour of the inlet valve is then to be observed with the optical sensor (see section 3.2.1) from above. By measuring the sample, height differences between the valve seat and the valve cover can be determined
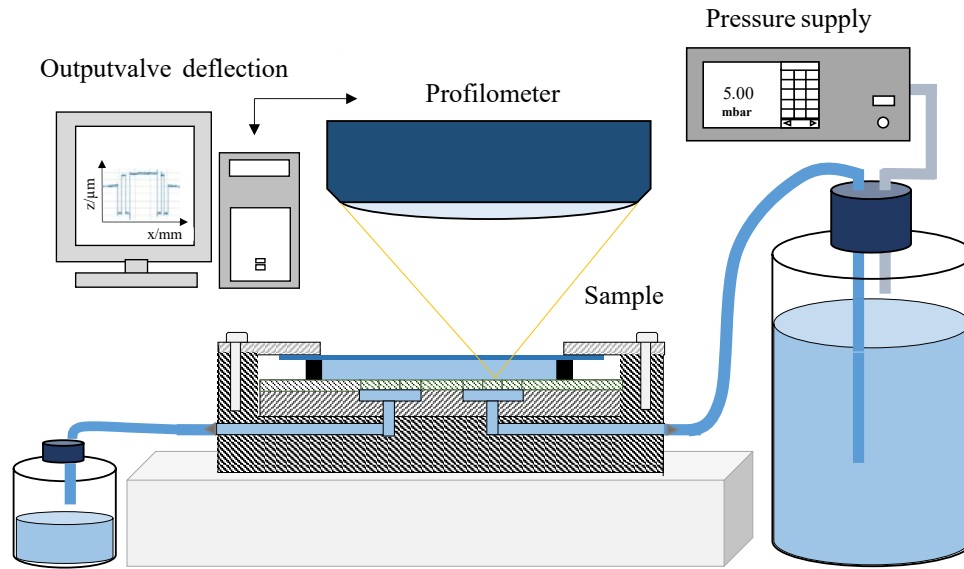
Figure 34: Measurement setup for valve deflection

with 30 nm by the instrument.

For the measurement constant pressure is given by the pressure regulator. The air pressure travels through a tube to a reservoir filled with air or water and ends up in the inlet valve. The valve is either covered by a glass plate or is completely accessible. Here, the deflections of the valve cover, which occur at the following pressures, are measured:

Pressure steps in mbar														
0	5	10	25	50	75	100	150	100	75	50	25	10	5	0

The ascending and then descending pressure values were elected to observe possible hysteresis effects within the medium water.

first, within the profilometer, a 3D scan of the valves is made with ten line scans per image. From this 3D image, the line scan in the middle was selected to generate a 2D image. Using a Python program, the valve deflection was subtracted from the height outside the valve to determine the deflection. For water measurements, the above calculation and calibration factor (see section 3.2.3) was multiplied to the certain valve displacement in comparison of the measurements with air an water.

With the above measurement setup, the following valve response is now to be investigated:

1. Sample without glass plate and air supply.

2. Sample with glass plate: assuming atmospheric pressure at the outlet.

   - Medium air
   - Medium water

3. Sample with glass plate: valve outlet is closed.

   - Medium air
   - Medium water

This measurement is primarily used to determine the spring constant. Since the spring constant is a constant, the determination of a deflection, at a specific pressure value, is theoretically sufficient for the calculation. However, water has a damping effect ,and a flatter course is assumed compared to measurements with air to determine the valve deflection.

According to Equation 24 it is assumed that the two diodes (inlet and outlet valve) have the same behaviour. To describe just one valve, the applied pressure values have to be halved for the z-axes of the deflection-pressure diagram.

Bubbles
In the course of the measurements, unwanted incidents due to the formation of bubbles occurred again and again. If a bubble appears in the system, further measurement data cannot be used in the optical measurements as a bubble reflects all the sensor's incoming light. The appearance of bubbles falsify the measurement values or simply make an evaluation impossible. Over time, however, the suspicion arose that there could be a connection between the appearance of the bubbles and the pressure. This behaviour was investigated by measuring the size of the bubbles with the help of 3D scans and documenting the pressure at which they appear. The limiting factor here is that it is assumed that even the smallest bubbles are present in the tubes or reservoir. Care was always taken to avoid bubbles by flooding the entire system before use and ensuring that no bubbles were visible in the tube. The position of the individual points where bubbles form was also documented and is presented in chapter 4.

3.2.6 Quasi-static flow measurements

The setup for measuring leakage rates and passive pressure is shown in Figure 35. Here the prepared valve sample with a glass plate is placed between an inlet reservoir and an outlet reservoir.
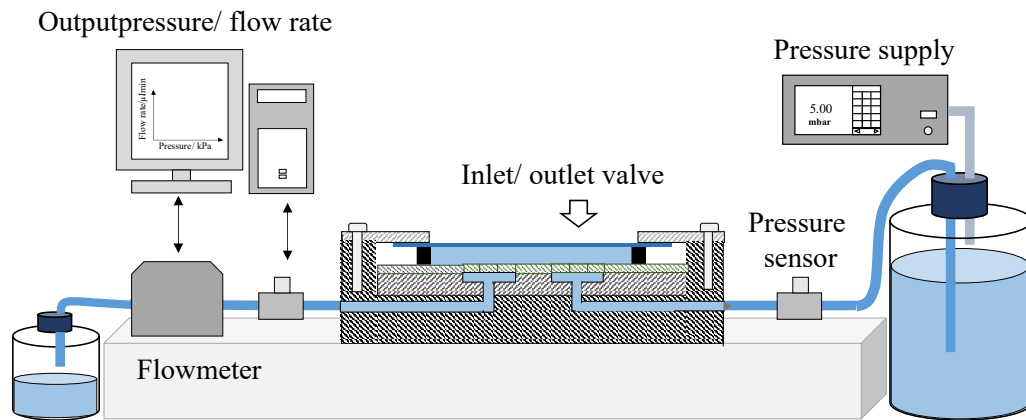
Figure 35: Measurement setup for flow measurements

Within the following measurements, the experiments are done with three different types of valve foils: normal valve geometries (V1.D1), normal valves with different smaller welding radius (V1.D2) and valves with different geometry (V2.D1). For further information, see Table 7.

In the following paragraph, the passive flow measurement and the measurement of the leakage will be described. In the case of water measurements,the inlet reservoir is always filled with a higher level of water than the position of the sample. This is done to avoid a change in the valve behaviour due to hydrostatic pressure (see section 3.2.1). It should be mentioned, that for the flow measurements ,two different mass flow meters for leakage rate (lower maximum value detection) and flow rate (higher maximum values) of FormalBronkhorst (Mini CORIL-FLOW),were used. However, both were interconnected, as shown in Figure 35.

Passive flow measurement
In passive flow measurement, the inlet reservoir is connected to the inlet reservoir (right) and the outlet valve to the outlet reservoir (left) employing tube systems. Since pressure losses are to be expected within the system due to fluidic resistances, such as tubes, two piezoresistive pressure sensors are connected to the tubes via T-pieces immediately upstream and downstream of the valves to check the pressure drop at the valve. The pressure at the valve can be determined by calculating the difference between the values measured at the

sensors. The pressure sensor is also connected to the sealed inlet reservoir via an air tube.

If I directed the fluid flow into the clamping device on the inlet side, the pressure acts in the valve's direction. A mass flow sensor is located between the piezoelectric pressure sensor and the outlet valve to determine the passive flow.

The pressure controller then runs through a pressure interval program and applies different pressures to the reservoir. The pressures displace the medium in the reservoir and direct it through the tubing to the device with the glass-lidded valve foils. Due to the parallel connection of the sensor, ideally, the same pressure acts on the sensor as is applied to the valve. This causes the piezoceramic of the sensor to undergo a small deformation, which generates an electrical voltage. generated. Using calibration curves, the measured piezoinduced voltage can be assigned to a specific pressure value. As described in the section 2.2.2, the valve cover is lifted and the fluid can pass. The pressure interval program that is run through to measure the passive flow, is shown below:

Pressure steps in mbar											
0	1	2	5	10	15	20	50	75	100	200	300
300	200	100	75	50	20	15	10	5	2	1	0

Leakage measurement

To measure the leakage rates, the valve is turned so that the pressure now acts in the opposite direction. The outlet valve is connected to the inlet reservoir and the inlet valve to the outlet reservoir. In this case, the mass flow sensor measures the flow that the valve could pass in the opposite direction to the valve opening behaviour (in the blocking direction). Also, in this case, the pressure controller runs through an interval program with different pressures applied to the inlet reservoir. The pressure interval program that is run through to measure the leakage rates, is shown below:

Pressure steps in mbar															
0	25	50	75	100	150	200	300	300	200	150	100	75	50	25	0

3.2.7   Dynamic valve deflection measurements

The dynamic behaviour of the passive valves is to be determined with an optical measuring system, the profilometer (FRT Micro-Prof Optical Profilometer, FRT CWL-X (S/N2100/0253-08)), using the measuring setup shown in Figure 36.
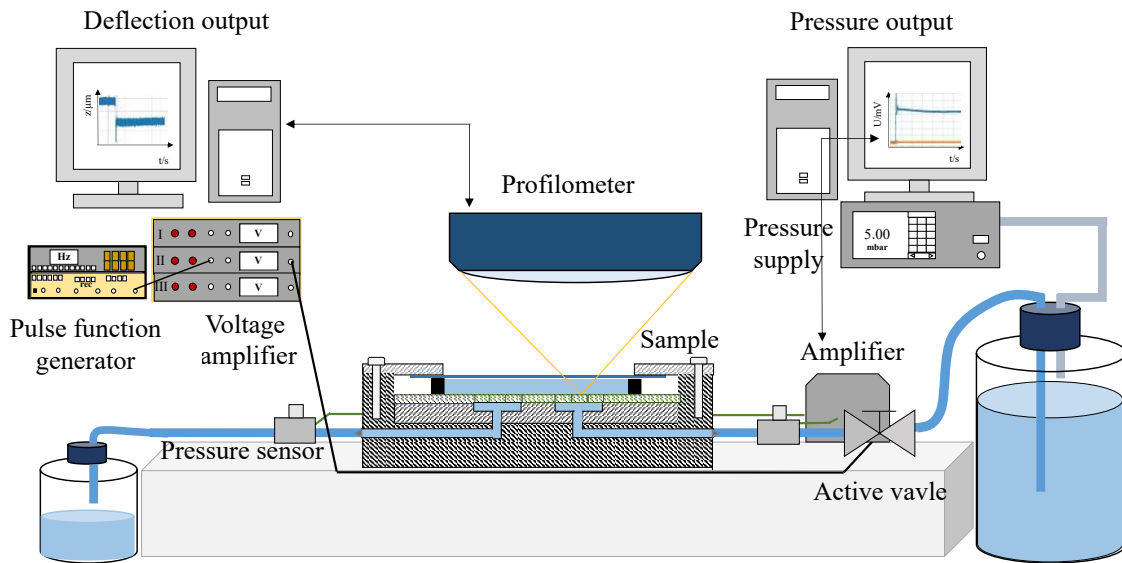
Figure 36: Measurement setup for dynamic valve behaviour

Because a glass plate is used above the valves instead of the normal white actuator membrane, an optical measuring method is possible. As with the quasi-static measurements of valve deflection, the light refraction was determined using a calibration procedure (see 3.2.3). This procedure ensures the comparability of air and water measurements.

For these measurements, the valve foil with inlet and outlet valve and glass plate was positioned with the focus of the profilometer (see section 3.2.1) on the cover of the inlet valve. The inlet valve was actuated by an active valve, which generated a sharp pressure pulse via a pulse generator frequency (Hameg Programmable Power Supply HM8142) with a square wave signal at 10Hz and amplified (Piezomechanik GmbH Analog Amplifier SVR 500-3). The active valve was connected to the inlet with a reservoir filled with either air or water. Within the water measurements, also the entire tubing system and the valve sample was filled with water (see Figure 3.2.2). A pressure sensor was connected between the active valve and the inlet valve, which determined the current pressure at the inlet valve through a voltage drop. Such a sensor was also located on the valve sample's outlet valve, and both were connected via a USB-6211 (National Instruments USB-6211 Multifunction I/O Device).

Utilizing a sensor calibration, the voltage drop of the pressure sensors between the sensor before the inlet valve of the sample and the sensor after the outlet valve of the sample could be assigned to the corresponding pressure values. Either air or water was pumped through the active valves. The two pressure sensors were to eliminate the hydrostatic pressure drop in the measurements caused by the falling water level based on the measured values.

The specific pressure differences were recorded with the DAQ-Express program. Analogous to these recordings, the dynamic valve deflection was recorded on another computer with the program CWL view, which recordings the CWL sensor for detection of the valve deflection. Both programs started at about the same time when the active valve was still closed. This value formed the initial reference. The pulse generator was then started ,and the active valve went into operation. Due to the initial reference, in which both the valve deflection and the pressure sensors were at 0, it was clearly recognisable from the records for pressure and the pulse reduction when the active valve opened. This made it possible to assign pressure values to the dynamic behaviour of the valve deflection. The optical measuring method allowed the investigation of the valve's step response with air and water as a medium. This method has never been used before and allows the user to determine the dynamic valve behaviour at different frequencies. Furthermore, the dynamic valve behaviour can be investigated experimentally with different media. So far, the valve behaviour has only been investigated for air measurements, but analytically calculated or simulated for water measurements.

After all relevant material and methods for characterisation of the valves are explained, the following chapter presents the results.

4 Results and discussion

In this chapter, the individual steps for determining the differences between measurements with medium air and water concerning the deflection of the passive valve are described. Derivations regarding the differences between flow measurements with water and air are described. The same valve samples were always used for all subsequent measurements ,and three different valve shapes (see Table 7) were present. Valves with geometry V1.D1,are used in the current micropump where valves of the type V2.D1 just differ from V1.D2 by a minimal increase in beam width. Finally, the valve (V1.D2), which is essentially identical in construction to valve (V1.D1), but with a significantly reduced welding radius, was used. For the V1.D1 series of measurements, the number of valves measured was n>7, for the V2.V1 series of measurements it was n=2, and for V1.D2 it was n>3. The same valve samples were always used for all subsequent measurements. Theoretically, a series of valves would also suffice for this statement. However, the use of different valves can have the advantage of correctly assigning differences between the media. If the differences between air and water measurements are the same for all valves, this further reinforces the valve model validity. The applied voltage -pressure here- equally applies at both resistors, hence one resistor gets the halved voltage, as described under Equation 24. The halving of the effective pressure applied was taken into account in all the following graphs, in which the glass plate covered the valves

Moreover, it has to be mentioned that in the case of some specific measurements, individual valves were excluded from the statistical evaluation. These valves showed an a-typical course during the measurements, as some of these valves did not open, or did not open at first and then abruptly.

There may be various reasons for these failures. One possibility could be that the test samples were not completely dry [51]. In such a case, capillary forces affect the valve and the necessary load for opening the valve increases. Even as care was taken to ensure that the valves were completely dried and blown through with compressed air (less than 500 mbar to avoid plastic deformation) after each measuring process, the closure of the valves could be attributed to these conditions. Another reason for the a-typical valve behaviour could be the handling of the valves. During the drying process of the valves in the cleanroom the glass plate was removed ,and the valve body was carefully lifted out to free the housing from water. This was done under laminar exhaust conditions, but it cannot be completely ruled out that particles got caught in the valve beams and affected the subsequent opening behaviour. For storage,

the inlet and outlet of the valve samples were connected and sealed with a tube. In this way, contamination by particles could be avoided, at least during storage. after each water measurement, the drying process took place, so it is conceivable that valves behave normally during one measurement and behave conspicuously during subsequent measurements.

It has therefore been specified exactly what valves were used for the statistical statements. for all the graphs below It is thus possible to understand at any time how the measurement results were obtained.

4.1   Valve deflection

In the beginning, the general considerations for the measurement through the glass plate attached to the valve samples in the medium air will be declared. The valve deflections under defined pressure are investigated with both media, air and water.

4.1.1   Initial considerations in relation to air measurements

The optical measurement results of the deflection of the valve cover by defined pressure, previously described under the section 3.2.5, are summarized in Figure 37.

For this purpose, the prepared valve samples were placed under the sensor. Various pressures were applied via the pressure transducer in the valve forward direction. The deflections of the valve cover generated by the respective pressures were measured with the optical sensor. As described in the paragraph before, different valve types from the V1.D1, V2.D2 and V1.D2 series,were used (see Table 7).

For validating the overall measurement setup, two considerations have been proofed.

Preliminary considerations
First, the valves of V1.D1 were used to check whether the assumption that the valve deflection is only caused by a pressure difference within a pressure gradient between inlet and outlet valve is correct. To confirm what was assumed, the sample outlet valve was closed ,and no flow was possible. However, as Figure 37 shown the gradient of the regression line (yellow) is constant. It is proof that the valve deflection can only occur due to pressure differences.

In the progress of the thesis so far, it has been proven that optical measurements with air
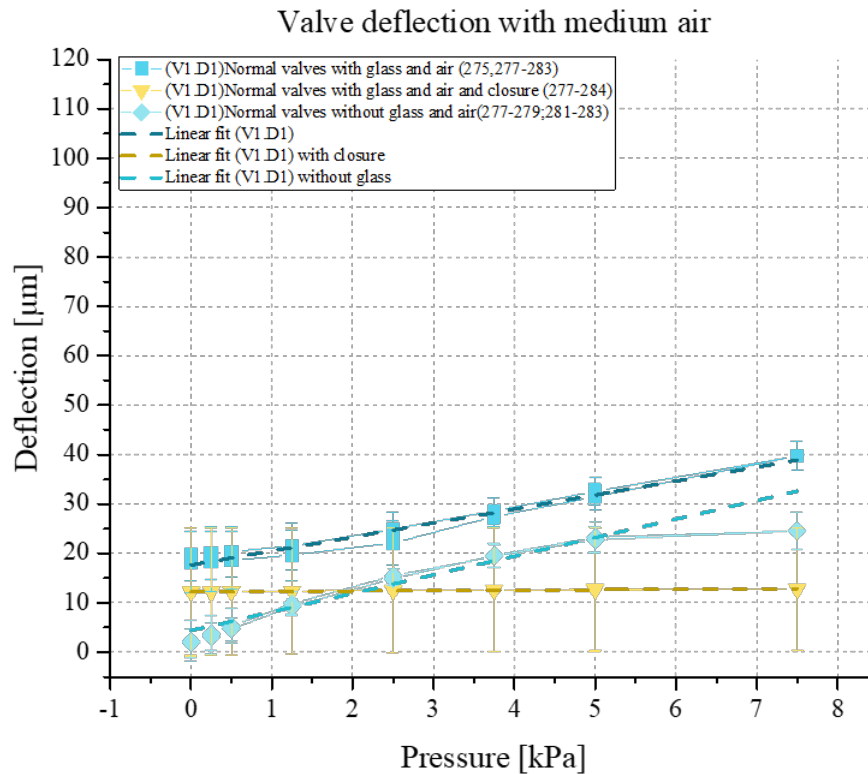
Figure 37: Results of the valve deflection with medium air using only valve type V1.D1

and water can be carried out equally through the setup using the calculated and validated factor 1.2 (see Table 10). Furthermore, it should now be determined whether, using the same valve series (V1.D1), differences in deflections can be observed when using the glass plate and without the glass plate. As described with Equation 24, it is assumed that by connecting the valves in series as resistors, the effective pressure applied is subsequently halved. For this purpose, air measurements were carried out with and without the glass plate.

Notable is that after installing the glass plate on the device, a higher initial gap can be mentioned than without glass. Figure 37 also shows that the regression line course (light blue, V1.D1 without glass) is steeper than with the glass plate (blue, V1.D1 with glass).

The reasons for this can be different. According to Equation 32, only two influencing factors are conceivable for a steeper gradient. Either there is an decrease in the applied pressure (),considering constant deflection (constant spring rate) or the spring rate (k_s) has increased with unchanged pressure. Both factors can contribute to a steeper slope. Since it is assumed that the inlet and outlet valves behave in the same way, it can be said that the prevailing

pressure should remain the same. Since the same valves were used for the measurement with and without glass plate (V1.D1), the spring stiffness is the same for both measurements. A straight calibration of the valve deflection with and without the glass plate has shown that the pressure at the valve must decrease when the glass plate is used. This is a systematic system behaviour in which the actual pressure applied to the valve behaves as follows:

$$p_{glass} = p_{applied} \cdot 0.8 \tag{25}$$

As there were no pressure sensors connected to the glass plate upstream and downstream of the valve, the cause of the pressure drop cannot be determined qualitatively. However, it is suspected that the cause lies in the measuring point with tube systems and reservoirs It can be assumed that the error is of a systematic nature, as it behaves the same for all pressures applied. Based on this observation, sensors were placed upstream and downstream of the system in all further measurements, following the valve deflection measurements.

In addition, since it cannot be assumed that the pressure drop on the measurement setup behaves in the same way for water and air, this discovery cannot be automatically transferred from air measurements to water measurements. A check of the behaviour of water measurements with and without a glass pane is also not possible by using an optical measuring device. However, at least the ratio of the deflection, using the glass plate, can be compared with medium air and water.

With regard to the enlarged initial gap with the lass plate compared to the measurement of the valve deflection without glass plate, the following can be assumed. Theoretically, a favourable underpressure between the outlet and inlet valve or an overpressure at the inlet valve could lead to an enlarged initial gap. Of course, it cannot be excluded that the handling of the valve samples could be a reason for the enlargement of the initial gap.The samples were prepared in a clean room, but lint from cleanroom wipes or other particles could have got between the valve arms when the samples were dried and disassembled and reassembled. Particles could also lead to an increase in the initial gap. Because of this, only vague statements can be made regarding the initial gap for all measurements with a glass plate.

4.1.2   Analyses of the valve deflection within medium air

For further considerations and analysing processes, the regression lines of the respective characteristic curves were formed. The results for all different valve types V1.D1, V2.D1 and V1.D2 (see Table 7), are shown under the following figure.
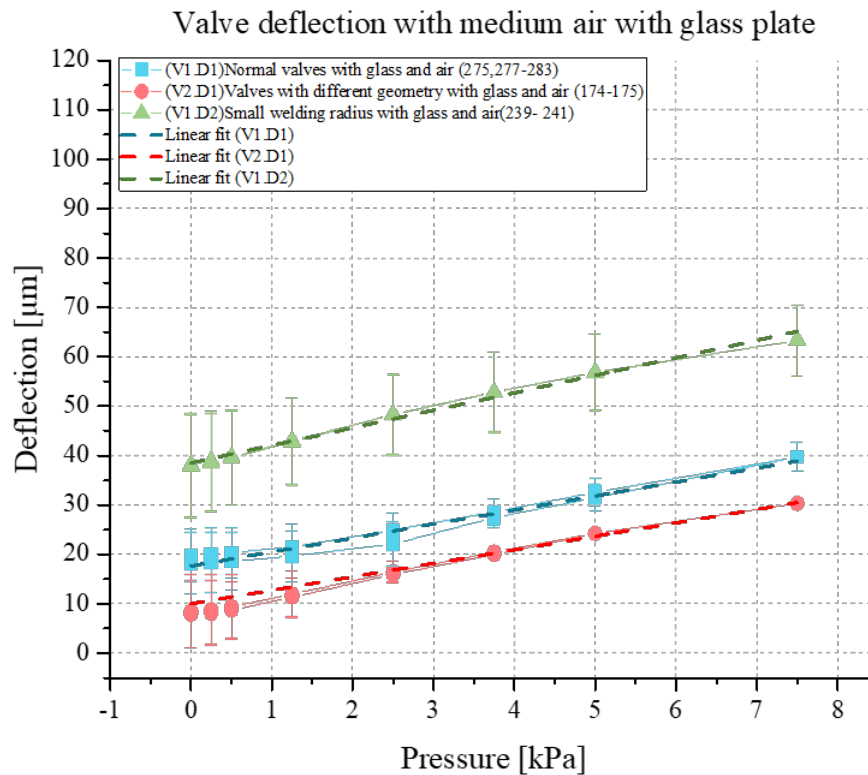
Figure 38: Results of the valve deflection with medium air and glass plate.

All relevant values for describing the regression lines of Figure 37 and Figure 38 are shown in tTable 11 below.

For further comparison, the spring stiffnesses were calculated using with Equation 29 and Equation 30 with the values from Table 6. Nevertheless, the formula is relatively inaccurate because the complex geometry of the ortho-planar valve is not completely represented,but rather a simplified column. With the help of this equation, at least the ratio of air to water measurements can be observed for this measurement setup. It can also be noted that V2.V1 has the highest spring stiffness, followed by V1.D1 ,and the smaller welding radius of V1.D2 reduces the spring stiffness. As a result, V1.D2 has the smallest value in terms of spring

Table 11: Regression lines for pressure dependent valve deflection within medium air

Equation	y = a + b*x				
Parameter	(V1.D1)	(V2.D1)	(V1.D2)	(V1.D1) with closure	(V1.D1) without glass
Intersection with Y-axis [µm]	17.65 ± 0.54	38.52 ± 0.38	9.99 ± 0.36	12.24 ± 0.01	4.37 ± 0.84
Gradient [µm/kPa]	2.83 ± 0.13	3.54 ± 0.11	2.73 ± 0.07	0.08 ± 0.00	3.76 ± 0.30
Error of the sum of quada	1.16	0.16	33.85	0	9.21
Pearson R	0.99	0.99	1	0.98	0.96
R-Quadrant(COD)	0.97	0.99	0.99	0.97	0.92
Cor. R-Quadrant	0.97	0.99	0.99	0.96	0.92

stiffness. For more detailed calculations, see Appendix B and Appendix C. Furthermore, the same measurements regarding valve deflection were carried out with water as the medium in order to be able to draw a comparison.

4.1.3   Analyses of the valve deflection within medium water

Also in these measurements, using the same measurement method described in the section 3.2.5, the deflection of the valves with glass covers at defined pressure was measured with a profilometer and are shown in Figure 39. Care was taken to ensure that the water level remained higher water level than the sample height (see section 3.2.1). Again the applied pressure was halved due to the series connection of the resistors assumed as valves ,and the deflection in the z-direction of the valves was multiplied by factor 1.2. This factor was described in section 3.2.3 and is used to compare water and air measurements with the profilometer as an optical measuring instrument. The results of the valve deflection within medium water and regression lines of the individual valve types V1.D1, V2.D1 and V1.D2 are plotted in the figure below.
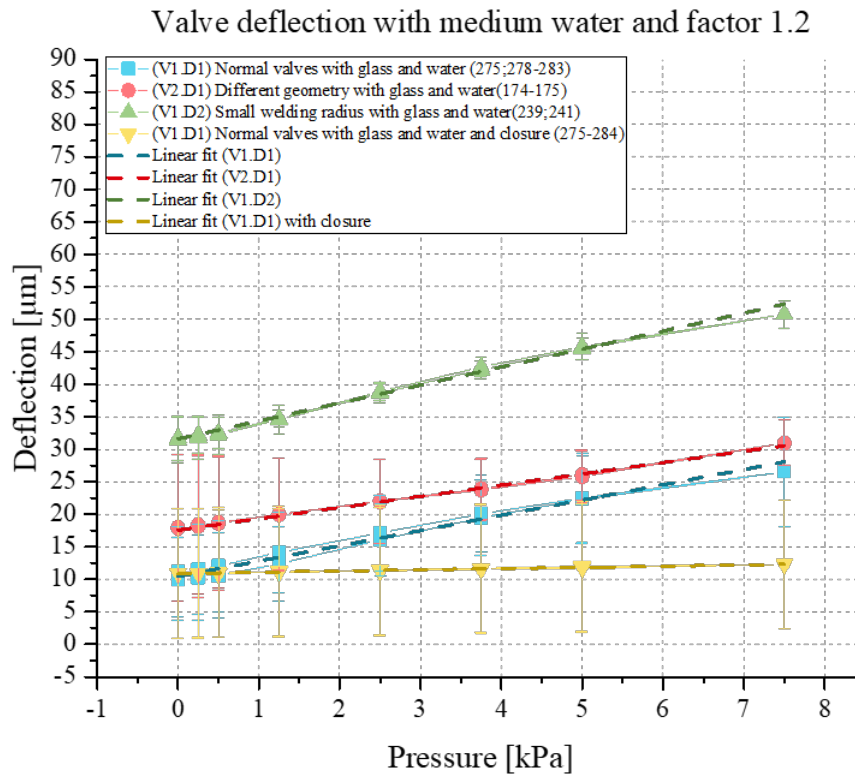
Figure 39: Results of valve deflection within medium water.

The values of the regression lines for the characteristic curves for water as a medium are presented in the table below for valve types V1.D1,V2.D2 and V1.D2 (see Table 7).

Table 12: Regression lines for pressure dependent valve deflection within medium water

Equation	y = a + b*x			
Parameter	(V1.D1)	(V2.D1)	(V1.D2)	(V1.D1) with closure
Intersection with Y-axis [µm]	10.46 ± 0.29	17.58 ± 0.17	31.60 ± 0.26	10.90 ± 0.03
Gradient [µm/kPa]	2.35 ± 0.10	1.73 ± 0.04	2.76 ± 0.08	0.19± 0.01
Error of the sum of quada	0.19	0.04	1.17	0.00
Pearson R	0.99	1.00	0.99	0.99
R-Quadrant(COD)	0.98	0.99	0.99	0.97
Cor. R-Quadrant	0.98	0.99	0.99	0.97

Since the different deflections of the same valve series in air and water are only dependent on the medium used, the spring stiffness can be specified again, starting with the highest value: V2.D1, V1.D1 and the smallest spring constant V1.D2.

4.1.4   Comparison of the valve deflection with medium air and water

After all relevant data on the deflection of the valves in the z-direction under the influence of different media have been recorded, they are now compared in the following. HAllvalve series characterised by different spring stiffnesses were measured, with the amount of deflection represents the relative value between pressure-dependent deflection and the original state without pressure. This difference was formed in order not to attribute the existing initial gap to the pressure-dependent deflection falsely. The results are shown iFigure 40 below. On the left-hand side under a) the results for air measurements and under b) on the right-hand side, the results of the measurements within medium water are represented.
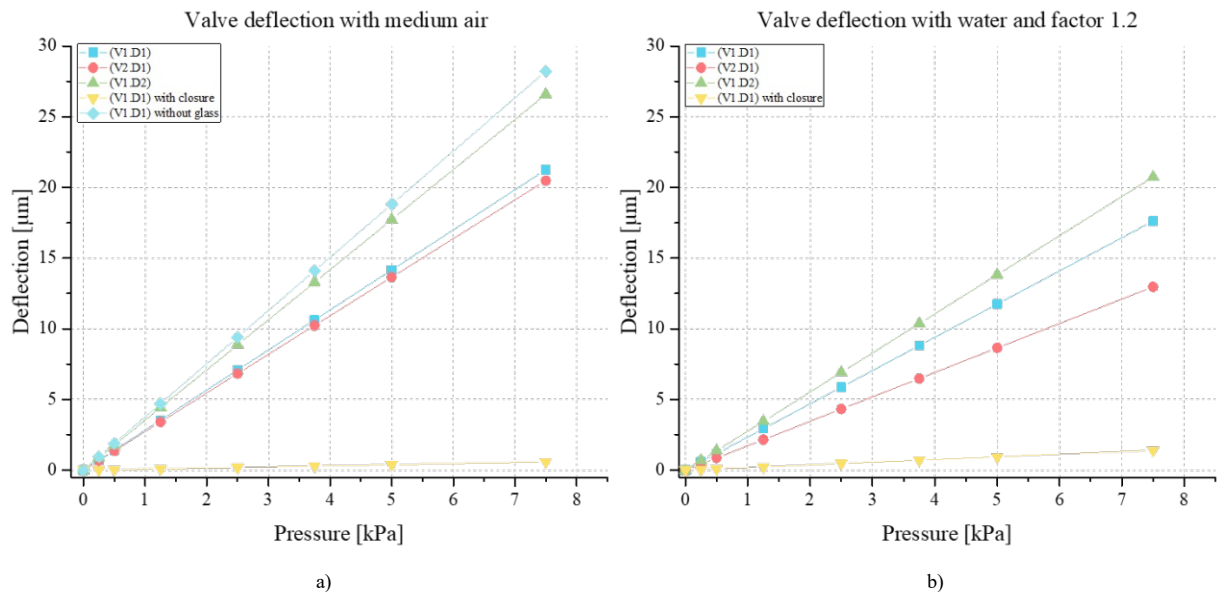
Figure 40: Results of valve deflection within medium a) air and b) water

Graphically, it can be clearly recognised how the dampening effect of the water medium is present in all valves. For a more detailed examination of the damping effect of air to water, two pressure values were examined more precisely for all valve series with the respective deflection of the specific valves. On the one hand, a relatively low pressure value of 500 Pa was chosen ,and on the other hand ,the maximum pressure value applied in this measurement at 7500 Pa. The results are presented in Table 13 below.

As you can see from the table, the valve with the highest spring stiffness V2.D1 has the highest damping factor from air to water. Valve series V1.D1 and V1.D2 behave relatively the same.

Table 13: Valve deflection in comparison of medium air and water

Valves	P [Pa]	z [m] in air	z [m] in water	ratio air/water
V1.D1	7500	2.12E-05	1.76E-05	1.2
V2.D1	7500	2.05E-05	1.30E-05	1.6
V1.D2	7500	2.66E-05	2.07E-05	1.3
Median				**1.4**
V1.D1	500	1.42E-06	1.17E-06	1.2
V2.D1	500	1.37E-06	8.64E-07	1.6
V1.D2	500	1.77E-06	1.38E-06	1.3
Median				**1.4**

The valve with the highest spring stiffness V2.D1 has the highest damping factor from air to water. Valve series V1.D1 and V1.D2 behave relatively the same. The limiting factor here is still that it is unclear where the pressure drop (see Equation 25) comes from when using the glass plate. For accurate quantification and future measurements, pressure sensors are needed before and after the valve samples. However, assuming a systematic measurement behaviour or measurement error, at least the ratio of the valve deflection from air to water can be described. It can be assumed that this factor 1.4 could be related to the ratio of the dynamic viscosity.

Considering the slope, the air measurements clearly show that the valve with the highest spring stiffness also has the lowest deflection. Based on this conclusion, the V2.D1 valves have the lowest deflection, followed by the V1.D1 valves and finally ,the V1.D2 valves with a smaller welding radius.

Here, too, the water measurements show that valves of the V2.D1 series have the lowest deflection. Valves of the V1.D1 series are again in the middle range ,and valves with a smaller welding radius (V1.D2) have the highest deflection according to their low stiffness.

It was also checked whether the damping could come from the water column above the valve cover. however, this can be ruled out,as the ratio of the density of air to water bears no relation to the derived factor of 1.4 (see Table 13). Another way to compare the valve deflections of the different valves under air and water conditions is a boxplot diagram. First of all, all valves are plotted within their initial gaps in comparison of medium air to water.

The following graph is plotted for further possible comparison of the values between air and water measurements (see Figure 41).

Initial gap

According to the following Figure 42, the initial gaps for two (V1.D1 and V1.D2) out of three valve series, were lower with water than with air as medium. For more information see section 4.1. Also, the valves with a small welding radius (V1.D2) have a significantly higher initial gap in all measurements than V1.D1 and V2.D1.
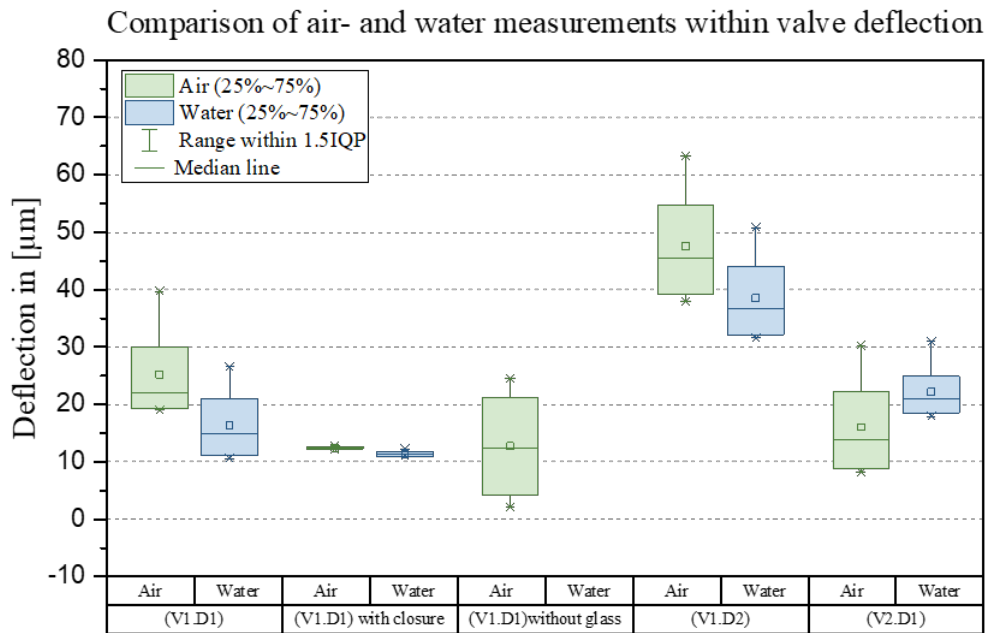
Figure 41: Box plot diagram of valve deflection within medium air and water for the different valve types V1.D1,V2.D1 and V1.D2

Further conclusions about the IG using the same measuring method are difficult to determine since it is unclear why the initial gaps are larger with the measurements without the glass plate. According to the values in Table 11 and Table 12 the values of the IG of the V1.D2 are in the air around two times higher than the IG of V1.D1 and four times higher than the values of V2.D1. In medium water, the IG of V1.D2 is three times higher than V1.D1 and 1.5 times higher than the valves V2.D1.

For further concrete statements, the initial gaps as shown Figure 41 are calculated out in order to avoid possible misinterpretations and are shown in the graph below (Figure 42).
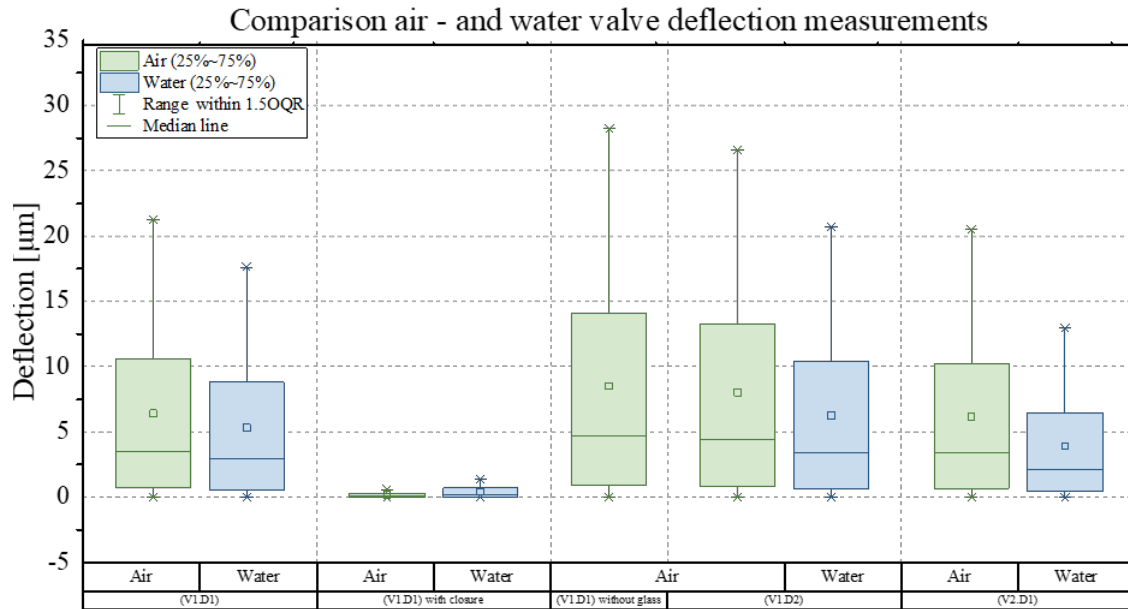
Figure 42: Box plot diagram of valve deflection within medium air and water for the different valve types V1.D1,V2.D1 and V1.D2.

As already discussed, the valves with the largest stiffness have the smallest deflection, which is also reflected in this diagram.

Since all deliberations on the measurements of valve deflection for water and air have been completed, the next paragraph addresses the flow measurements to the medium air and water.

4.2 Flow measurements

In this paragraph, the results of the passive flow measurements described in the section 3.2.6 are recorded and discussed. On the one hand, the passive flow rate for air and water, and on the other hand, the leakage rates were determined.

4.2.1 Passive flow measurement with medium air and water

In this measurement, the passive flow rate is measured at the outlet valve employing a flow sensor. The applied pressure changes the flow rate through the valve. As with the previous measurement, this is a quasi-static system. The results of this measurement for air and water will be discussed later. Again, the applied pressure was halved to infer the behaviour of a valve (see Equation 24).
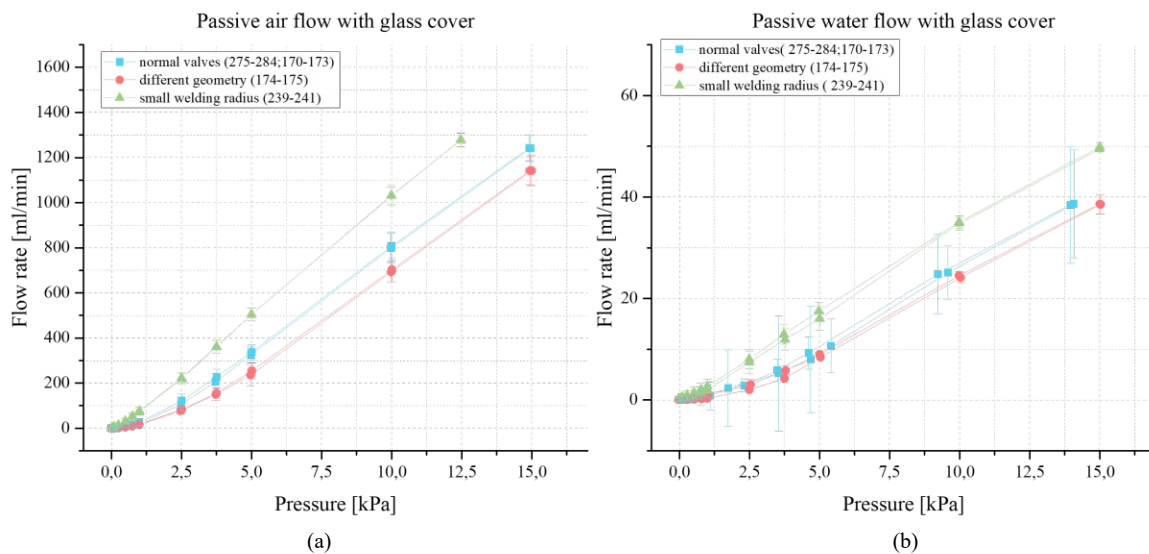
Figure 43: Passive flow measurements with medium a) air and b) water with valves V1.D1,V2.D1 and V1.D2

As already described in the section 3.1.1, the opening behaviour of valves can be compared with the behaviour of diodes. In passive flow measurements, the forward region of the diode behaviour is considered. By linearising the graph with respect to the threshold value U_{thresh}, a differential resistance R_{diff} can be determined by applying a tangent and reading off U_{thresh}. These values might be particularly relevant for future electrical network models in relation ortho-planar valves. For this purpose, the measured values were analysed. The values are summarized in Table 14.

Table 14: Graphical determination of the differential resistance and the trehshold voltage in the linear range of the valve series V1.D1, V2.D1 and V1.D2

Medium	Parameter	V1.D1	V2.D1	V1.D2
Air	R_{diff} [Pa min/ml]	1.19E+01	1.10E+01	8.62E+00
	R_{diff} [Pa s/m³]	7.14E+08	6.62E+08	5.17E+08
	U_{tresh} [Pa]	2.40E+03	2.50E+03	4.00E+02
Water	R_{diff} [Pa min/ml]	3.33E+02	3.85E+02	3.33E+02
	R_{diff} [Pa s/m³]	2.00E+10	2.31E+10	2.00E+10
	U_{tresh} [Pa]	4.00E+02	2.40E+03	2.00E+02
	Ratio (R_{air}/R_{water})	0.036	0.029	0.026

As can be clearly seen in the table, the valves behave very differently in air and water. Considering first the values for air, it is noticeable that the differential resistances are relatively the same for all valves. Nevertheless, it can be seen that the valve with the lowest spring stiffness V1.D2 achieves the steepest slope for the differential resistance. Then, regarding the flow, the valve with the lowest spring stiffness V1.D2 allows a higher flow the fastest and vice versa, the one with the highest stiffness, the lowest and the slope of the straight line is the flattest. Since the two valves, V1.D1 and V2.D1 have the same slope but run differently, the threshold voltage must be considered. Here, valve V1.D1 has a minimally lower voltage than the values of V2.D1, which explains the earlier rise of graph V1.D1. The valves V2.D2 have a deficient value for the low voltage to be applied. The maximum flows are about 1200 ml/min at an applied pressure of 15 kPa. This value is approx. 30 times higher than the maximum for water measurements.

Considering the water measurements, the values for the flow are many times lower than the ones for air. Looking at the maximum values, these are approx. 40 ml/min for the water measurements at an applied pressure of 15 kPa. This is a factor of 30 compared to the maximum values for air. As in the previous measurements with air, the spring stiffness are again relevant. Valve V1.D2 has the steepest curve. However, this time, the differential resistance of V2.D2 shows a higher value than the other two valves. In general, the values for the differential resistance are approximately the same. Decisive here is the threshold pressure which heralds the start of the flow. As with air, V1.D2 has the lowest threshold pressure, followed by V2.D1 and then V2.V1. This behaviour is again due to the increasing spring stiffness from V1.D2 to V1.D1 and finally V2.D1.

The differences between air and water measurements are, however, mainly determined by the U_{thresh}, which shows a strongly differentiated behaviour with the different valves. However,

the damping of the gradient is almost the same for all valves from water to air. It is recommended to use the valve-specific values for further modelling.

Looking at Figure 44 it can be clearly seen, that air has many times higher flow rates than water.
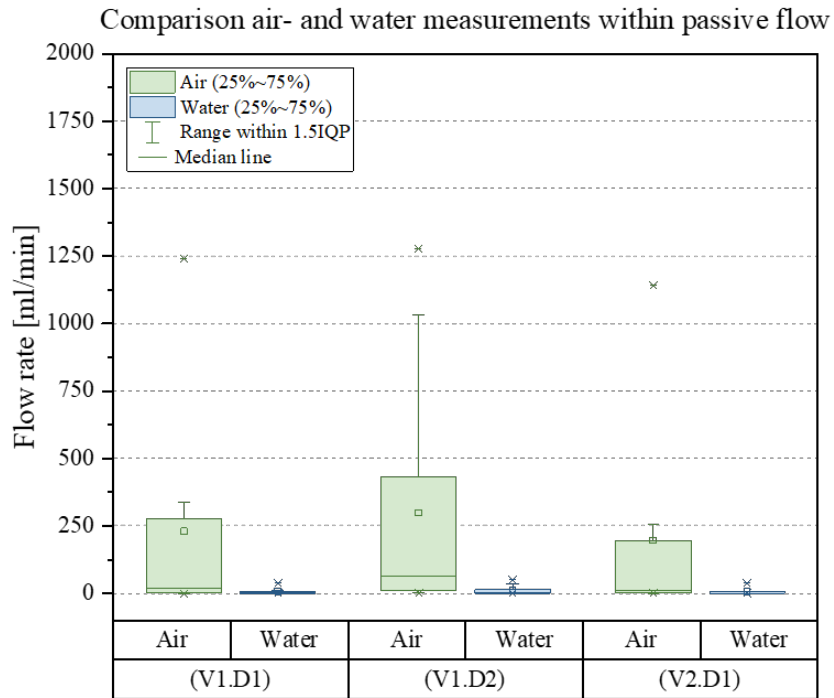
Figure 44: Comparison of results for passive flow within medium air and water with valve type V1.D1,V2.D1 and V1.D2

As described above, valve V1.D2 has higher flow rates than V1.D1 and V2.D1 due to its low spring stiffness.

Now that all the statements regarding passive flow measurements have been made, the leakage rates will be discussed in more detail.

4.2.2 Leakage measurements with medium air and water

About the leakage rate, the results are shown in the following Figure 45. The measurement method used here is described in section 3.2.6. Again, valves of the V1.D1, V2.D1 and V1.D2 series were used (see Table 7).
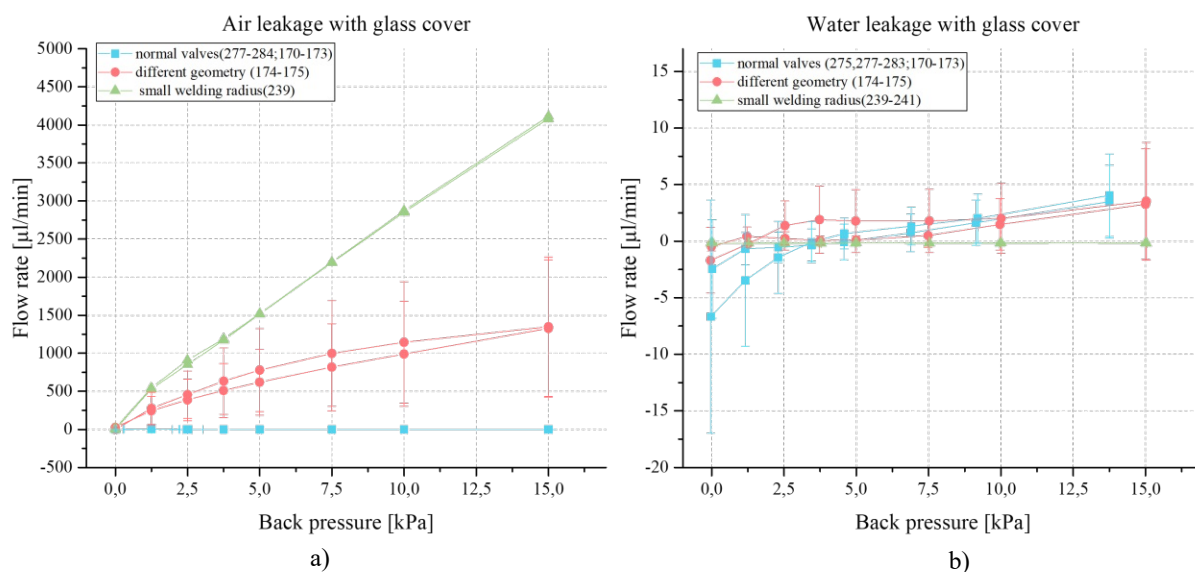
Figure 45: Leakage of the valves V1.D1,V2,D1 and V1.D2 with medium air a) and medium b) water

For a better understanding, all relevant statistical values are shown in the Table 15.

Table 15: Presentation of the relevant data on the leakage rate of the valve series V1.D1,V2.D1 and V1.D2

Medium	Samples	Average [μl/min]	STD	Min [μl/min]	Median [μl/min]	Max[μl/min]
	V1.D1	0.2	0.1	0.0	0.2	0.4
Air	V2.D1	660.5	425.3	0.0	627.5	1348.6
	V1.D2	1659.9	1291.6	0.0	1352.3	4112.5
	V1.D1	-0.1	2.6	-6.7	-0.1	4.0
Water	V2.D1	1.0	1.4	-1.7	0.9	3.5
	V1.D2	-0.2	0.0	-0.2	-0.2	-0.2

It should be noted that only one valve was used in the air measurements for valve series V1.D2 instead of three in the in Figure 45 a), as two valves showed a-typical behaviour for

the air but not for the water measurements. This behaviour was checked and confirmed by new measurements. Therefore, a statement regarding the leakage rate in comparison to the other series is only vaguely possible. What can be said about the leakage rates in comparison to air and water is that valves of the V1.D1 series have a shallow leakage rate for air compared to the other valve series V2.D1 and V1.D2. Valves of type V1.D1, however, has the highest leakage rate in water. All valves have a shallow leakage rate with air and water measurements with maximum flow rates below 5.0 µl/min. In contrast, in the air measurements, the leakage rate in air for valve series V1.D2 (sample 239) increases up to 4000 µm/min at a pressure of 15 kPa.

4.3 Bubbles

As described in the section 3.2.5, bubbles repeatedly occurred throughout the measurements, making it impossible to evaluate the results. Therefore, these were examined for position and pressure dependence. An example of the evaluation is shown in Figure 46. A pressure value and the number of bubbles were transmitted and observed for each bubble that occurred. Figure 46 shows only the beginning of bubble formation and ends with 15 kPa and should serve as a showcase.
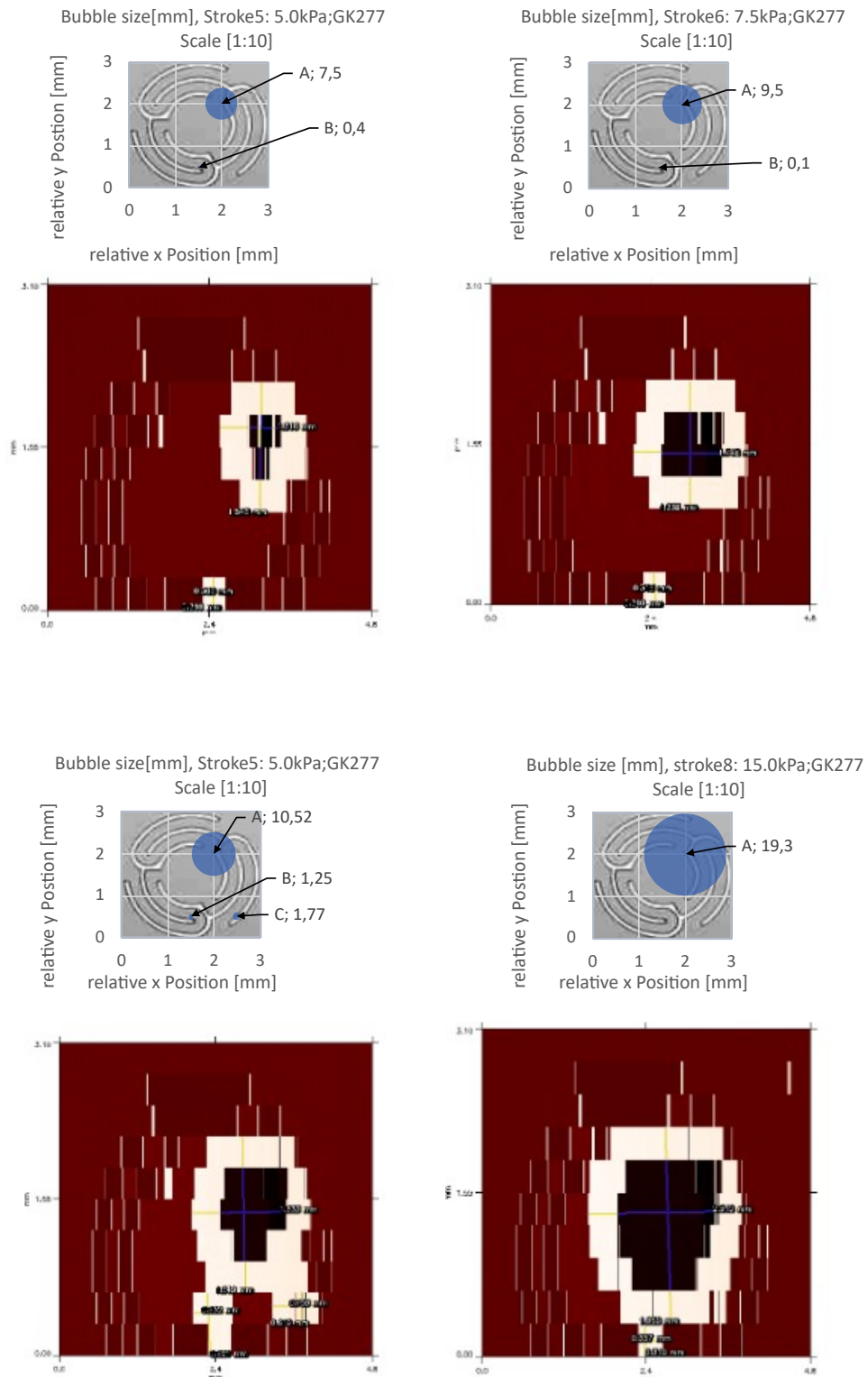
Figure 46: 3D images of bubble formation as a function of applied pressure and subsequent representation of the position and size in a scaled representation of the valve used

It was interesting to see how the bubbles behave when the pressure decreases. When the pressure decreases, the bubbles expand. It must be mentioned that adhesion forces act on

Comparison between bubble size [mm] and applied pressure [kPa]
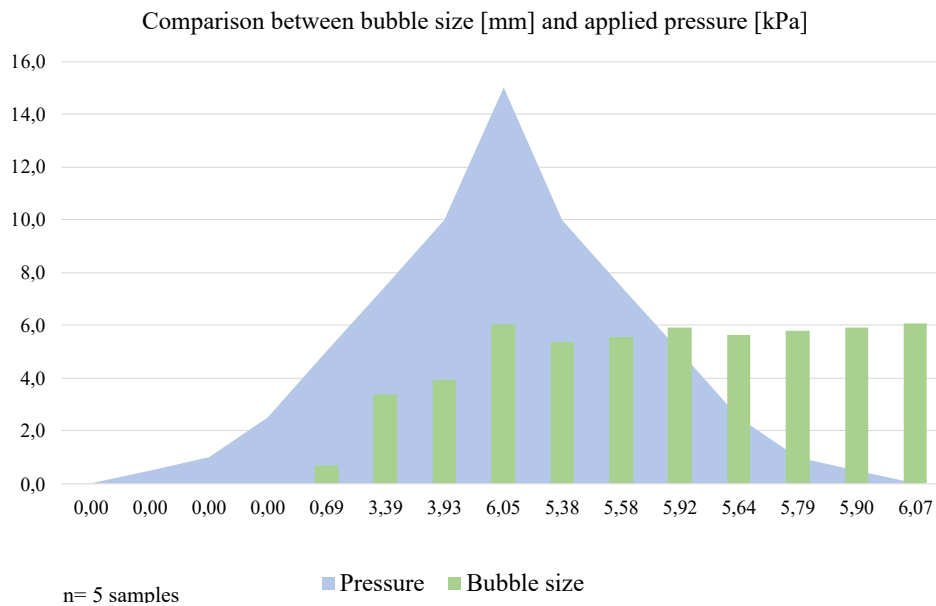
Figure 47: Comparison between bubble size [mm] and applied pressure [kPa]

the disc and the bubble remains on the disc due to this. It has also been found that the bubbles always appear at the points with the highest stress peaks, i.e. at the end of the arms. Figure 47 It shows how the bubble size changes depending on the pressure. Bubbles only appear above a value of approx. 20 mbar ,and the size increases on average with decreasing pressure. Due to higher adhesion forces to glass, but a certain size, the bubbles have always adhered to the glass pane. Therefore the course probably behaves differently than under the influence of an actuator membrane. In addition, the glass pane is rigid, and the actuator membrane is movable, which is another influencing factor.

Now that the results of the bubbles that occur during measurements with water have been discussed, the last point to be presented is the results of the dynamic measurements.

4.4   Dynamic measurements

The measurement procedure for the dynamic measurement method is shown in section 3.2.7. For these measurements, only valves of the series (V1.D1) have been randomly tested so far. With the help of this method, the specific natural frequencies of the valves under the

influence of the medium air and water are to be examined, among other things. This will allow conclusions to be drawn about the entire system. It will also be investigated whether the oscillation behaviour of the valve has a negative influence on the pump performance.
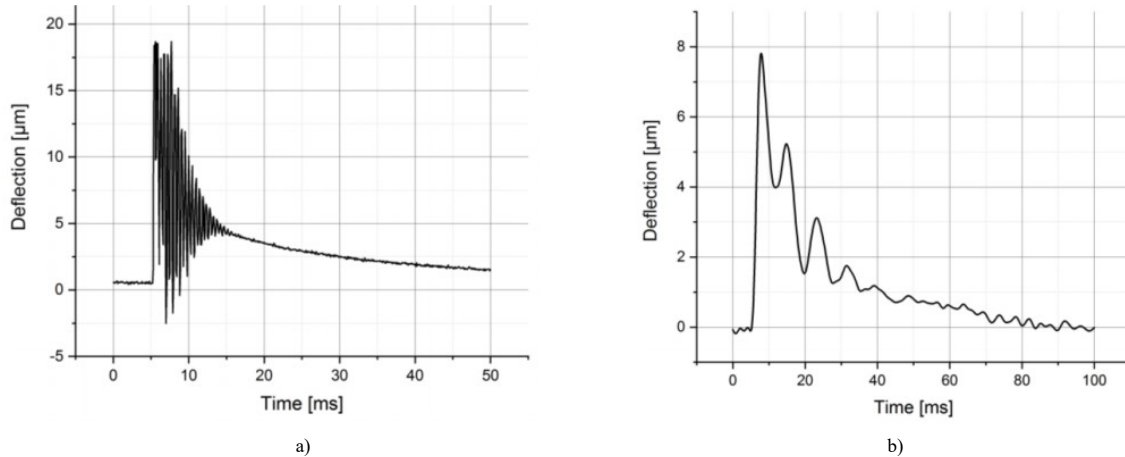
Figure 48: Measured dynamic valve deflection during actuation with a sharp pressure impulse (10Hz) with medium a) air and b) water

A short air pressure pulse at the valve leads to a deflection with subsequent oscillation, dependent on the corresponding spring constant of the respective valves and is shown under Figure 48 a). The oscillation is unwanted as it leads to turbulence and thus increases the fluidic resistance. Instead of this, water is damping the oscillation and limits the disturbance, but also leads to a slow valve movement (see Figure 48 b)) with the consequence of lower usable actuator frequencies. The flow rate of the stainless steel piezoelectric diaphragm pump stagnates and starts to decrease in the range of 30-40 Hz due to this reduced valve performance. The valve has in medium air a resonance frequency of around 2.15 kHz, and within the water as a medium, a resonance frequency around 130 Hz. For further qualitative statements, however, further investigations must be carried out to include the influence of the measurement setup.

This measuring method for measuring the dynamic deflection of valve with the aid of an optical sensor was developed in the course of this work. However, further validation measures must be carried out in order to be able to determine the influence of the tube system within the measurement setup on the deflection of the valve sample. However, the procedure offers subsequent research work the possibility of a more precise evaluation of dynamic systems under the influence of air and water.

5 Conclusion and Future scope

Following is a brief summary of the whole thesis with decisive considerations and outcomes. In this section, the most important findings of the preceding considerations and measurements regarding quasi-static valve deflection, quasi-static measurement of leakage and flow rates are presented. Subsequently, the findings regarding the formation of bubbles are briefly presented. Finally, the findings of the dynamic measurements are discussed. These results are intended to form the basis for new modelling or validate old assumptions and provide a great opportunity for further optimisation measures regarding passive check valves.

Quasi-static measurements

Most of the characterisation tests with passive check valves are only carried out with air as the medium. However, the medium used for the micropump is often liquid. In the case of medical products, for example, dug dosing systems, drugs are injected in liquid form. Due to the fact that no measuring method has been available to date for investigating valves, especially their deflection under applied pressure, one has been developed for this purpose. Until now, valve behaviour under the influence of water has been calculated or simulated. However, measured values provide a quantification of such models. Under normal use (see Figure 23 where the pump is assembled), there is an actuator foil above the inlet and outlet valves. This actuator is an optical barrier between possible optical sensors and the valves. If this barrier is removed, measurements with air are possible, as the air escaping from the valve does not damage the sensitive sensor. With water, however, the situation is different. The leakage of water at the valves could irreversibly damage the optical sensor (see section 3.2.1). In the first step of this work, a procedure was developed to use optical sensors to characterise valves under the influence of water. For this purpose, the actuator above the valve was removed, and a very thin transparent plate (glass) was attached (see Figure 26). This construction made it possible to observe the valves visually.

In the next step, the completely new measuring method used was calibrated by calculation and measurement. The aim was to ensure that it is possible to compare air and water measurements with each other. Under normal use of the optical sensor (see Figure 20), there is only air between the sensor head and the valve sample. Within the new developed measurement, there was also a glass plate above the valve for the air measurements. For water measurements, a glass plate and the medium water was between the glass plate and the valve (see Figure 28). These different materials or media influence the results of the optical sensor. The calibration was first carried out mathematically and then looked up under

section 3.2.3. A factor of 1.2 was calculated for air/water valve deflection (see Table 10). Subsequently, this factor was validated by measuring different metal foils (see Figure 32). This showed that a factor of 1.2 was also determined. It is now possible to compare the measurement results with air and water using the optical sensor.

Furthermore, in order to be able to determine the valve behaviour under the influence of different media, different valve series were used: V1.D1, V2.D1 and V1.D1. The parameters for the different valves are described under Table 6. The valves are each variable either by geometry or welding radius. In order to be able to characterise the valves using air and water as medium, different measurements were carried out with the prepared samples.

First, measurements to determine the valve deflection within medium air and water are done. The measurement for the valve deflections due to applied pressures are carried out with the test set-up from section 3.2.5. First of all, measurements were carried out on the V1.D1 valve series with and without a glass plate. It was noticed that there is a pressure difference between the pressure applied and the pressure actually applied (see Equation 25). This pressure drop is most likely due to the measurement setup. It was also found that there is an increased initial gap in the valves with glass plates compared to those without glass plates. This is also most likely due to the measurement setup. Statements on the IG (see Figure 2.2.2 under Initial Gap) can therefore only be made to a limited extent. If so, then only in relation to each other, i.e. measurements with air and measurements with water. However, it is noticeable that in all measurements with reduced welding radius (V1.D2), the initial gaps were increased compared to the other valve series. It can therefore be assumed that the reduced welding radius increases the undesired initial gap.

It was calculated that for the valve samples with a glass plate, the applied pressure must be halved afterwards. This is based on the assumption of a series connection of the two valve resistors (see Equation 24). Subsequently, the optical measurement was carried out with air and water for all valve series (V1.D1, V2.D1, V1.D2). The spring stiffness was determined graphically and mathematically once during these measurements (see Appendix B and Appendix C). It was shown that the smaller welding radius of V1.D2 has an enormous influence on the spring stiffness and reduces it by approx. 20 %. The theory that ta pressure drop only causes the deflection was also verified. This statement proved to be true (see Figure 37).

If the measurements are compared with air and water, it is noticeable that the deflections behave in the same way with regard to their spring stiffness. The magnitude of the spring

79

stiffnesses behaves as follows in successive order: V2.D1, V2.D1 and V1.D2. As can be seen in Table 14, the ratios of air and water measurements behave the same for all valves, regardless of the pressure applied. The ratio of the deflections of the air and water measurements is 1.4. One can therefore speak of a systematic behaviour. regarding the measurements of the valve deflection, it must be said that to be able to make quantitative statements, a measurement with a pressure sensor before and after the valve sample would be necessary. This could prove the pressure drop that is only calculated so far. Due to this fact, pressure sensors were used afterwards.

The section about bubbles (see section 4.3),is mentioned as an important knowledge for future measurements. It is essential that there are no bubbles in the total water inflow. If bubbles appear in the system, boundary layers form ,and the optical measurement cannot be used. For each measurement, care was taken to ensure that the entire tube system was flushed once before the measurements and that no bubbles were visible. The filling of the valve samples should also be looked up in the section 3.2.2 for future measurements. Regarding the formation of bubbles, it can be stated that it is assumed that in the event of bubbles forming, these are primarily caused by bubbles already present in the system. Degassed water should be used in all cases for future measurements. It has also been noticed that the size of the bubbles changes with the pressure applied. During the measurements taken, it was also noticed that the bubbles only appear at a pressure of larger than 4kPa (see Figure 47). However, as mentioned, this must be checked using a degassed liquid. In the literature, it was noticed that metal was often used for this purpose in order to avoid bubbles. To a certain extent, bubbles are difficult to avoid. Under paper [24], rib structures on the chamber were used to remove bubbles from the system. This could be checked in future work. In addition, the evaluation of bubble size through the 3D data set is very tedious, as the bale size was measured manually for all valves at fifteen different pressures applied. Edge detentions could automatically calculate the optical data via python script and a statement made about the size. Using image processing, "Sobel-filters" could be used for edge detection and "Region growing" for segmentation.

After the measurements of the valve deflection were completed, the passive flow was measured (see measurement setup 3.2.6). Again, for this manner all three valve types were used (see Table 6). The values from the Table 14 are particularly relevant here. Since passive valves are comparable with diodes (see section 3.1.1), the linear range of the flow characteristic was considered under this table. All three valves have the same ratio of air to water measurements. At an applied pressure of 15 kPa, an air to water attenuation of approximately 30 can be observed . The flow rate of the different valves is again due to their spring stiffness.

V2.D1 has the highest spring constant, followed by V2.D1 and finally V1.D2. These values of the differential resistances can be used for further simulations. Pressure sensors before and after the valves were used. However, it was not possible to calculate this characteristic curve using formulas. For further measurements, it is recommended first to determine the spring stiffness of the valves using FEM simulation. This value is particular and depends on the specific valve design. No formula was found that adequately describes the spring stiffness.

With regard to the leakage rates of the valves in comparison with air and water, it can be said that relatively low leakage rates were found in both water and air (see Table 15).

Dynamic measurements
The structure for the dynamic measurements can be found under section 3.2.7. Therefore, V1.D1, V2.D1 and V1.D2 were used again. For these measurements, a pressure pulse is triggered very close to the valve and the valve deflection is observed using a profilometer. This procedure needs to be improved in further work, as it is suspected that the influence of the tube system has a relatively strong influence due to the oscillating behaviour of the medium. Subsequent measurements should try to bring the pressure pulse even closer to the valve inlet, as this is crucial for deflection. The less tube there is between the inlet valve and the pressure pulse, the less influence the measuring system has on the deflection. However, it can be observed that with air, there is a much higher frequency and deflection of the valve at the same pressure compared to the water measurements (see section 4.4).

Glossary

The next list describes several symbols that will be later used within the body of the document

β_T	Compressibility coefficient
η	Dynamic viscosity
λ	Wave length
ρ	Density
τ	Stress
A	Sureface
b	Width
c	Speed of light
d	Diameter
E	Young's modulus
F	Force
g	Gravity
h	Height
I	Moment of interior
i	Current
j	Number of valve beams
k	Stiffness
m	Mass

n	Refractive index
P	Pressure
q	Charge
U	Voltage
V	Volume
v	Velocity
z	Deflection
AC	Alternating current
AP	Operating point
BaTiO	Barium titanate
C	Capacitor
DC	Direct current
DI water	Deionized water
EMFT	Research Institution for Microsystems and Solid State Technologies
IG	Initial Gap
MEMS	Microelectromechanical systems
NC	Normally closed
NO	Normally open
NPWT	Negative Pressure Wound Therapy
OADR	Old Age Dependency Ratio
PET	Polyethylene terephthalate
PTZ	Zitronate titanate
PZT	Plumbum zirconate titanate
R	Resistor
SAWHI	Aubcutaneous Abdominal Wound Healing Impairment

List of Figures

List of Tables

Appendix: A

The following section presents formulas found in the literature for calculating the components used in ortho-planar valves.

For a radial flow between two parallel disks forming a fluidic ring, the Navier-Stokes equations can be used and lead to the following expression (26) for the variable hydraulic resistance R_v of the valve [21]:

$$R_v = \frac{6\eta}{\pi z^3} \log\left(\frac{r_o}{r_i}\right) \tag{26}$$

where x is the valve defection, r_s is the radius of the valve disc (surface of the disc), and r_i is the radius of the inlet channel of the valve (inlet surface).

Another possible explanation for valve resistance reads as follows:

$$Q = \frac{e}{\eta} \cdot p^3 \tag{27}$$

where Q is the fluidic flow and e is the specific parameter depending on the valve behaviour, the value p presents the applied pressure.

Considering the presented model Figure 15, a check valve is represented by its differential valve resistance and by the opening behaviour (capacitor) in parallel. In this context, the fluidic capacity of the valve is calculated from the displacement due to flap deflection [53]:

$$C_v = \frac{d_i}{dp} \int_0^1 w(z)dz \cdot h \tag{28}$$

d is the valve diameter of the inner diameter of the valve, dp the pressure differences, w the valve opening, z the valve deflection and h valve thickness.

In terms of resistance, all formulas were compared with the actual measurement results. None of the formulas was sufficient for an accurate model description. Equation 27 showed relatively good agreement, at least for high-pressure values (in the linear range of the diode characteristic) using the medium air. However, this was not the case for medium water.

Appendix B

For a rough comparison of the different valves, the specific spring stiffness was calculated for the V1.D1, V2.D1, and V1.D2 series valves. The formula Equation 30 used for this purpose (for further information, see section 2.2.2). Following expressions considering the deflection (z) and the stiffness (k_s):

$$F = \frac{F_{total}}{j} \quad \text{and} \quad I = \frac{bh^3}{12} \tag{29}$$

with

$$k_s = \frac{12EI}{l^3} \tag{30}$$

The total spring stiffness is expressed as:

$$k_{total} = j \cdot k_s \tag{31}$$

The valve specific parameters can be found under Table 6.

In addition, the spring stiffness was determined from the measured values (medium air with glass plate). According to Hook's law, the pressure-dependent deflection of the check valve z can be simplified as follows [21, 63]:

$$z = \frac{(A_i) \cdot (dp)}{k_{total}} \tag{32}$$

where A_i is the surface of the inlet, dp the pressure difference and k_{total} the valve stiffness depending on the sum of valve beams.

The results are presented in the table below:

However, itEquation 30 has inaccuracies with regard to the complex geometry. In addition, no pressure sensor was detected during the measurements of the valve deflection (Equation 32). It is assumed that there is a pressure drop due to the measurement setup (tube system, etc.). For subsequent measurements, pressure sensors were therefore always attached before and after the valve sample. Since the pressure drop was the same for all valves, a systematic error is assumed. This means that it is at least possible to determine which valve has the highest and lowest spring resistance. However, for qualitative statements, measurements

must be carried out again with pressure sensors before and after the valve.

The following values were obtained with both formulas:

Table 16: Spring stiffness of V1.D1, V2.D1 and V1.D2

Samples	ktotal (Eq:31) [N/m]	ktotal (Eq:32) [N/m]
V1.D1	517.29	623.82
V2.D1	541.67	647.18
V1.D2	/	498.63

To calculate the spring stiffness, only a pressure value difference is necessary. For the calculations and the determination of k_{total} from the measured values, the pressure value 7500 Pa was used. What is interesting about the results is that it can be seen that valves with a smaller welding radius have a significantly lower spring resistance with the same valve geometry. The small welding radius thus reduces the spring stiffness by approx—20%.

Appendix C

In this section, a factor is calculated using a formula Equation 33 in relation to the valve deflection under the influence of air and water.

$$z = \frac{(A_i) \cdot (dp)}{k_{total}} \cdot factor \tag{33}$$

These values are not qualitative, as a pressure drop from the system is assumed. The values must therefore be checked. However, it can be proven that the same factors for water and air measurements can be calculated for all valves of different types using the calculated spring stiffnesses (see Table 16).

For this purpose, the low pressure value at 500 Pa and the maximum pressure value at 7500 Pa were used. The results are presented in the table below Table 17.

Table 17: Valve deflection in comparison of medium air (factor α) and water(factor β)

Valves	P [Pa]	factor α air	factor β water	ratio γ water/air	ratio δ air /water
V1.D1	500	8.29E-01	6.88E-01	8.29E-01	1.21E+00
V2.D1	500	8.48E-01	5.37E-01	6.33E-01	1.58E+00
V1.D2	500	8.29E-01	6.47E-01	7.80E-01	1.28E+00
V1.D1	7500	8.29E-01	6.88E-01	8.29E-01	1.21E+00
V2.D1	7500	8.48E-01	5.37E-01	6.33E-01	1.58E+00
V1.D2	7500	8.29E-01	6.47E-01	7.80E-01	1.28E+00
Median		**0.8**	**0.6**	**0.7**	**1.4**

The calculated fit for water and air was also shown graphically in the figure below (Figure 49).
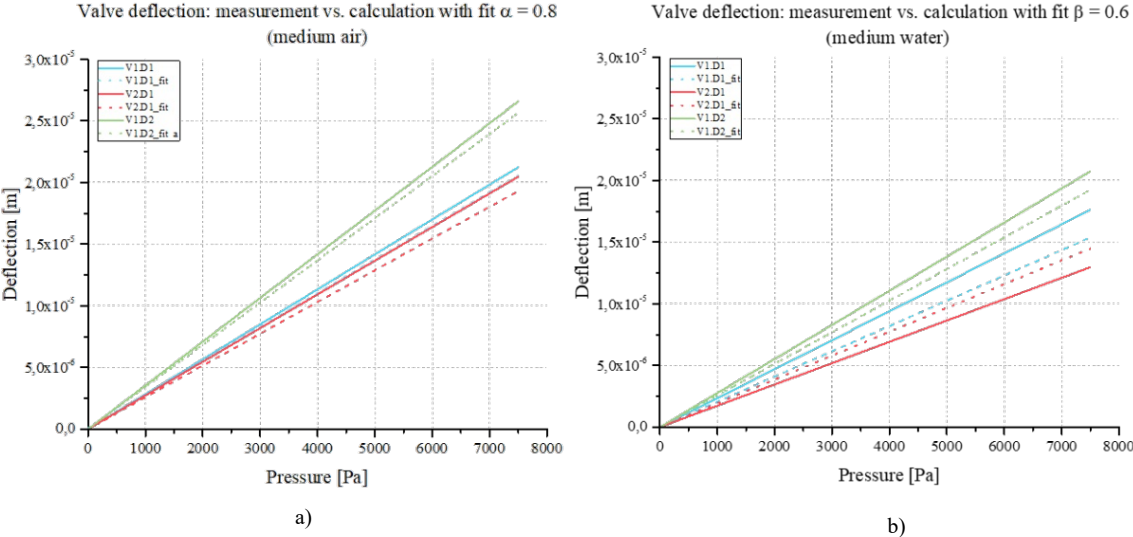
Figure 49: Valve deflection within medium a) air(fit α) and b) water (fit β)

It can be seen that a constant factor for air and a constant factor for water can be identified regardless of the pressure applied. However, it is not possible to make a qualitative statement about the calculated values, as k_{total} values for these complex geometries are normally simulated by FEM and deviate from the analytical calculations.

References

[1] Fraunhofer Research Institution for Microsystems and Solid State Technologies EMFT. *The smallest micropump in the world - Fraunhofer EMFT*. 13.05.2021. URL: https://www.emft.fraunhofer.de/en/mediacenter/press-briefings/2015-11-16_smallest-micropump.html.

[2] Brand S. "Microdosing systems: micropumps the beating heart of microfluidics." In: 2006 ().

[3] Peter Woias. "Micropumps—past, progress and future prospects". In: *Sensors and Actuators B: Chemical* 105.1 (2005), pp. 28–38. ISSN: 09254005. DOI: 10.1016/j.snb.2004.02.033.

[4] Agnes Beate Bußmann et al. "Piezoelectric titanium based microfluidic pump and valves for implantable medical applications". In: *Sensors and Actuators A: Physical* 323 (2021), p. 112649. ISSN: 09244247. DOI: 10.1016/j.sna.2021.112649.

[5] Partha Kumar Das and A. B. M. Toufique Hasan. "Mechanical micropumps and their applications: A review". In: AIP Conference Proceedings. Author(s), 2017, p. 020110. DOI: 10.1063/1.4984739.

[6] *Micropump Market by Share, Size, Growth and Analysis – 2027 | MRFR*. 30.04.2021. URL: https://www.marketresearchfuture.com/reports/micro-pump-market-1300.

[7] United Nations, Department of Economic and Social Affairs, and Population Division. "World Population Ageing 2019: Highlights". In: (2019).

[8] Iñaki Martín Lesende et al. "Functional decline and associated factors in patients with multimorbidity at 8 months of follow-up in primary care: the functionality in pluri-pathological patients (FUNCIPLUR) longitudinal descriptive study". In: *BMJ open* 8.7 (2018), e022377. DOI: 10.1136/bmjopen-2018-022377.

[9] K. Jeitler et al. "Continuous subcutaneous insulin infusion versus multiple daily insulin injections in patients with diabetes mellitus: systematic review and meta-analysis". In: *Diabetologia* 51.6 (2008), pp. 941–951. ISSN: 0012-186X. DOI: 10.1007/s00125-008-0974-3. URL: https://link.springer.com/content/pdf/10.1007/s00125-008-0974-3.pdf.

[10] Dörthe Seidel et al. "Negative Pressure Wound Therapy vs Conventional Wound Treatment in Subcutaneous Abdominal Wound Healing Impairment: The SAWHI Randomized Clinical Trial". In: *JAMA surgery* 155.6 (2020), pp. 469–478. DOI: `10.1001/jamasurg.2020.0414`.

[11] Fraunhofer Research Institution for Microsystems and Solid State Technologies EMFT. *The smallest micropump in the world - Fraunhofer EMFT*. 4.05.2021. URL: `https://www.emft.fraunhofer.de/en/mediacenter/press-briefings/2015-11-16_smallest-micropump.html`.

[12] Agnes Bußmann et al. "Microdosing for Drug Delivery Application – a Review". In: (2021).

[13] S. Mohith, P. Navin Karanth, and S. M. Kulkarni. "Recent trends in mechanical micropumps and their applications: A review". In: *Mechatronics* 60 (2019), pp. 34–55. ISSN: 09574158. DOI: `10.1016/j.mechatronics.2019.04.009`.

[14] Laxman Saggere. "Membrane Actuation for Micropumps". In: *Encyclopedia of Microfluidics and Nanofluidics*. Ed. by Dongqing Li. Boston, MA: Springer US, 2008, pp. 1078–1082. ISBN: 978-0-387-32468-5. DOI: `10.1007/978-0-387-48998-8_871`.

[15] Ronghui Zhang et al. "Development and Characterization a Single-Active-Chamber Piezoelectric Membrane Pump with Multiple Passive Check Valves". In: *Sensors (Basel, Switzerland)* 16.12 (2016). DOI: `10.3390/s16122108`.

[16] "Stainless steel micropumps at Fraunhofer EMFT". In: (). URL: `https://www.emft.fraunhofer.de/content/dam/emft/en/documents/Infosheets/14_E_Stainless%20steel%20micropumps.pdf`.

[17] *Microdosing systems and micropumps for medical technology*. URL: `https://www.emft.fraunhofer.de/content/dam/emft/en/documents/Infosheets/16_E_Microdosing%20systems%20and%20micropumps%20for%20medical%20technology.pdf`.

[18] S. Mohith, P. Navin Karanth, and S. M. Kulkarni. "Recent trends in mechanical micropumps and their applications: A review". In: *Mechatronics* 60 (2019), pp. 34–55. ISSN: 09574158. DOI: `10.1016/j.mechatronics.2019.04.009`.

[19] A. Nisar et al. "MEMS-based micropumps in drug delivery and biomedical applications". In: *Sensors and Actuators B: Chemical* 130.2 (2008), pp. 917–942. ISSN: 09254005. DOI: `10.1016/j.snb.2007.10.064`.

[20]   Qifeng Cui, Chengliang Liu, and Xuan F. Zha. "Simulation and optimization of a piezoelectric micropump for medical applications". In: *The International Journal of Advanced Manufacturing Technology* 36.5-6 (2008), pp. 516–524. ISSN: 0268-3768. DOI: 10.1007/s00170-006-0867-x.

[21]   S. Fournier and E. Chappel. "Modeling of a Piezoelectric MEMS Micropump Dedicated to Insulin Delivery and Experimental Validation Using Integrated Pressure Sensors: Application to Partial Occlusion Management". In: *Journal of Sensors* 2017 (2017), pp. 1–7. ISSN: 1687-725X. DOI: 10.1155/2017/3719853. URL: https://downloads.hindawi.com/journals/js/2017/3719853.pdf.

[22]   A. Shabanian et al. "A novel piezo actuated high stroke membrane for micropumps". In: *Microelectronic Engineering* 158 (2016), pp. 26–29. ISSN: 01679317. DOI: 10.1016/j.mee.2016.03.016.

[23]   Qiao Sheng Pan et al. "Piezoelectric micropump using dual-frequency drive". In: *Sensors and Actuators A: Physical* 229 (2015), pp. 86–93. ISSN: 09244247. DOI: 10.1016/j.sna.2015.03.029.

[24]   H. K. Ma, R. H. Chen, and Y. H. Hsu. "Development of a piezoelectric-driven miniature pump for biomedical applications". In: *Sensors and Actuators A: Physical* 234 (2015), pp. 23–33. ISSN: 09244247. DOI: 10.1016/j.sna.2015.08.003.

[25]   Rakesh Kumar Haldkar, Vijay Kumar Gupta, and Tanuja Sheorey. "Modeling and flow analysis of piezoelectric based micropump with various shapes of microneedle". In: *Journal of Mechanical Science and Technology* 31.6 (2017), pp. 2933–2941. ISSN: 1738-494X. DOI: 10.1007/s12206-017-0536-z.

[26]   Kwang W. Oh and Chong H. Ahn. "A review of microvalves". In: *Journal of Micromechanics and Microengineering* 16.5 (2006), R13–R39. ISSN: 0960-1317. DOI: 10.1088/0960-1317/16/5/R01.

[27]   Jingshi Dong et al. "Performance of single piezoelectric vibrator micropump with check valve". In: *Journal of Intelligent Material Systems and Structures* 31.1 (2020), pp. 117–126. ISSN: 1045-389X. DOI: 10.1177/1045389X19880024.

[28]   Olivier Smal et al. "Modelling, characterization and testing of an ortho-planar microvalve". In: *Journal of Micro-Nano Mechatronics* 4.3 (2008), pp. 131–143. ISSN: 1865-3928. DOI: 10.1007/s12213-008-0015-9.

[29]   Xiaoqiang Wu et al. "Advances in passive check valve piezoelectric pumps". In: *Sensors and Actuators A: Physical* 323 (2021), p. 112647. ISSN: 09244247. DOI: 10.1016/j.sna.2021.112647.

[30]   Nam-Trung Nguyen et al. "Micro check valves for integration into polymeric microfluidic devices". In: *Journal of Micromechanics and Microengineering* 14.1 (2004), pp. 69–75. ISSN: 0960-1317. DOI: `10.1088/0960-1317/14/1/309`.

[31]   *Microdosing systems and micropumps for medical technology.* URL: `https://www.emft.fraunhofer.de/content/dam/emft/en/documents/Infosheets/16_E_Microdosing%20systems%20and%20micropumps%20for%20medical%20technology.pdf`.

[32]   D. C. S. Bien, S. J. N. Mitchell, and H. S. Gamble. "Fabrication and characterization of a micromachined passive valve". In: *Journal of Micromechanics and Microengineering* 13.5 (2003), pp. 557–562. ISSN: 0960-1317. DOI: `10.1088/0960-1317/13/5/305`.

[33]   Min Hu et al. "A silicon-on-insulator based micro check valve". In: *Journal of Micromechanics and Microengineering* 14.3 (2004), pp. 382–387. ISSN: 0960-1317. DOI: `10.1088/0960-1317/14/3/010`.

[34]   Nam-Trung Nguyen and Thai-Quang Truong. "A fully polymeric micropump with piezoelectric actuator". In: *Sensors and Actuators B: Chemical* 97.1 (2004), pp. 137–143. ISSN: 09254005. DOI: `10.1016/S0925-4005(03)00521-5`.

[35]   Thai-Quang Truong and Nam-Trung Nguyen. "A polymeric piezoelectric micropump based on lamination technology". In: *Journal of Micromechanics and Microengineering* 14.4 (2004), pp. 632–638. ISSN: 0960-1317. DOI: `10.1088/0960-1317/14/4/026`.

[36]   Bo Li et al. "Development of large flow rate, robust, passive micro check valves for compact piezoelectrically actuated pumps". In: *Sensors and Actuators A: Physical* 117.2 (2005), pp. 325–330. ISSN: 09244247. DOI: `10.1016/j.sna.2004.06.029`.

[37]   Jing Shi Dong et al. "Design and experimental research on piezoelectric pump with triple vibrators". In: *Microsystem Technologies* 23.8 (2016), pp. 3019–3026. ISSN: 0946-7076. DOI: `10.1007/s00542-016-3029-6`.

[38]   Jing Shi Dong et al. "Design of a piezoelectric pump with dual vibrators". In: *Sensors and Actuators A: Physical* 257 (2017), pp. 165–172. ISSN: 09244247. DOI: `10.1016/j.sna.2017.02.001`.

[39]   Eric Chappel. "A Review of Passive Constant Flow Regulators for Microfluidic Applications". In: *Applied Sciences* 10.24 (2020), p. 8858. DOI: `10.3390/app10248858`.

[40]   Xiaoqiang Wu et al. "Advances in passive check valve piezoelectric pumps". In: *Sensors and Actuators A: Physical* 323 (2021), p. 112647. ISSN: 09244247. DOI: `10.1016/j.sna.2021.112647`.

[41]   Hamid Asadi Dereshgi, Huseyin Dal, and Mustafa Zahid Yildiz. "Piezoelectric microp-umps: state of the art review". In: *Microsystem Technologies* 7 (2021), p. 9765. ISSN: 0946-7076. DOI: `10.1007/s00542-020-05190-0`.

[42]   Olivier Smal et al. "Modelling, characterization and testing of an ortho-planar micro-valve". In: *Journal of Micro-Nano Mechatronics* 4.3 (2008), pp. 131–143. ISSN: 1865-3928. DOI: `10.1007/s12213-008-0015-9`.

[43]   John J. Parise, Larry L. Howell, and Spencer P. Magleby. "Ortho-planar linear-motion springs". In: *Mechanism and Machine Theory* 36.11-12 (2001), pp. 1281–1299. ISSN: 0094114X. DOI: `10.1016/S0094-114X(01)00051-9`.

[44]   Olivier Smal, Bruno Dehez, Benoît Raucent, Michaël De Volder, Jan Peirs, Dominiek Reynaerts, Frederik Ceyssens, Johan Coosemans, Robert Puers. "Modelling and Char-acterisation of an Ortho-Planar Micro-Valve." In: (2006).

[45]   Roxana Künzel. "Modelierung und Optimierung der fluidischen Eigenschaften von pas-siven Membranventilen einer Titan-Micropumpe: Master Thesis". In: (2018).

[46]   Xinjie Zhang and Zhenyu Zhang. "Microfluidic Passive Flow Regulatory Device with an Integrated Check Valve for Enhanced Flow Control". In: *Micromachines* 10.10 (2019). DOI: `10.3390/mi10100653`.

[47]   Arun Gunda et al. "Proportional Microvalve Using a Unimorph Piezoelectric Microac-tuator". In: *Micromachines* 11.2 (2020). DOI: `10.3390/mi11020130`.

[48]   Jin-Ho Kim, C. J. Kang, and Yong-Sang Kim. "A disposable polydimethylsiloxane-based diffuser micropump actuated by piezoelectric-disc". In: *Microelectronic Engi-neering* 71.2 (2004), pp. 119–124. ISSN: 01679317. DOI: `10.1016/j.mee.2003.10.005`.

[49]   Guru Prasath Natarajan, Sung-Jin Kim, and Chang-Wan Kim. "Analysis of Membrane Behavior of a Normally Closed Microvalve Using a Fluid-Structure Interaction Model". In: *Micromachines* 8.12 (2017). DOI: `10.3390/mi8120355`.

[50]   Judy L. Lin and Jason M. Clevenger. "Modeling and optimizing passive valve designs for the implantable Gold Micro-Shunt used in glaucoma treatment". In: *Computers & Structures* 87.11-12 (2009), pp. 664–669. ISSN: 00457949. DOI: `10.1016/j.compstruc.2008.09.005`.

[51]   Zhen-Hao Lin et al. "Fluid-Structure Interaction Analysis on Membrane Behavior of a Microfluidic Passive Valve". In: *Membranes* 10.10 (2020). ISSN: 2077-0375. DOI: `10.3390/membranes10100300`.

[52]   M. S. Groen. *Microvalves for precise dosing.* 2015. ISBN: 9789036539616. DOI: `10.3990/1.9789036539616`.

[53] Markus Herz. "Optimierung der Förderrate einer piezoelektrischen Mikropumpe_final". In: (2011).

[54] Chiang-Ho Cheng and Yi-Pin Tseng. "Characteristic studies of the piezoelectrically actuated micropump with check valve". In: *Microsystem Technologies* 19.11 (2013), pp. 1707–1715. ISSN: 0946-7076. DOI: `10.1007/s00542-013-1857-1`.

[55] Olivier Smal et al. "Modelling, characterization and testing of an ortho-planar micro-valve". In: *Journal of Micro-Nano Mechatronics* 4.3 (2008), pp. 131–143. ISSN: 1865-3928. DOI: `10.1007/s12213-008-0015-9`.

[56] S. Fournier and E. Chappel. "Modeling of a Piezoelectric MEMS Micropump Dedicated to Insulin Delivery and Experimental Validation Using Integrated Pressure Sensors: Application to Partial Occlusion Management". In: *Journal of Sensors* 2017 (2017), pp. 1–7. ISSN: 1687-725X. DOI: `10.1155/2017/3719853`.

[57] Francisco Antonio Perdigones, Antonio Luque, and Jose M. Quero. "Correspondence Between Electronics and Fluids in MEMS: Designing Microfluidic Systems Using Electronics". In: *IEEE Industrial Electronics Magazine* 8.4 (2014), pp. 6–17. ISSN: 1932-4529. DOI: `10.1109/MIE.2014.2318062`.

[58] Prof. Dr. Bock. "Skriptum: Grundlagen der Elektrotechnik und Elektronik". In: (2014), pp. 53–56.

[59] Joachim Specovius, ed. *Grundkurs Leistungselektronik: Bauelemente, Schaltungen und Systeme*. 9., überarbeitete und aktualisierte Auflage. Lehrbuch. Wiesbaden: Springer Vieweg, 2018. ISBN: 978-3-658-21169-1.

[60] P. Voigt, G. Schrag, and G. Wachutka. "Electrofluidic full-system modelling of a flap valve micropump based on Kirchhoffian network theory". In: *Sensors and Actuators A: Physical* 66.1-3 (1998), pp. 9–14. ISSN: 09244247. DOI: `10.1016/S0924-4247(97)01783-4`.

[61] Tarik Bourouina and Jean-Paul Grandchamp. "Modeling micropumps with electrical equivalent networks". In: *Journal of Micromechanics and Microengineering* 6.4 (1996), pp. 398–404. ISSN: 0960-1317. DOI: `10.1088/0960-1317/6/4/006`.

[62] Dieter Guicking. *Schwingungen: Theorie und Anwendungen in Mechanik, Akustik, Elektrik und Optik*. Lehrbuch. Wiesbaden: Springer Vieweg, 2016. ISBN: 978-3-658-14135-6. DOI: `10.1007/978-3-658-14136-3`. URL: `https://link.springer.com/content/pdf/10.1007%2F978-3-658-14136-3.pdf`.

[63]   Olivier Smal, Benoît Raucent, and Hervé Jeanmart. "Fluid flow modelling of a micro-valve". In: *International Journal for Simulation and Multidisciplinary Design Optimization* 3.2 (2009), pp. 356–362. ISSN: 1779-627X. DOI: 10.1051/ijsmdo/2009011.

[64]   Silke Stempin Dominik Surek. "Angewandte Strömungsmechanik für Praxis im Stuidum". In: 2007 ().

[65]   Jason K. Lee et al. "Measurement Methods for Solubility and Diffusivity of Gases and Supercritical Fluids in Polymers and Its Applications". In: *Polymer Reviews* 57.4 (2017), pp. 695–747. ISSN: 1558-3724. DOI: 10.1080/15583724.2017.1329209.

[66]   Leopold Böswirth and Sabine Bschorer. "Strömung kompressibler Fluide". In: *Technische Strömungslehre*. Ed. by Leopold Böswirth and Sabine Bschorer. Wiesbaden: Vieweg+Teubner Verlag, 2012, pp. 266–292. ISBN: 978-3-8348-1718-1. DOI: 10.1007/978-3-8348-8647-7{\textunderscore}11.

[67]   Leopold Böswirth and Sabine Bschorer, eds. *Technische Strömungslehre*. Wiesbaden: Vieweg+Teubner Verlag, 2012. ISBN: 978-3-8348-1718-1. DOI: 10.1007/978-3-8348-8647-7.

[68]   Prof. Dr.-Ing. Ralph Schneider. "Regelungstechnik". In: (2014).

[69]   Yann Quinsat and Christophe Tournier. "In situ non-contact measurements of surface roughness". In: *Precision Engineering* 36.1 (2012), pp. 97–103. ISSN: 01416359. DOI: 10.1016/j.precisioneng.2011.07.011.

[70]   M. Pagem and C. Boust. "3D SURFACE ACQUISITION: COMPARISON OF TWO MICROTOPOGRAPHIC EQUIPMENTS WHEN MEASURING MATERIALS OF CULTURAL HERITAGE". In: (). URL: https://f-origin.hypotheses.org/wp-content/blogs.dir/1101/files/2019/01/2016_MPAGE_CIE_Article-1.pdf.

[71]   Bronkhorst. *Coriolis Massendurchfluss-Messprinzip*. 21.05.2021. URL: https://www.bronkhorst.com/de-de/service-und-support/theorien-und-technologien/coriolis-massendurchfluss-messprinzip/.

[72]   "Mini cori-flow: Kompakte Coriolis-Massendurchflussmesser & -regöer für Flüssigleoten und Gase". In: (). URL: https://www.wagner-msr.de/files/wagner-mess-regeltechnik/Downloads/Prospekte/Bronkhorst/961030--folder%20mini%20cori-flow%20revc.pdf.

[73]   Gottfried Schröder and Hanskarl Treiber. *Technische Optik: Grundlagen und Anwendungen*. 11., bearbeitete und aktualisierte Auflage. Kamprath-Reihe. Würzburg: Vogel Business Media, 2014. ISBN: 9783834361882. URL: http://www.content-select.com/index.php?id=bib_view&ean=9783834361882.